Supporting Information for

Original article

P450-mediated dehydrotyrosine formation during WS9326 biosynthesis proceeds *via* dehydrogenation of a specific acylated dipeptide substrate

Songya Zhang[a], Lin Zhang[b], Anja Greule[c], Julien Tailhades[c,d,e], Edward Marschall[c,d,e], Panward Prasongpholchai[f], Daniel J. Leng[f], Jingfan Zhang[g], Jing Zhu[a], Joe A. Kaczmarski[h], Ralf B. Schittenhelm[c,i], Oliver Einsle[b], Colin J. Jackson[e,h], Fabrizio Alberti[f,g], Andreas Bechthold[j], Youming Zhang[a], Manuela Tosin[f,*], Tong Si[a,*], Max J Cryle[c,d,e,*]

[a]*CAS Key Laboratory of Quantitative Engineering Biology, Shenzhen Institute of Synthetic Biology, Shenzhen Institute of Advanced Technology, Chinese Academy of Sciences, Shenzhen 518055, China*

[b]*Institut für Biochemie, Albert-Ludwigs-Universität Freiburg, Freiburg 79104, Germany*

[c]*Department of Biochemistry and Molecular Biology, The Monash Biomedicine Discovery Institute, Monash University, Clayton, VIC 3800, Australia*

[d]*EMBL Australia, Monash University, Clayton, VIC 3800, Australia*

[e]*ARC Centre of Excellence for Innovations in Peptide and Protein Science, Clayton, VIC 3800, Australia*

[f]*Department of Chemistry, University of Warwick, Gibbet Hill Road, Coventry, CV4 7AL, UK*

[g]*School of Life Sciences, University of Warwick, Gibbet Hill Campus, Coventry, CV4 7AL, UK*

[h]*Research School of Chemistry, the Australian National University, Acton, ACT 2601, Australia*

[i]*Monash Proteomics and Metabolomics Facility, Monash University, Clayton, VIC 3800, Australia*

[j]*Institute of Pharmaceutical Sciences, Albert-Ludwigs-Universität Freiburg 79104, Germany*

Received 6 February 2023; received in revised form 16 March 2023; accepted 16 March 2023

*Corresponding authors.

E-mail addresses: M.Tosin@warwick.ac.uk (Manuela Tosin), tong.si@siat.ac.cn (Tong Si); max.cryle@monash.edu (Max J Cryle).

1. SI Tables

Table S1. Plasmids used in this study.

Name	Description	Reference
pIJ790	λ-Red plasmid, temperature sensitive replicon	[1]
pBluescript II SK(+)	Cloning vector, lacZ'(α-complementation)	Stratagene
pKC1132	Conjugative vector, non-replicative in *Streptomyces*	[2]
pUZ8002	Helper plasmid for conjugating plasmid containing the oriT sequence, RK2-derived (IncP-1α group), tra1 and tra2 region	[3]
pBSK-Sas16	Plasmid containing gene *sas16* for subcloning	This study
pKCLP2-gusA	pKCLP2 derivative with *gusA* gene	[4]
pTESa	pSET152 derivatives; attP flanked by loxP site, ermEp1 promoter flanked by *tfd* terminator sequences	[4]
pLERECJ	Carrying aac(3)IV flanked by loxP-sites	[5]
pKCLP2-gusA-sas16::*aac3*	Vector for gene deletion of *sas16*	[6]
pSET152-hyg	ΦC31 attachment site, integrative, HygR	Lab stock
pSET152-sas16	For gene *sas16* complementation	This study
pSET152-sas16-F250T	For complementation of Sas16 with point-mutation F250T	This study
pSET152-sas16-A246G	For complementation of Sas16 with point-mutation A246G	This study
pSET152-sas16-Y248N	For complementation of Sas16 with point-mutation Y248N	This study
pSET152-sas16-AY246-248GN	For complementation of Sas16 with point-mutation AY246-248GN	This study
pSET152-sas16-YF248-250NT	For complementation of Sas16 with point-mutation YF248-250NT	This study
pSET152-sas16-AF246-250GT	For complementation of Sas16 with point-mutation AF246-250GT	This study
pSET152-sas16-AYF-246-248-250GNT	For complementation of Sas16 with point-mutation AYF-246-248-250GNT	This study
pET28a(+)	Protein expression vector carrying an N-terminal His_6-Tag/thrombin/T7 promoter, f1 ori, pBR322 ori	Invitrogen
pBluescript SK(-)	Cloning vector, lacZ'(α-complementation)	Stratagene
pUC19	Cloning and sequencing vector for E. coli	Invitrogen
pBSK-Sas16	Plasmid containing gene *sas16* for subcloning	This study
pET28-Sas16	Vector for protein expression of Sas16	This study
pET28-Sas16-F250T	Vector for protein expression of Sas16-F250T	This study
pET26 PuR	Vector for protein expression of PuR	[7]
pET26 PuxB A105V	Vector for protein expression of PuxB	[7]
pET21-sfp-R4-4	Vector for protein expression of sfp-R4-4	[8]
pET-Trx_1c	Vector with an internal hexahistidine tag and a protease cleavage site between the fusion protein and the cloned protein sequence Trx- PCP, T7 promoter	[9]
pET-Trx-A-NMt-PCP	Vector for protein expression of A-NMT-PCP domain, based on pET-Trx-1c	This study
pBSK-NMt	Plasmid containing MTase encoding gene for subcloning	This study
pSC101-ccdA	Vector for counterselection	[10]
P15A-ccdB-amp	Vector for counterselection	[10]
pBAC1F16	Plasmid containing the WS9326A BGC for heterologous expression	This study
pBAC1F16-Nmet-amp-ccdB	Plasmid for the point-mutation of N-methyltransferase domain	This study
pBAC1F16-D2014Q	Plasmid for the point-mutation of N-methyltransferase domain	This study
pBAC1F16-D2014A	Plasmid for the point-mutation of N-methyltransferase domain	This study

Table S2. Primers used in this study.

Primer	Sequence (5' to 3')	Purpose
Vsas4-KO-F	CAGCGACTTGAGCAGTCTCTCGG	For PCR verification of exconjugant *S. lividans* 1326::1F16
Vsas4-KO-R	AGTAGCTGAGGCACACCAGCAC	
Vsas18-KO-F	TGCTGGTCACCAACCACCACA	For PCR verification of mutant *S. lividans* 1326::1F16::pKC1132-sas18
Vsas18-KO-R	TGTTCGAGGATCAGCCGGATGC	
apra-M-R	GGCTCTTCTCCTTGAGCCACCT	
P450pET-F	ATAgaattcATGACCGACGCCGAGACG	For the construction of plasmid pET28-Sas16
P450pET-R	TCActcgagCTACCAGCCGATCGTCAGCTT	
For_A_NMt_PCP_NcoI	ATTccatgGACACCCTGCCCGCCCTG	For the construction of plasmid pET-Trx-A-NMt-PCP
Rev_A_NMt_PCP_XhoI	ATTctcgagAACGCTCCAATTCGATGCG	
SAS16F	ATATaagctcCCGACTACACCGGCATCCTC	For the construction of plasmid pKCLP2-gusA-sas16::aac3
SAS16R	ATATgaattcGCTCGTCGTCCACCGTGTC	
SAS16-ApraF	CGCAAGAAATGACCTCAGCTCAGATATAGGGGTAACGTCATGGATATCTCTAGATACCG	
SAS16-ApraR	GATGCAGCGGTCGCGTTCGGCGTGAACCTTCATGGCGCCTAAACAAAAGCTGGAGCTC	
pET28a-sas16-NdeI-GA-F	CTGGTGCCGCGCGGCAGCCATATGACCGACGCCGAGACGAAG	For construction of mutant sas16-F250T expression vector
pET28a-sas16-HindIII-GA-R	GGTGCTCGAGTGCGGCCGCAAGCTTCTACCAGCCGATCGTCAGCT	
sas16-MFrg1-F	TCGCGGACGTGCTCATAGTC	For construction of plasmid pSET152-sas16
sas16-MFrg1-R	GAGCAGCAGCATCTTGGTCATCA	
F250T-F	GACTATGAGCACGTCCGCGAGCTGGCCCGCATCAATGG	For site-directed single mutation at position 246, 248, 250 of Sas16
F250T-R	TGATGACCAAGATGCTGCTGCTCgcgggcaacgagaccatcgt	
A246G-R	TGATGACCAAGATGCTGCTGCTCgggggctacgagttcatcgt	
Y248N-R	TGATGACCAAGATGCTGCTGCTCgcgggcaacgagttcatcgt	
AY246-248GN-R	TGATGACCAAGATGCTGCTGCTCgggggcaacgagttcatcgt	For site-directed double mutation at position 246, 248, and 250 of Sas16
YF248-250NT-R	TGATGACCAAGATGCTGCTGCTCgcgggcaacgagaccatcgt	
AF246-250GT-R	TGATGACCAAGATGCTGCTGCTCgggggctacgagaccatcgt	
AYF-246-248-250GNT	TGATGACCAAGATGCTGCTGCTCgggggcaacgagaccatcgt	For site-directed mutations at position 246, 248, 250 of Sas16
nMTsas16-D2104Q-F	gtctgatcatggcgccggtcgccccgcacgtggagctgtactggggtgccTTTGTTTATTTTTCTAAATAC	Oligonucleotides containing the D2104Q site mutation for counterselection[10]
nMTsas16-D2104Q-R	gggtcggcggcggtctgccggcgcagggtctcgatgaccgtgccggacagAGCCCCATACGATATAAGTTGT	
nMTsas16-D2104Q-Res	gggtcggcggcggtctgccggcgcagggtctcgatgaccgtgccggacagCTGggcaccccagtacagctccacgtgcggggcgaccggcgccatgatcagac	For point mutations of D2104Q in plasmid pBAC1F16
nMTsas16-D2104A-F	gtctgatcatggcgccggtcgccccgcacgtggagctgtactggggtgccTTTGTTTATTTTTCTAAATAC	Oligonucleotides containing the D2104A site mutation for counterselection[10]
nMTsas16-D2104A-R	gggtcggcggcggtctgccggcgcagggtctcgatgaccgtgccggacagAGCCCCATACGATATAAGTTGT	
nMTsas16-D2104A-Res	gggtcggcggcggtctgccggcgcagggtctcgatgaccgtgccggacagGGCggcaccccagtacagctccacgtgcggggcgaccggcgccatgatcagac	For point mutations of D2104A in plasmid pBAC1F16
Vnmet-ccdB-F	ACAAGTGGCAGGTCATCAAC	For verification of the mutagenesis in NMt domain of Sas17
amp-ccdB-R	AGCCCCATACGATATAAGTTG	
VNmetQ2104-R	AAGTACTGCGCCACCGAGTTG	

Table S3. Strains used in this study.

Strains	Relevant characteristics	Reference
S. asterosporus DSM 41452	Wild type strain of WS9326A producer	DSMZ
S. asterosporus DSM 41452::pUC19Δ3100spec	*S. asterosporus* DSM 41452 strain containing plasmid pUC19Δ3100spec	[11]
S. asterosporus DSM 41452::pKC1132-sas18	Gene inactivation of *sas18* in the WT strain	This study
S. *lividans* 1326::1F16	*S. lividans* 1326 containing BAC plasmid pBAC1F16	This study
S. asterosporus Δ*sas16*	Gene *sas16* deletion in the WT strain	[11]
S. asterosporus Δ*sas16*:: pSET152-sas16	Sas16 overexpression in the mutant *S. asterosporus* DSM 41452 Δ*sas16*	This study
S. asterosporus Δ*sas16*::pSET152-sas16-F250T	Complementation of gene *sas16* with F250T mutation in *S. asterosporus* DSM 41452 Δ*sas16*	This study
S. asterosporus Δ*sas16*:: pSET152-sas16-A246G	Complementation of gene *sas16* with A246G mutation in *S. asterosporus* DSM 41452 Δ*sas16*	This study
S. asterosporus Δ*sas16*:: pSET152-sas16-Y248N	Complementation of gene *sas16* with Y248N mutation in *S. asterosporus* DSM 41452 Δ*sas16*	This study
S. asterosporus Δ*sas16*:: pSET152-sas16-AY246-248GN	Complementation of gene *sas16* with AY246-248GN mutation in *S. asterosporus* DSM 41452 Δ*sas16*	This study
S. asterosporus Δ*sas16*:: pSET152-sas16-YF248-250NT	Complementation of gene *sas16* with YF248-250NT mutation in *S. asterosporus* DSM 41452 Δ*sas16*	This study
S. asterosporus Δ*sas16*:: pSET152-sas16-AF246-250GT	Complementation of gene *sas16* with AF246-250GT mutation in *S. asterosporus* DSM 41452 Δ*sas16*	This study
S. asterosporus Δ*sas16*:: pSET152-sas16-AYF-246-248-250GNT	Complementation of gene *sas16* with AYF-246-248-250GNT mutation in *S. asterosporus* DSM 41452 Δ*sas16*	This study
E. coli DH5α	General cloning host	Invitrogen
E. coli ET12567(pUZ8002)	Methylation-deficient *E. coli* strain for conjugation with the helper plasmid	Lab stock
E. coli BW25113	Host for DNA recombination	[5]
E. coli BL21 star (DE3)	Protein expression host	Invitrogen
E. coli BL21(DE3) pLysS	Protein expression host	Invitrogen
E. coli Gbred-gyrA462	Host for ccdB counterselection	[10]
E. coli DH10 β/ pBAC1F16	E. coli harboring BAC plasmid pBAC1F16	This study
E. coli DH10 β/pSC101-ccdA/pBAC1F16	For point-mutation of N-methyltransferase domain in Sas17	This study
E. coli DH10 β/pSC101-ccdA/pBAC1F16-Nmet-amp-ccdB	For point-mutation of N-methyltransferase domain in Sas17	This study
E. coli DH10 β/pSC101-ccdA/pBAC1F16-NmetD2104Q-amp-ccdB	For point-mutation of D2104Q in N-methyltransferase domain in Sas17	This study
E.coli DH10 β/pSC101-ccdA/pBAC1F16-NmetD2104A-amp-ccdB	For point-mutation of D2104A in N-methyltransferase domain in Sas17	This study
E. coli BL21 (DE3)::pET28-Sas16	For Sas16 protein expression	This study
E. coli BL21 (DE3)::pET28-Sas16-F250T	For Sas16-F250T protein expression	This study
E. coli BL21 (DE3)::pET-Trx_1c-A-NMt-PCP	For Trx-A-NMt-PCP protein expression	This study
S. lividans 1326/1F16 NmetD2104Q	For inactivation of NMt domain of Sas17	This study
S. lividans 1326::1F16 NmetD2104A	For inactivation of NMt domain of Sas17	This study
S. asterosporus DSM 41452 ΔNmet	In-frame deletion of gene encoding MTase in the WT strain	[11]
S. lividans 1326::1F16::pKC1132-sas18	For inactivation of gene sas18 in *S. lividans 1326*::1F16	This study

Table S4. Data collection and refinement statistics for $P450_{Sas}$

Data set	
Space group	P 4_2 2_1 2
Cell constants a, b, c [Å] α, β, γ [°]	112.8, 112.8, 146.2 90, 90, 90
Resolution limits [Å]	146.15 – 2.0 (2.05 – 2.0)
Completeness (%)	100 (100)
Unique reflections	64321
Multiplicity (%)	26.6 (28.1)
R_{merge}*	0.236 (1.802)
$R_{p.i.m.}$	0.047 (0.345)
Mean I/σ(I)	13.1 (2.5)
$CC_{1/2}$	0.998 (0.390)
Refinement statistics	
R_{cryst}†	0.20
R_{free}	0.24
r.m.s.d. bond lengths [Å]	0.0235
r.m.s.d. bond angles [°]	2.30
Average B-factor [$Å^2$]	27
PDB Code	7OQ6

*$R_{merge} = \Sigma_{hkl} [(\Sigma_i |I_i - \langle I \rangle|)/\Sigma_i I_i]$;

†$R_{cryst} = \Sigma_{hkl} ||F_{obs}| - |F_{calc}||/\Sigma_{hkl} |F_{obs}|$;

RMSD: Root Mean Square Deviation is the square root of the mean of the square of the distances between the matched atoms.

Table S5. Structure of WS9326 derivatives determined by HR-MS and MS² fragmentation. For MS² traces see SI Figures S12-S16.

Number	Name	m/z [M+H]⁺ Theoretical Weight (Da)	m/z [M+H]⁺ Observed Weight (Da)	Error △(ppm)	Molecular Formula	Chemical Structure	Producer
1	**WS9326K**	1055.5090	1055.5072	1.7	$C_{54}H_{70}N_8O_{14}$	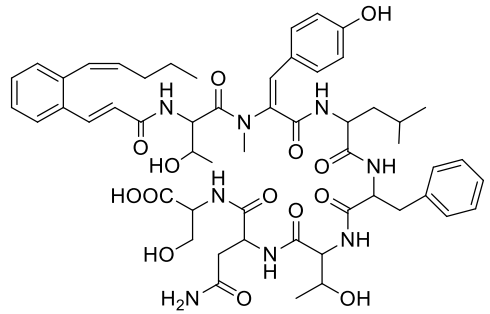 Pentenylcinnamoyl-Thr-NMet-Dht-Leu-Phe-Thr-Asn-Ser-OH	WT and Mutant Δ*sas16*
2	**WS9326L**	1057.5246	1057.5231	1.4	$C_{54}H_{72}N_8O_{14}$	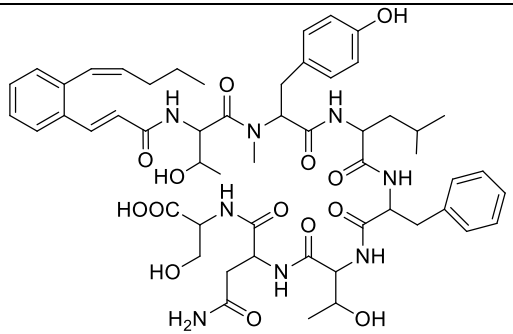 Pentenylcinnamoyl-Thr-NMet-Tyr-Leu-Phe-Thr-Asn-Ser-OH	WT and Mutant Δ*sas16*
3	**WS9326M**	856.4497	856.4489	1.0	$C_{47}H_{61}N_5O_{10}$	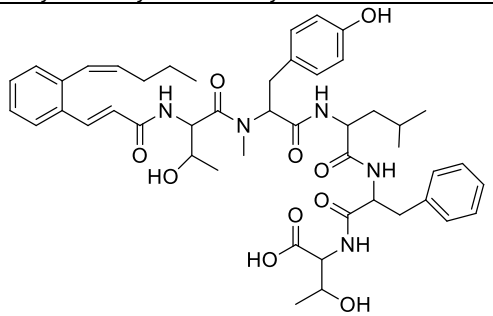 Pentenylcinnamoyl-Thr-NMet-Tyr-Leu-Phe-Thr-Asn-Ser-OH	WT and Mutant Δ*sas16*

4	**WS9326N**	842.4340	842.4332	1.0	$C_{46}H_{59}N_5O_{10}$	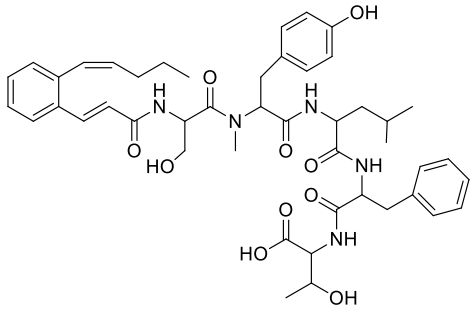 Pentenylcinnamoyl-Ser-NMet-Tyr-Leu-Phe-Thr-OH	WT and Mutant Δ*sas16*
5	**WS9326O**	495.2495	495.2491	0.8	$C_{28}H_{34}N_2O_6$	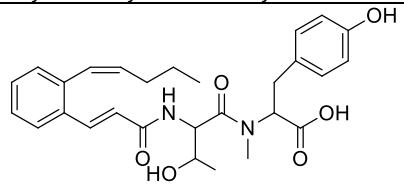 Pentenylcinnamoyl-Thr-NMet-Tyr-OH	Mutant Δ*sas16*
6	**WS9326X**	1038.4828	1038.4821	0.6	$C_{54}H_{67}N_7O_{14}$	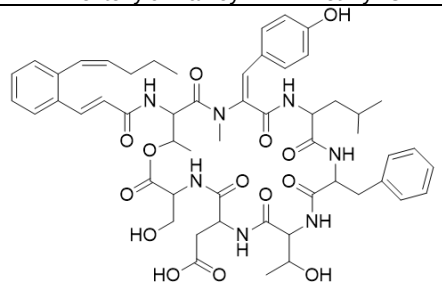 Pentenylcinnamoyl-Thr-NMet-Dht-Leu-Phe-Thr-Asp-Ser-O-	Mutant *S. lividans 1326*::1F16

Table S6. Summary of NMR Data for WS9326M (DMSO-d_6). For NMR spectrum see SI Figures S32-S36.

position		δ_C (ppm)	δ_H (*J* in Hz)	^{1}H-^{1}H COSY	HMBC
Acyl	1	165.8			
	2	122.8	6.79, 1H, d(15.5)	7.56	165.8, 133, 132.8, 136.7(weak)
	3	136.7	7.56, 1H, d(15.5)	6.79	165.8, 132.8, 136.9, 133, 128.7, 125.8, 122.8
	4	132.8			
	5	os			
	6	os			
	7	os			
	8	os			
	9	136.7			
	10	134	5.82, 1H, dt(11.2, 7.8)	6.56, 1.97	136.7, 21.9, 29.9
	11	127	6.56, 1H, d(11.2, 8.7)	5.82, 1.97	29.9
	12	29.9	1.96, 2H, m	1.35	
	13	21.9	1.35, 2H, m	0.79	
	14	13.5	0.79, 3H, m	1.35	
^{1}Thr	NH		8.48, 1H, brs	4.34	
	α	53	4.34, 1H, brs	8.48	165.7, 171.5, 65.8, 19.4
	β	65.8	3.06, 1H, brs		0.68
	γ	19.4	0.68, 3H, os		
	C=O	171.5			
^{2}Tyr	NMe	28.8	2.75, 3H, s		171.5, 60.7
	α	60.7	5.03, 1H, m	2.96, 2.79	168.5, 127.2
	β	33.6	2.96, 1H, m		168.5, 127.2, 130.1
			2.79, 1H, m		168.5, 127.2, 130.1
	1	127.2			
	2,6	130.1	7.03, 2H, m	6.66	156
	3,5	115.4	6.66, 2H, m	7.03	156
	4	156			

	C=O	168.5			
^{3}Leu	NH		9.28, 1H, brs		
	α	58.2	4.14, 1H, os	8.03(NH), 1.18, 1.06	
	β	40.4	1.18, 1.06, 2H, m	4.14, 1.05	58.2, 172.1
	γ	23.7	1.05, H, m	0.56	
	δ	22.5	0.56, 3H	1.05	
		22.6	0.69, 3H, m		
	C=O	172.1			
^{4}Phe	NH		8.28, 1H, brs		
	α	54	4.57,1H, m	8.28	137.6, 170.9, 37.7
	β	37.7	3.06, 1H, m		137.6, 129.4
			2.71,1H, os		
	1	137.6			
	2,6	127.7	7.24, 2H, os	7.17	37.7, 125.8, 129.1
	3,5	125.8	7.17, 2H, os		
	4	129.1			
	C=O	170.9			
^{5}Thr	NH		8.28, 1H		
	α	54.3	4.77, 1H, m	8.28, 3.85	164.5, 170.7
	β	67.1	3.85, 1H, m	1.02	170.7
	γ	19.6	1.02, 3H, os	3.85	
	OH	n/d			
	C=O	170.7			

Note: assignments based on HSQC, COSY, and HMBC experiments. os = overlapping signal, n/d = no data, brs = broad signal.

Table S7. Summary of NMR Data for WS9326N (DMSO-d_6). For NMR spectrum see SI Figures S37-S41.

position		δ_C (ppm)	δ_H (*J* in Hz)	^{1}H-^{1}H COSY	HMBC
Acyl	1	167.5			
	2	120.9	6.45, 1H, d(16.2)	7.70	167.5, 141.4, 132.1, 126.9
	3	141.4	7.70, 1H, d(16.2)	6.45	167.5, 137.4, 132.1, 126.4, 120.9
	4	126.9	n/d		
	5	os			
	6	os			
	7	os			
	8	os			
	9	137.4	n/d		
	10	132.7	6.53, 1H, d(11.5)	5.74,	137.4, 128.9, 29.8
	11	128.9	5.74, 1H, dt(11.5, 7.4)	6.53, 2.06	128.9, 137.4, 29.8, 22.2
	12	29.8	2.06, 2H, m	1.38	
	13	22.2	1.38, 2H, m	0.84	
	14	13.6	0.84, 3H, m	1.38	
^{1}Ser	NH		os		
	α	67.6	4.12, 1H, brs		166.9
	β	48.4	3.16, 1H, brs		
	C=O	166.9			
^{2}Tyr	NMe	28.1	2.78, 3H, s		
	α	60.9	5.03, 1H, m	2.45, 2.78	
	β	34.2	2.78, 1H, m	2.45, 5.03	173.6, 128.6, 135.8, 134.3, 137.4, 138.6
			2.45, 1H, m		
	1	128.6			
	2,6	os			
	3,5	os			
	4	os			
	C=O	173.6			

^{3}Leu	NH				
	α	66.9	3.87, os	1.03	
	β	38.8	1.03, 1.24, 2H, m		
	γ	22.2	1.36, H, m		22.2, 21.8
	δ	22.2, 21.8(os)	0.79(os, 3H),0.77(os, 3H)		
	C=O	172.1			
^{4}Phe	NH				
	α	54.1	4.54,1H, m	3.03, 2.78	
	β	os	3.03, 1H, m		127.5, 132.7
			2.78,1H, os		
	1	os			
	2,6	os			
	3,5	os			
	4	os			
	C=O	n/d			
^{5}Thr	NH		8.12		
	α	54.5	4.79, 1H, m		
	β	66.8	3.88, 1H, m	1.04	
	γ	os	1.04, 3H, os	3.88	
	OH	n/d			
	C=O	n/d			

Note: assignments based on HSQC, COSY, and HMBC experiments. os = overlapping signal, n/d = no data, brs = broad signal.

Table S8. Summary of NMR Data for WS9326X (DMSO-d_6). For NMR spectrum see SI Figures S42-S46.

position		δ_C (ppm)	δ_H (*J* in Hz)	^{1}H-^{1}H COSY	HMBC
Acyl	1	165.3			
	2	122.5	6.69, 1H, d(15.2)		165.3, 133.0
	3	137.4	7.42, 1H, d(15.2)		165.3
	4	133.0	-		
	5	126.0	7.53, 1H, d(7.1)		137.4, 129.6
	6	129.6	7.33, 1H, m		
	7	127.3	7.20, 1H, m		
	8	129.6	7.60, 1H, d(9.5)		
	9	137.0			
	10	126.8	6.50, 1H, d(11.1)	5.82	134.1
	11	134.1	5.82, 1H, m	2.00	
	12	29.8	2.00, 2H, m	1.36	
	13	21.9	1.36, 2H, m	0.79	
	14	13.6	0.79, 3H, t(7.4)	1.36	
^{1}Thr	NH		8.72, 1H, d(9.5)		165.3, 53.2
	α	53.2	5.33, 1H, t(9.0)	5.01	169.0
	β	73.3	5.01,1H, m	1.15	
	γ	16.5	1.15, 3H, d(6.3)		
	C=O	169.0			
^{2}△Tyr	NMe	34.2	2.98, 3H, s		169.0, 128.4
	α	128.4		6.13	
	β	131.4	6.13, 1H, s		165.6, 128.4, 131.7
	1	122.9			
	2, 6	131.7	7.39, 2H, d(8.2)	6.58	
	3, 5	114.7	6.58, 2H, d(8.2)		158.1
	4	158.1			
	C=O	165.6			
^{3}Leu	NH		9.23, 1H, d(2.65)		165.6, 53.8

	α	53.8	4.06, 1H, m	1.26	39.0
	β	39.0	1.26, 2H, m	4.06	
	γ	23.3	0.88, 1H, m		22.1, 22.0
	δ	22.1	0.75, 3H, d(6.8)		
		22.0	0.63, 3H, brs		
	C=O	172.1			
[4]Phe	NH		9.15, 1H, d(8.3)	4.33	55.6, 36.2, 172.1
	α	55.6	4.33, 1H, m	NH(9.15), 3.27	
	β	36.2	3.27, 1H, m	4.33	138.6, 128.9
			2.71, 1H, m	4.33	
	1	138.6			
	2,6	128.9	7.32, 2H, d(7.6)		
	3,5	127.9	7.27, 2H, t(14.9)	6.68	
	4	123.0	6.68, 1H, m		
	C=O	170.1			
[5]Thr	NH		7.53, 1H, d(7.41)	4.38	170.1, 68.1, 170
	α	57.0	4.38, 1H, m	NH(7.53)	
	β	68.1	4.27, 1H, m	0.63	
	γ	22.9	0.63, 3H, brs	4.27	
	C=O	170.0			
[6]Asp	NH		8.48, 1H, d(7.2)		170.0, 35.8
	α	50.6	4.45, 1H, m	2.64	171.0,171.8
	β	35.8	2.64, 1H, m	4.45	
	γC=O	171.8			
	C=O	171.0			
	OH		2.53, 1H, t(16.7)		56.0, 60.7,168.8
[7]Ser	NH		8.50, 1H, d(9.5)	4.33	
	α	56.0	4.33, 1H, m	NH(8.50)	168.8
	β	60.7	3.24, 1H, m(5.2)	4.33	
			3.16, 1H, t(19.3)		

	OH		4.81, 1H, brs		60.7
	C=O	168.8			

Note: assignments based on HSQC, COSY, and HMBC experiments. os = overlapping signal, n/d = no data, brs = broad signal.

Table S9. Structural comparisons of known P450 structures with similarity to $P450_{Sas}$ as revealed by a Dali search.[12]

Rank	PDB ID	Chain	Z-score	RMSD	Residues matched	Residues total	% ID	Role*	Citation
1	5Y1I	B	43.7	2.3	367	394	38	Macrolide FD-891 biosynthesis (GfsF)	[13]
35	2Z36	A	42.0	2.7	372	403	39	MoxA Cyp105	[14]
38	3ABB	A	41.1	2.5	355	383	42	Filipin biosynthesis CYP105D6	[15]
44	5FOI	B	40.4	2.6	359	388	35	Mycinamicin VIII C21 hydroxylase (MycC1)	[16]
51	5X7E	A	40.0	2.8	366	404	38	Vitamin D3 dihydroxylase	[17]
108	2WI9	A	38.5	3.3	360	396	38	Pikromycin biosynthesis (PikC)	[18]
137	1UED	A	38.1	2.8	355	391	32	OxyC from vancomycin biosynthesis	[19]
196	1OXA	A	37.5	3.2	358	403	35	Erythromycin biosynthesis (EryF)	[20]
222	3MGX	B	37.2	2.7	354	391	25	OxyD from balhimycin biosynthesis	[21]
288	4PXH	E	36.7	3.0	357	407	23	$P450_{sky}$-PCP complex	[22]
421	1LFK	A	35.3	3.2	345	375	31	OxyB from vancomycin biosynthesis	[23]

* Blue text indicates a role in hydroxylation of a macrolide or large non-polar molecule; red text indicates oxidation of a peptidyl-PCP substrate; green text indicates β-hydroxylation of an aminoacyl-PCP substrate.

Table S10. Summary of putative peptide intermediate species captured in *S. asterosporus* strains.

S. asterosporus strain	Wild type [a]			Δ*sas16*::pSET152-sas16[b]			Δ*sas16*[b]		
Probe utilised/ intermediates offloaded from:	**1** (Tyr)	**2** (Gly)	**3** (β-Ala)	**1** (Tyr)	**2** (Gly)	**3** (β-Ala)	**1** (Tyr)	**2** (Gly)	**3** (β-Ala)
M1	*m/z* 649*** (**4**) and 647** (**5**)	*m/z* 529** (**6**)	*m/z* 543*** (**7**)	*m/z* 649** (**4**) and 647* (**5**)	n.d.	*m/z* 543** (**7**)	*m/z* 649** (**4**)	n.d.	*m/z* 543** (**7**)
M2		*m/z* 704** (**8**)	*m/z* 720** (**18**) and 718**(**9**)		*m/z* 704*(**8**)	*m/z* 720** (**18**) and 718** (**9**)		n.d.	n.d.
M3	*m/z* 923* (**10**)	*m/z* 817* (**11**)	*m/z* 831* (**12**)	n.d.	n.d.	*m/z* 831*(**12**)	n.d.	n.d.	n.d.
M4	*m/z* 1072* (**19**) and 1070* (**13**)			*m/z* 1072*(**19**) and 1070*(**13**)			*m/z* 1072*(**19**)		
M5	*m/z* 1171* (**14**)	*m/z* 1065* (**15**)	*m/z* 1081* (**20**) and 1079*(**16**)	n.d.	n.d.	*m/z* 1081*(**20**)	n.d.	n.d.	*m/z* 1081*(**20**)

[a] grown in liquid culture and on plates, 2mM probe concentration; [b] grown on plates, 2mM probe concentration; *** high abundance, clearly detectable species; ** detectable species; * species present in traces; n.d. = not detectable; *m/z* putative intermediate $[M+H]^+$ masses given, with those in red featuring dehydrotyrosine (Dht). For proposed species structures and HR-MS^n analysis see **SI Figures S27-30**.

2. SI Figures

Figure S1. UV/Vis spectra of P450$_{Sas}$ and binding responses for possible soluble substrates. (A) P450$_{Sas}$ UV/Vis spectrum showing the resting state heme Soret absorption (blue) and the reduced, CO-complexed form (red). (B) Possible soluble substrates for P450$_{Sas}$, including intermediates at the amino acid, peptide, and cyclic peptide state. (C) Final spectra after titration of the potential soluble substrates.

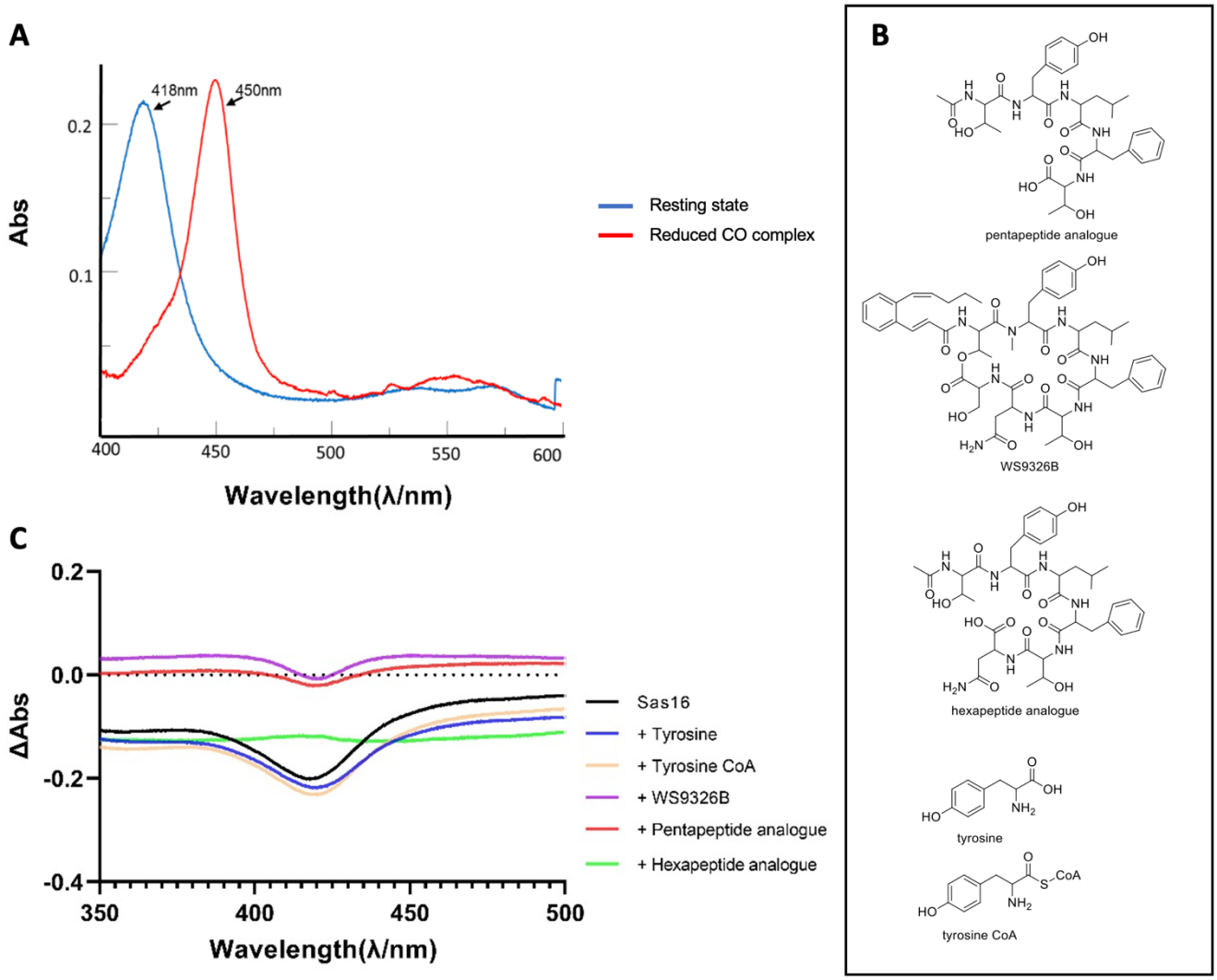

Figure S2. Conserved sequence regions of 20 P450 enzymes implicated in the β-hydroxylation of PCP-bound amino acid residues and a comparison to P450$_{Sas}$. Sequence residues indicated (based on numbering of OxyD$_{bal}$) are responsible for maintaining the arrangement of secondary structure elements and active site of these P450s to allow them to bind and hydroxylate their PCP-bound amino acid substrates; comparison to Sas16 shows a very high level of mismatches with this consensus sequence (17) as opposed to P450s involved in the β-hydroxylation of aminoacyl-PCPs (0-6, average <1 per sequence). This does not support the presence of the conserved active site geometry of β-hydroxylating P450s and implies the substrate of Sas16 is not an aminoacyl-PCP.

P450	**B-B$_2$ loop N-term.**		**B-B$_2$ loop C-term.**						**F-helix**				**G-helix**					**I-helix**			**β-1 sheet**			**Mis-matches**
	69	72	82	83	84	86	89	90	171	172	173	174	187	188	189	190	193	228	229	235	282	283	284	
OxyD $_{bal}$	G	I	S	G	G	M	V	S	H	A	F	G	A	H	T	E	V	N	C	G	A	M	H	0
OxyD $_{van}$	G	I	S	G	G	M	V	S	H	A	F	G	A	H	T	E	V	N	C	G	A	M	H	0
OxyD $_{cep}$	G	I	S	G	G	M	V	S	H	A	F	G	A	H	T	E	V	N	C	G	A	M	H	0
OxyD $_{pek}$	G	I	S	G	G	M	V	S	H	A	F	G	A	H	T	E	V	N	C	G	A	M	H	0
OxyD $_{veg}$	G	I	S	G	G	M	V	S	H	A	F	G	A	H	T	E	V	N	C	G	A	M	H	0
NikQ	G	L	A	A	G	M	*I*	T	*F*	A	W	S	A	H	T	E	L	N	C	G	V	M	H	2
SanQ	G	L	A	A	G	M	*I*	T	*F*	A	W	S	A	H	T	E	L	N	C	G	V	M	H	2
PyrI	G	L	A	G	*G*	M	*I*	T	T	A	L	*D*	A	*Q*	S	*D*	*N*	N	C	G	A	L	H	5
RubC2	G	L	A	S	G	M	V	T	H	A	W	S	A	K	S	E	L	N	C	G	S	L	H	0
NovI	G	L	A	S	G	M	V	T	H	A	W	S	A	K	N	E	L	N	C	G	S	L	H	0
CouI	G	L	A	S	G	M	V	T	H	A	W	S	A	K	N	E	L	N	C	G	S	L	H	0
CloI	G	L	A	S	G	M	V	T	H	A	W	S	A	K	N	E	L	N	C	G	S	L	H	0
SimI	G	L	A	S	*R*	M	*L*	T	H	A	L	S	A	K	N	E	L	N	C	G	S	L	H	2
CinD	G	L	G	G	G	M	V	T	A	A	L	S	A	R	N	E	L	N	C	G	S	M	H	0
SalD	G	L	G	A	G	M	V	T	T	A	L	S	A	R	N	E	L	N	C	G	S	M	H	0
Sky32	G	L	A	A	G	M	V	T	S	A	L	S	A	R	N	E	L	N	C	G	A	M	H	0
TioI	G	L	A	G	G	M	V	T	N	A	L	S	A	R	N	*Q*	L	N	C	G	A	M	H	1
Ecm12	G	L	A	G	G	M	V	T	L	A	L	S	A	R	N	E	G	N	C	G	A	M	H	0
TrsB	G	L	A	G	G	M	V	S	E	A	L	S	A	R	N	E	L	N	C	G	*G*	M	H	1
ZmbVIIc	G	L	A	G	G	M	V	T	*A*	A	*V*	A	A	H	*H*	E	*S*	*H*	C	G	A	*A*	H	6
Matches %[a]	100	100	100	100	95	100	100	100	50	100	95	95	100	95	95	90	80	95	100	100	950	95	100	0-6
Suggested Consensus[b]	**G**	V I L	(1)	(1)	**G**	**M**	V I L	S T	H	**A**	W F L	(1)	**A**	(2)	(3)	**E**	L V	**N**	**C**	**G**	(1)	L M	**H**	
Sas16	*T*	I	*D*	A	*K*	*L*	T	*M*	*I*	*M*	*V*	G	**A**	*N*	*E*	**E**	*K*	*M*	*T*	*A*	*V*	*E*	*I*	**17**

[a] Percentage of residues matching to the consensus rule, based upon identity.

[b] Identity residues are emboldened and underlined; 1-3 similar residues indicated in normal font. Exceptions are: (1) Small residue (S, G, A), (2) Positively Charged Residue (K, H, R), (3) Hydrophilic Residue (N, T, S).

Figure S3. Sequence alignment of the aminoacyl-PCP β-hydroxylating P450 $OxyD_{bal}$ with $P450_{Sas}$. Highlighted sequence residues as indicated in SI Figure S2 that are responsible for maintaining the arrangement of secondary structure elements and active site of $OxyD_{bal}$ (as found in the structure of this P450, PDB code: 3MGX); colours are the same as in Figure 2A.

```
OxyD      -------MQTTNAVDLGNPDLYTTLERHARWRELAAEDAMVWSDPGSSPSGFWSVFSHRA     53
Sas16     MTDAETKMAKCPVAPHGWPNPLL-----PEYDQLPEGRPL-TQVTMPSGSKAWLVAQHDH     54
                 * .  ..  * *:         .: :*     :  .    * *  * * .*

OxyD      CAAVLAPSAPL-TSEYGMMIGFDR-----DHPDNSGGRMMVVSEHEQHRKLRKLVGPLLS     107
Sas16     IQRLLADNRFSVEPHPTFPIRFPAPQELLDMIARDAKNLLVTMDPPRHTRVRQMALPDFT     114
             :** .      .  : * *       *   ... .::*. :  :* ::*::. * ::

OxyD      RAAARKLAERVRIEVGDVLGRVL-----DGEVCDAATAIGPRIPAAVVCEILGVPAEDED     162
Sas16     IKAAEKLRP----RMQDLIDYYLDKMEAEGAPADLVQALALPFPAQVICELAGIPENDRE     170
            **.**      .: *::.  *     :*  .* . *:.  :** *:**: *:* :*.:

OxyD      MLIDLTNHAFGGEDELFDGMTPRQAHTEILVYFDELITARRKEPGDDLVSTLVTDDD---     219
Sas16     IFTRNAAIMVG-TRHSYTMEQKLAANEELMKYFAALVTEKQSNPTDDMLGNFIARAGKTD     229
          ::   :   .*   . :       *: *:: **  *:* ::.:* **::..:::  .

OxyD      -LTIDDVLLNCDNVLIGGNETTRHAITGAVHALATVPGLLTALRDGSA-DVDTVVEEVLR     277
Sas16     EFDHHGLTLMTKMLLLAGYEFIVNRIALGIQALVENPEQLAALRADLPGLMPKTVDEVLR     289
           :  ..: *  . :*:.* *   : *: .::**.  *  *:*** .    : ..*:****

OxyD      WTSPA-MHVLRVTTADVTINGRDLPSGTPVVAWLPAANRDPAEFDDPDTFLPGRKPNRHI     336
Sas16     YYSLVDEIIARVALEDVEIDGVTIKAGEGILVLKGLGDRDPSKYPNPDVFDIHRDSRDHL     349
          : * .   : **:  ** *:*  : :*  ::.    .:***::: :**.*   *. . *:

OxyD      TFGHGMHHCLGSALARIELSVVLRVLAERVSRVDLEREPAWLRAIVVQGY---RELPVRF     393
Sas16     AFGYGVHQCLGQHVARLMLEMCLTSLVERFPGLHLVEGDEPIEL--IDGLPPVHKLTIGW     407
          :**:*:*:***. :**: *.: *  *.**.  :.* .    :.   ::*    ::* : :

OxyD      TGR 396
Sas16     --- 407
```

Figure S4. Structural comparisons of $P450_{Sas}$ with P450 homologues involved in the modification of peptidyl carrier protein-bound substrates. Structures include OxyB (A, pale pink; PDB code: 1LFK, chain A) and OxyC (B, pale blue; PDB code: 1UED, chain A) from the GPA cyclisation pathway of vancomycin (upper), together with OxyD (C, pale orange; PDB code: 3MGX, chain A) and $P450_{sky}$ (D, pale yellow PDB code: 4L0E, chain A) shown to be responsible for the β-hydroxylation of aminoacyl-PCP substrates in balhimycin and skyllamycin respectively(lower). $P450_{Sas}$ (chain A) is coloured using the scheme found in Figure 2.

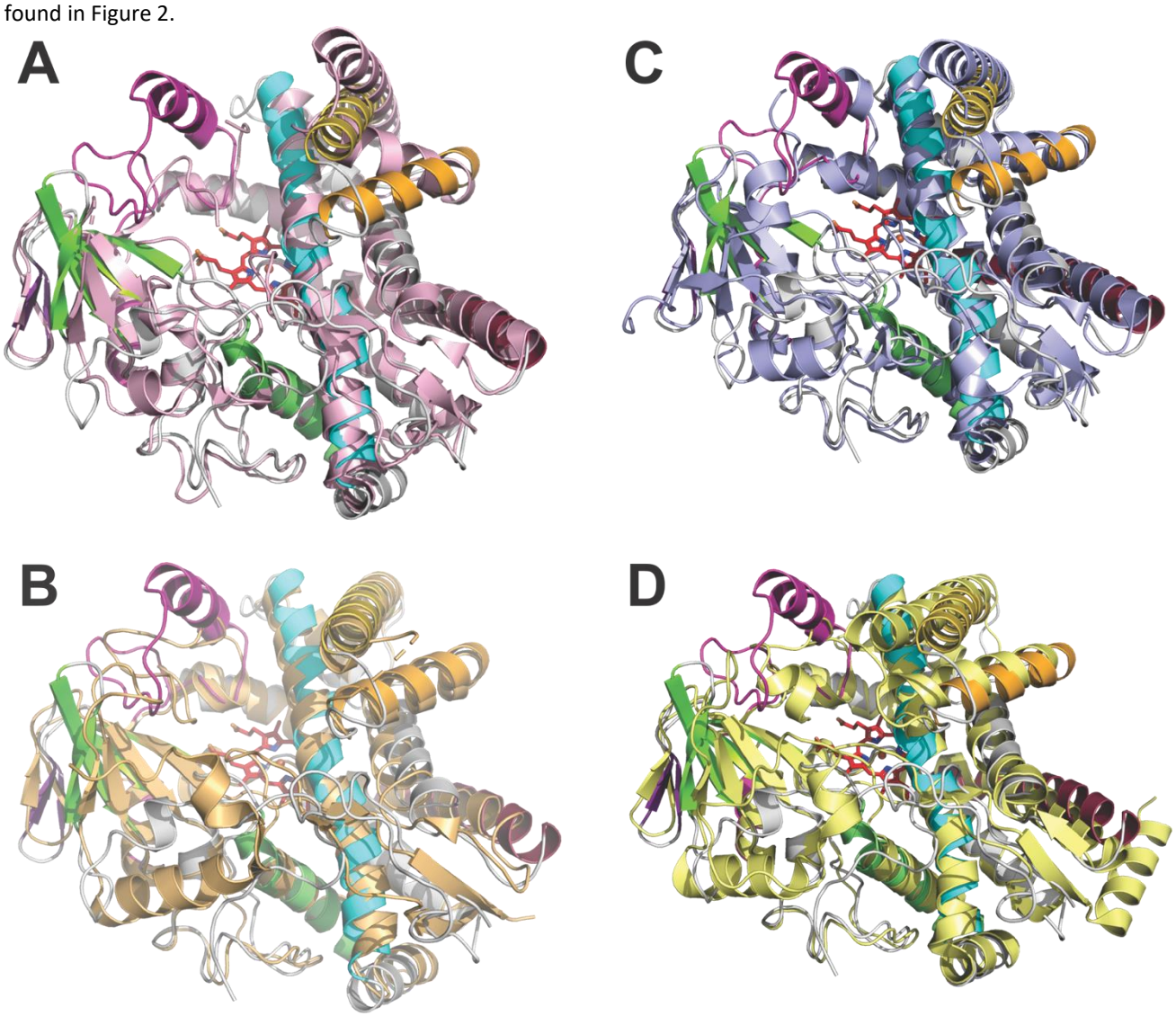

Figure S5. Modelling and molecular dynamics simulations to probe conformations of $P450_{Sas}$ N-terminal and C-terminal loops. (A) Comparison of the C-terminal loops of chain A of the crystal structure of $P450_{Sas}$ (blue), the final frame of a 1 µs MD simulation initiated from chain A of $P450_{Sas}$ (orange), a physics-based model of $P450_{Sas}$ generated using the AlphaFold v2.0[24] Google Colab notebook (magenta), and the crystal structure of $P450_{sky}$ (4PWV, green). Significant crystal packing interactions are observed between the C-terminal loop and the neighbouring chain in the asymmetric unit (grey surface) in the $P450_{Sas}$ crystal structure. The alpha-carbons of Leu397 ($Leu397_{C\alpha}$) are shown as spheres, heme is shown as yellow sticks, and the C11 disulfide bond is shown as ball-and-sticks. (B) Plots showing the distance between $Leu397_{C\alpha}$ and the heme iron during two independent molecular dynamics simulations initiated from chain A of the $P450_{Sas}$ crystal structure. (C) Alternate view highlighting the distinct conformations of the N-terminal region in the crystal structure of $P450_{Sas}$, final frame of the 1 µs MD simulation (replicate 1), AlphaFold2 model, and $P450_{sky}$ (PDB 4PWV). While the C-terminal loop's apex lies *between* the heme and the N-terminal region in $P450_{sky}$ and the AlphaFold2 model of $P450_{Sas}$, it does not protrude as far into the active site in the crystal structure of $P450_{Sas}$, possibly due to being blocked by the conformation of the N-terminal region that is induced by the presence of the C11 disulfide bond.

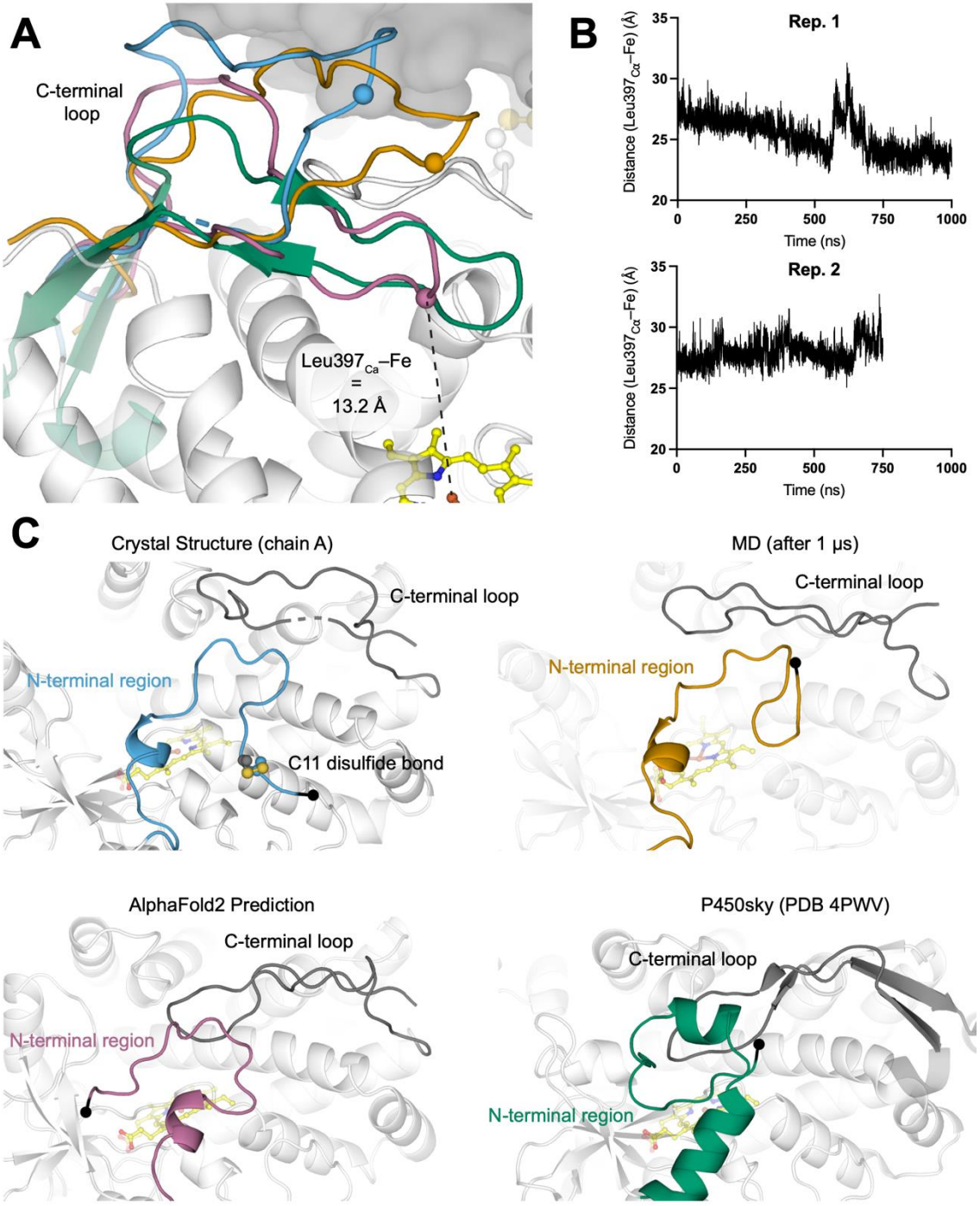

Figure S6. P450$_{Sas}$ active site mutants constructed for *in vivo* analysis. (A) Partial alignment of P450$_{Sas}$ sequence with OxyB$_{bal}$ including the I-helix that contains the active site residues critical for oxygen activation in the majority of P450 enzymes (typically an acid/ alcohol pair, highlighted in green), showing the three positions explored through mutation of the Sas16 gene in vivo (A246, Y248, F250, shown in yellow); mutations converted the equivalent positions into the residues found in OxyB$_{bal}$ and included all single mutants (A246G, Y248N, F250T), the three possible double mutants (AY to GN, YF to NT, AF to GT) and the triple mutant (AFY to GNT). (B) Analysis of strains containing the comparable mutations in the sas16 gene. HPLC-MS chromatograms monitoring for the mass of WS9326A ([M-H]$^-$ 1035, negative mode) were obtained from the culture of *S. asterosporus* Δsas16::pSET152-sas16-F250T (black, (1)), *S. asterosporus* Δsas16::pSET152-sas16-A246G (red, (2)), *S. asterosporus* Δsas16::pSET152-sas16-Y248N (green, (3)), *S. asterosporus* Δsas16::pSET152-sas16-AY246-248GN (blue, (4)), *S. asterosporus* Δsas16::pSET152-sas16-YF248-250NT (purple, (5)), *S. asterosporus* Δsas16::pSET152-sas16-AF246-250GT (maroon, (6)), *S. asterosporus* Δsas16::pSET152-sas16-AYF-246-248-250GNT (pale green (7)), *S. asterosporus* Δsas16 (pale blue, (8)), *S. asterosporus* Δsas16::pSET152-sas16 (orange, (9)) and the wildtype strain (magenta, (10)).

A.

```
OxyD      -LTIDDVLLNCDNVLIGGNETTRHAITGAVHALATVPGLLTALRDGSA-DVDTVVEEVLR   277
Sas16     EFDHHGLTLMTKMLLLAGYEFIVNRIALGIQALVENPEQLAALRADLPGLMPKTVDEVLR   289
           :  ..: *  . :*:.* *   : *: .::**.  *  *:*** .    : ..*:****
```

B.

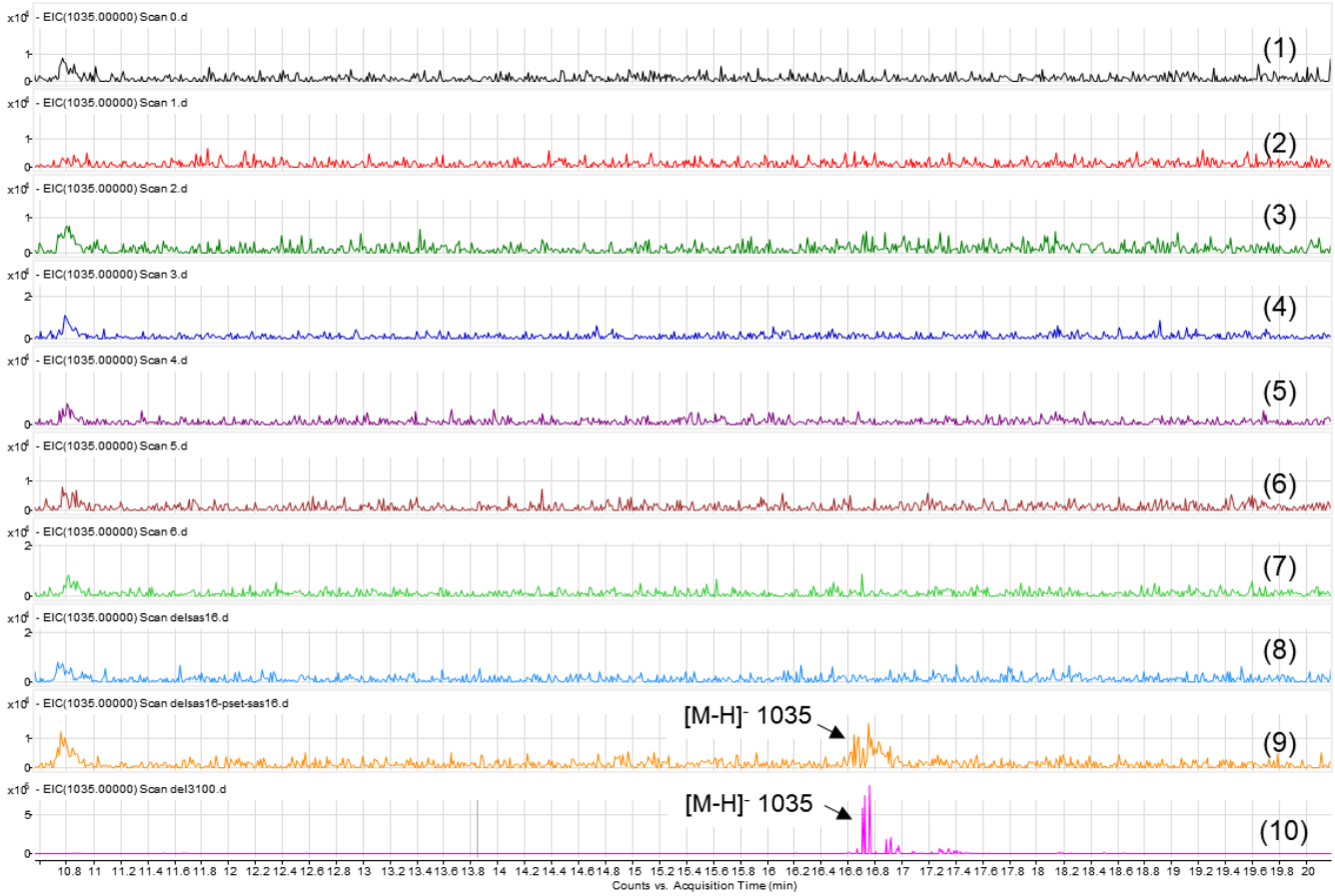

Figure S7. Comparison of reduced CO difference spectra of $P450_{Sas}$ together with protein expression (wild type and F250T mutant). (A) $P450_{Sas}$ UV/Vis spectrum showing the resting state heme soret (wild type – red; F250T mutant – green) and difference spectra of the reduced, CO-complexed form (wild type – black; F250T mutant - blue) showing that both enzymes are apparently correctly folded. (B) SDS-PAGE gel of purified $P450_{Sas}$ proteins showing identical behaviour.

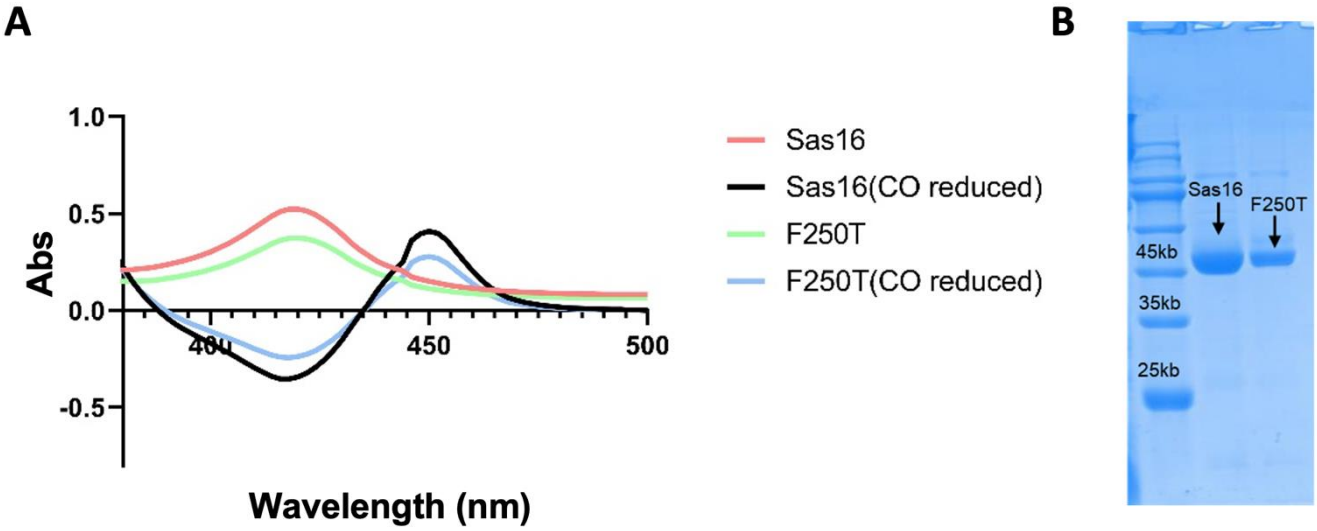

Figure S8. Analysis of the *in vitro* activity of the Sas17 module 2 Trx-A-NMt-PCP construct. (A) Loading of Tyr by the A-domain following by cleavage with methylamine, confirming PCP-loading by detection of the methylamide by LCMS. (B) Activity of the NMt domain confirmed by loading Tyr-CoA using Sfp followed by incubation with SAM, methylamine cleavage and subsequent LC MS analysis.

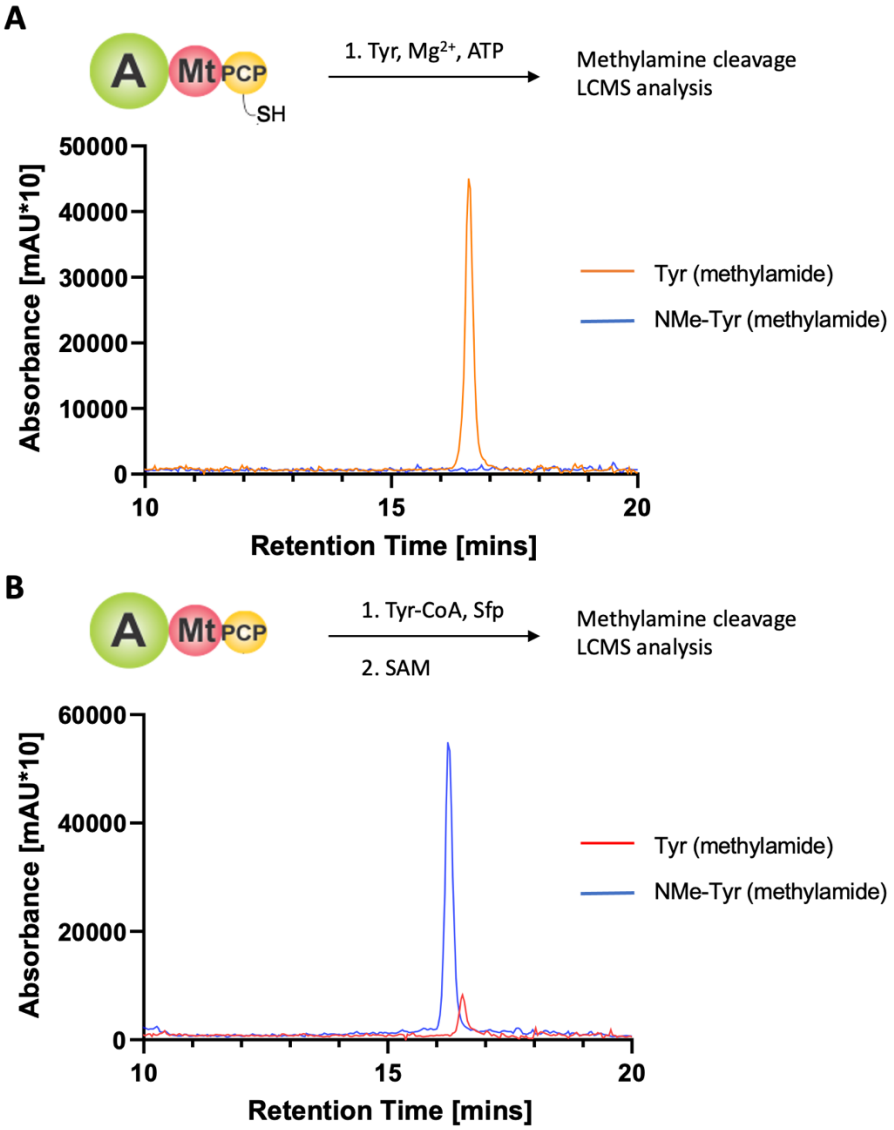

Figure S9. Generating the point-mutations (D2014Q, D2014A) of the NMt domain in Sas17. (A) Scheme of the workflow to generate in vivo point mutations of the BAC plasmid pBAC1F16 using ccdB counterselection recombineering. Step 1: plasmid pBAC1F16 was transformed into strain DH10 β/pSC101-ccdA to yield DH10 β/pSC101-ccdA/1F16, then the cassette amp-ccdB was integrated into plasmid pBAC1F16 through homologous recombination to yield DH10 β/pSC101-ccdA/1F16-Nmet-amp-ccdB. For mutant verification, a 1.8 kb PCR fragment was amplified using primers: Vnmet-ccdB-F and amp-ccdB-R, see the resulting fragment in (B); Step 2: the ssDNA oligonucleotides containing target mutation, through Red-ET homologous recombination, the D2104 site was replaced into Q, yielding the mutant DH10 β/pSC101-ccdA/1F16-NmetD2104Q-amp-ccdB, which was verified by colony PCR using Vnmet-ccdB-F and VNmetQ2104-R (C); the mutation was further verified by sequencing (E). Using the same strategy, the D2014A mutant (DH10 β/pSC101-ccdA/1F16-NmetD2104A-amp-ccdB) was constructed, with the corresponding colony PCR and sequencing result was shown in panels (D) and (F).

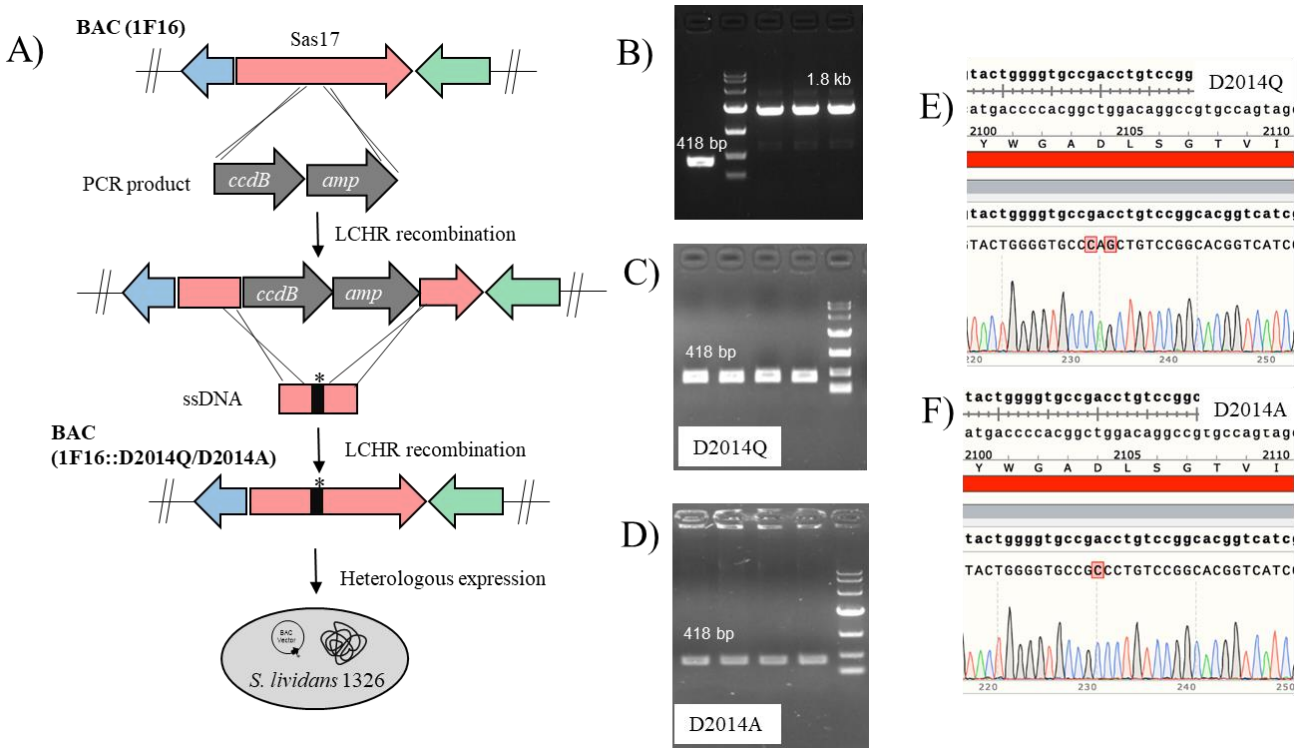

Figure S10. HRMS analysis of the secondary metabolites from *S. lividans* 1F16 together with those bearing mutations in the Sas17 NMt domain (*S. lividans* 1F16 NmetD2104Q, *S. lividans* 1F16 NmetD2104A); the cell cultures of the mutants were also supplemented with N-methyltyrosine and N-methyltyrosine SNAC. WS9326 production was abolished for both NMt mutants, with recovery of WS9326A production generated by supplementation of these mutant strains with NMe-Tyr SNAc. Upper trace – wild type production of WS9326A; traces #2-3 – D2014Q and D2014A mutants showing a loss of WS9326A production; traces #4-5 mutants supplemented with N-methyltyrosine SNAc showing production of WS9326A; traces #4-5 mutants supplemented with N-methyltyrosine showing no recovery of WS9326A production.

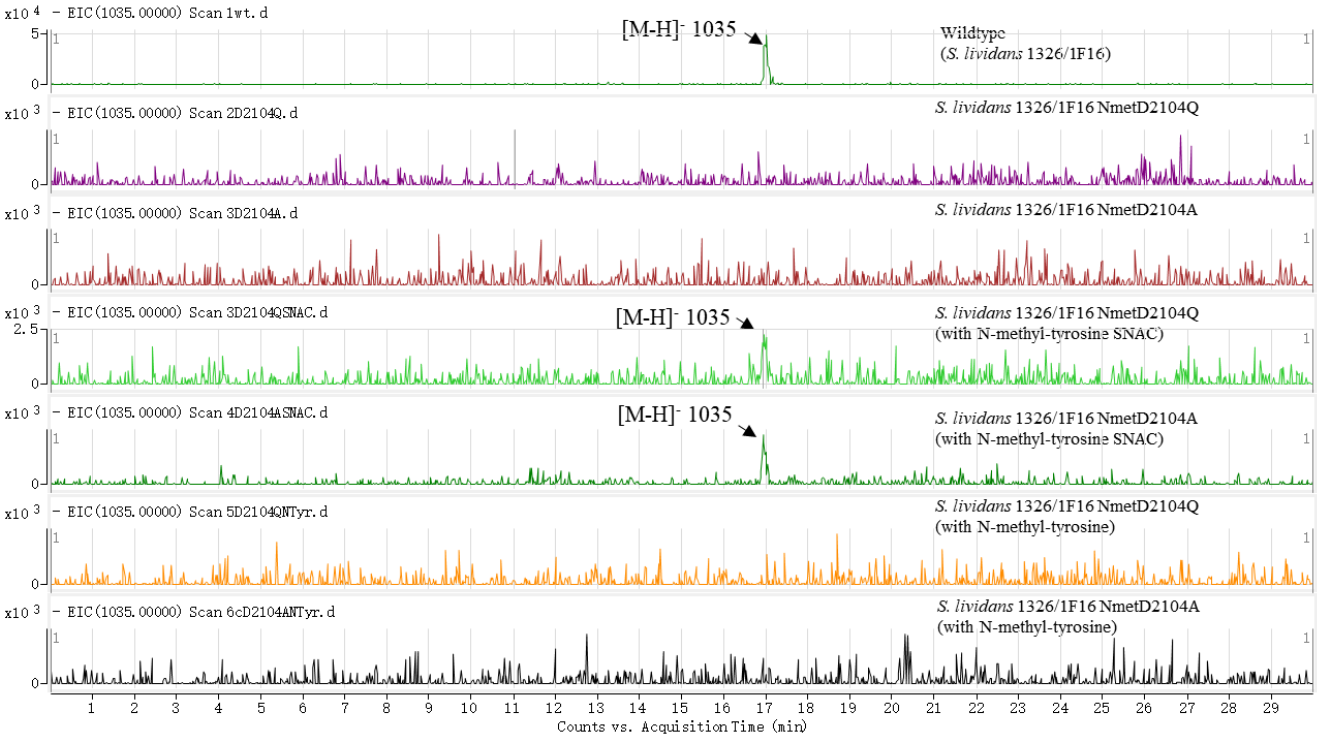

Figure S11. *In vitro* P450$_{Sas}$ binding and turnover assays using dipeptidyl substrates. (A) LCMS trace of the products of turnover of the cinnamoyl-Val-NMe-Tyr-loaded Sas17 module A-NMt-PCP protein following incubation with P450$_{Sas}$ and after methylamine cleavage; only starting material was detected (red), with no evidence of elimination (green) or hydroxylation (purple) of the Tyr residue. (B) CMS trace of the products of turnover of the cinnamoyl-Thr-NMe-Tyr-loaded Sas17 module A-NMt-PCP protein following incubation with P450$_{Sas}$ and after methylamine cleavage; only starting material was detected, with no evidence of elimination or hydroxylation of the Tyr residue. (C) Effect of cinnamoyl-Val-NMe-Tyr-loaded Sas17 module A-NMt-PCP protein on the UV/Vis absorption spectrum of P450$_{Sas}$, showing only a decrease of the soret band and no activation (Type I) shift. (D) Effect of cinnamoyl-Thr-NMe-Tyr-loaded Sas17 module A-NMt-PCP protein on the UV/Vis absorption spectrum of P450$_{Sas}$, showing only a decrease of the soret band and no activation (Type I) shift. Results using both Bz-Thr-NMe-Tyr and cinnamoyl-Thr-Tyr loaded Sas17 module A-NMt-PCP protein were the same as for the two substrates in this figure.

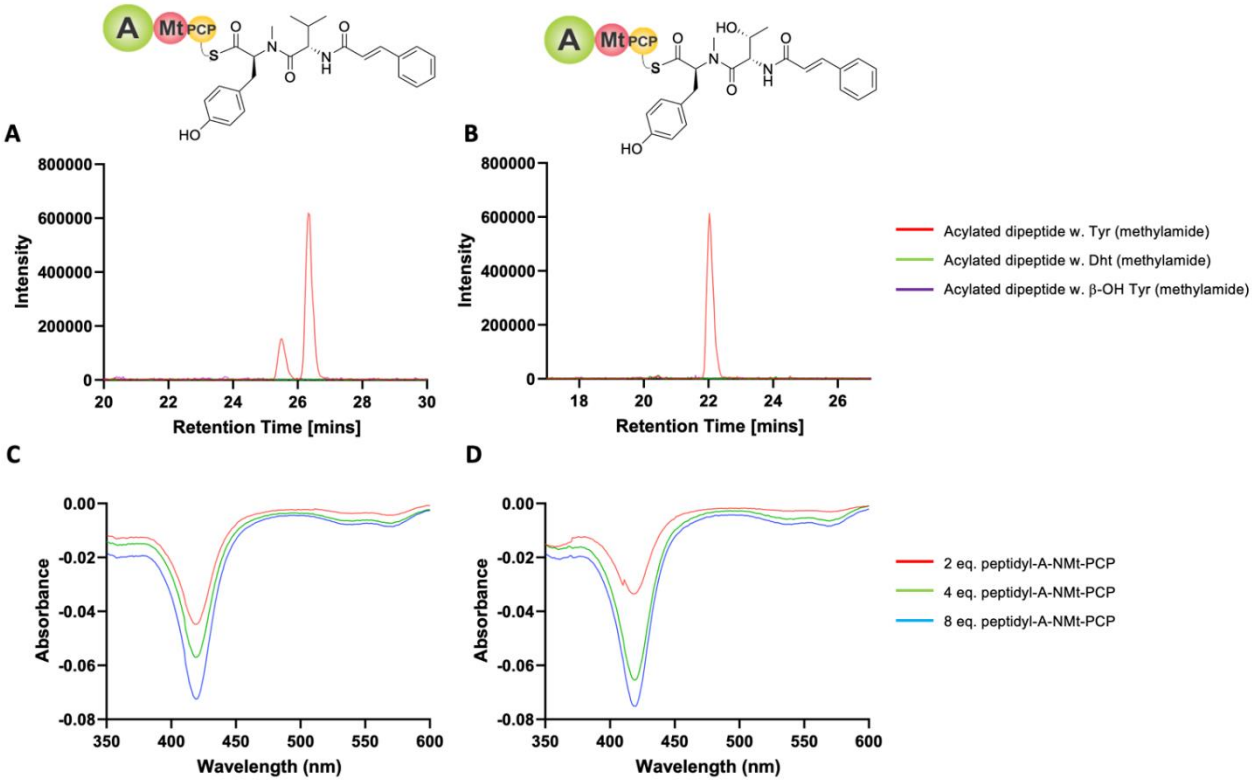

Figure S12. MS² fragmentation analysis of WS9326K.

del3100 WT SG 4d-positive #4823 RT: 15.87 AV: 1 NL: 1.19E6
F: FTMS + c ESI d Full ms2 1055.5072@hcd40.00 [73.0000-1095.0000]

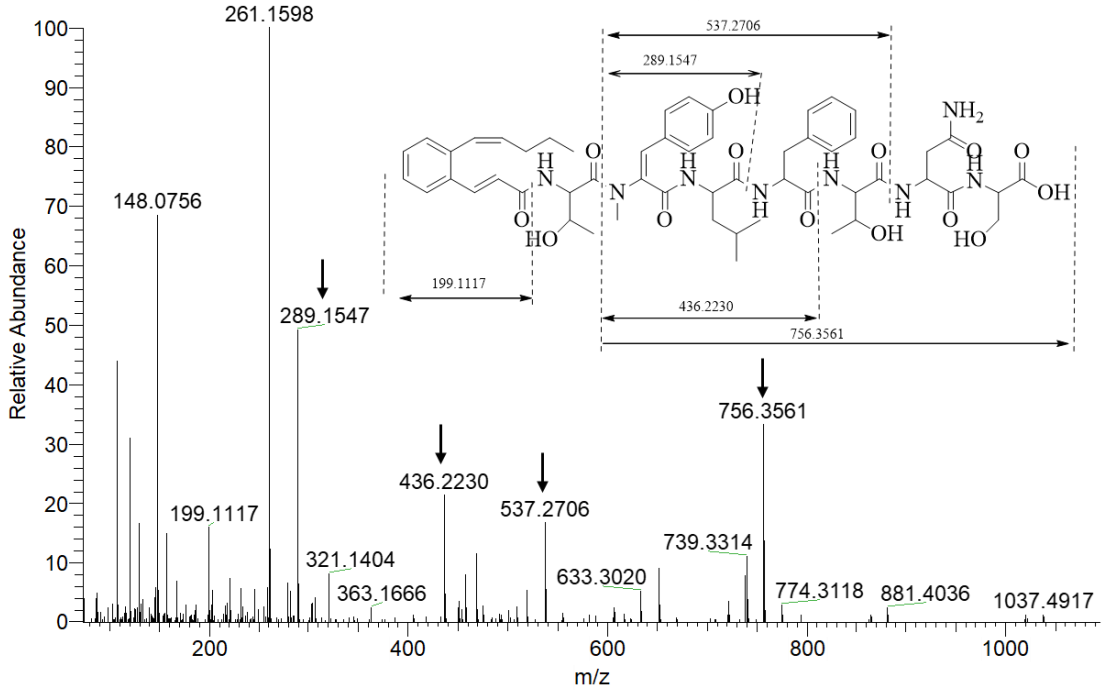

Figure S13. MS² fragmentation analysis of WS9326L.

del3100 sas16[M-H]-1055化合物 #3799 RT: 16.76 AV: 1 NL: 1.13E6
F: FTMS + c ESI d Full ms2 1057.5231@hcd40.00 [73.3333-1100.0000]

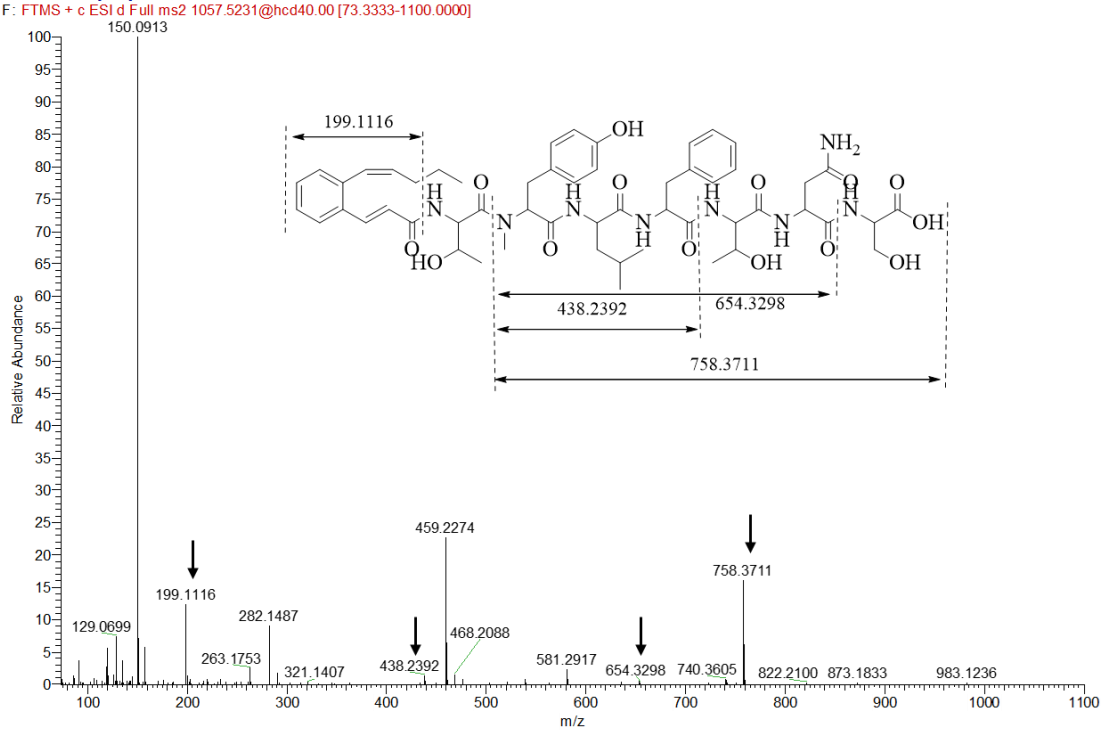

Figure S14. MS² fragmentation analysis of WS9326N.

del3100 WT SG 4d-positive #5564 RT: 17.63 AV: 1 NL: 1.35E6
F: FTMS + c ESI d Full ms2 842.4332@hcd40.00 [58.6667-880.0000]

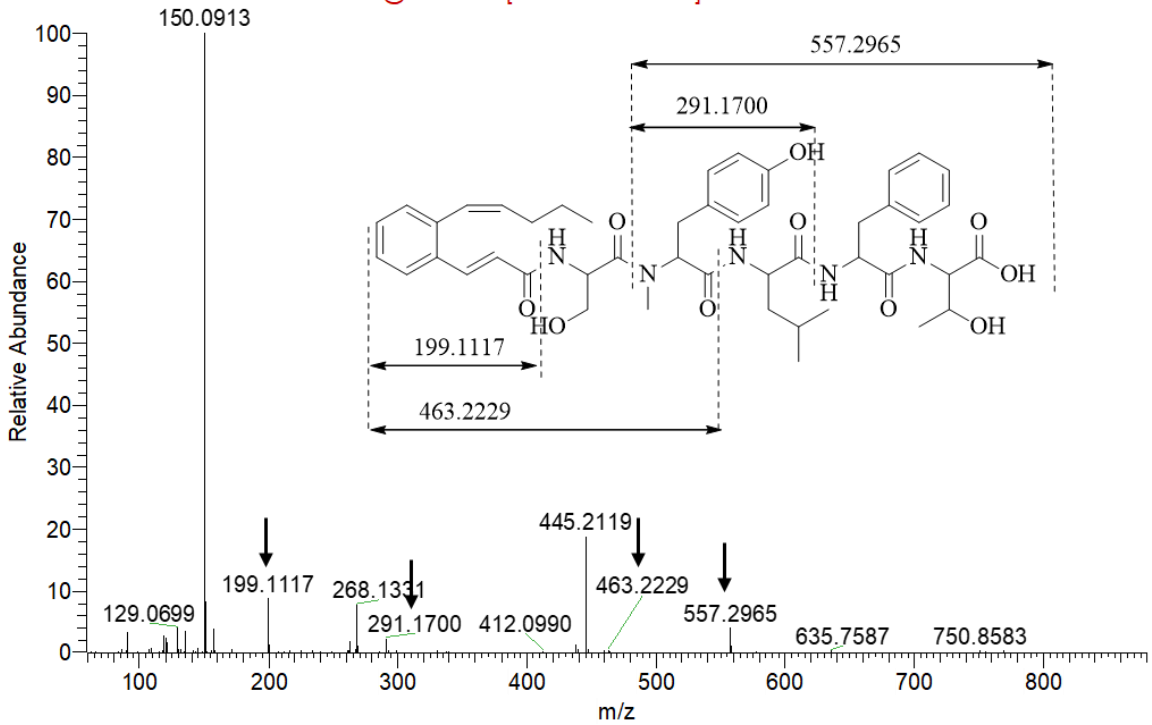

Figure S15. MS² fragmentation analysis of WS9326M.

del3100 WT SG 4d-positive #5727 RT: 18.02 AV: 1 NL: 1.88E6
F: FTMS + c ESI d Full ms2 856.4489@hcd40.00 [59.6667-895.0000]

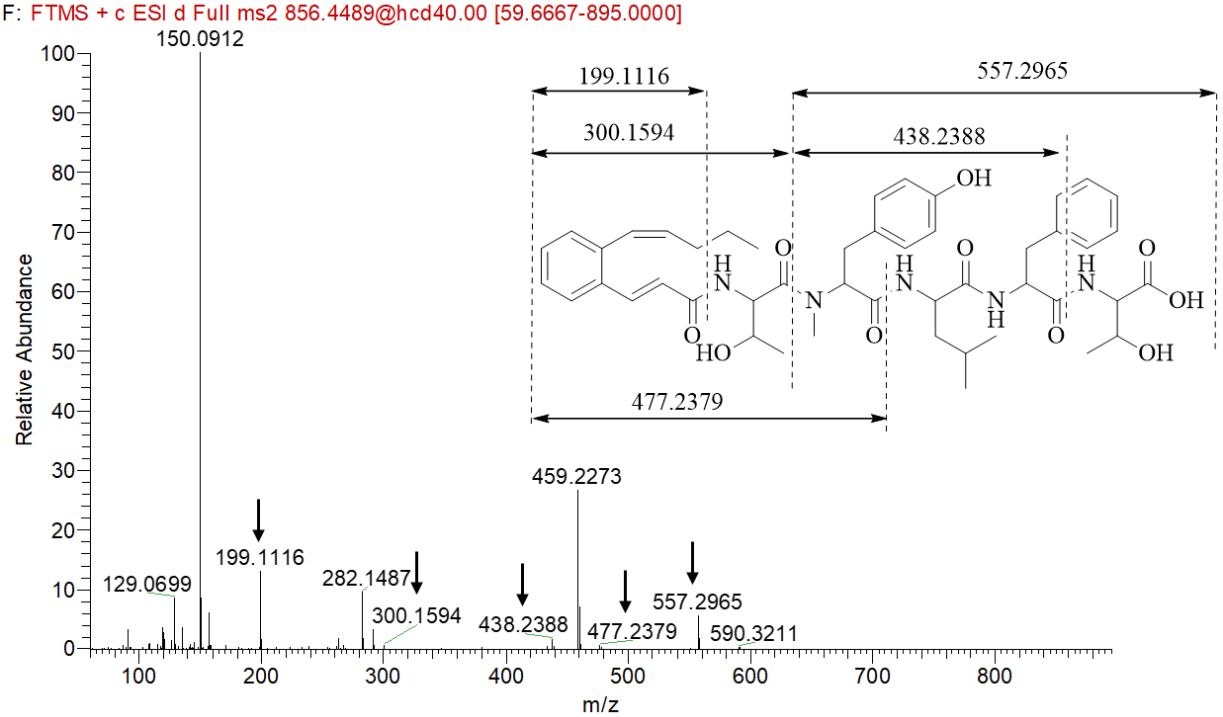

Figure S16. MS^2 fragmentation analysis of WS9326O.

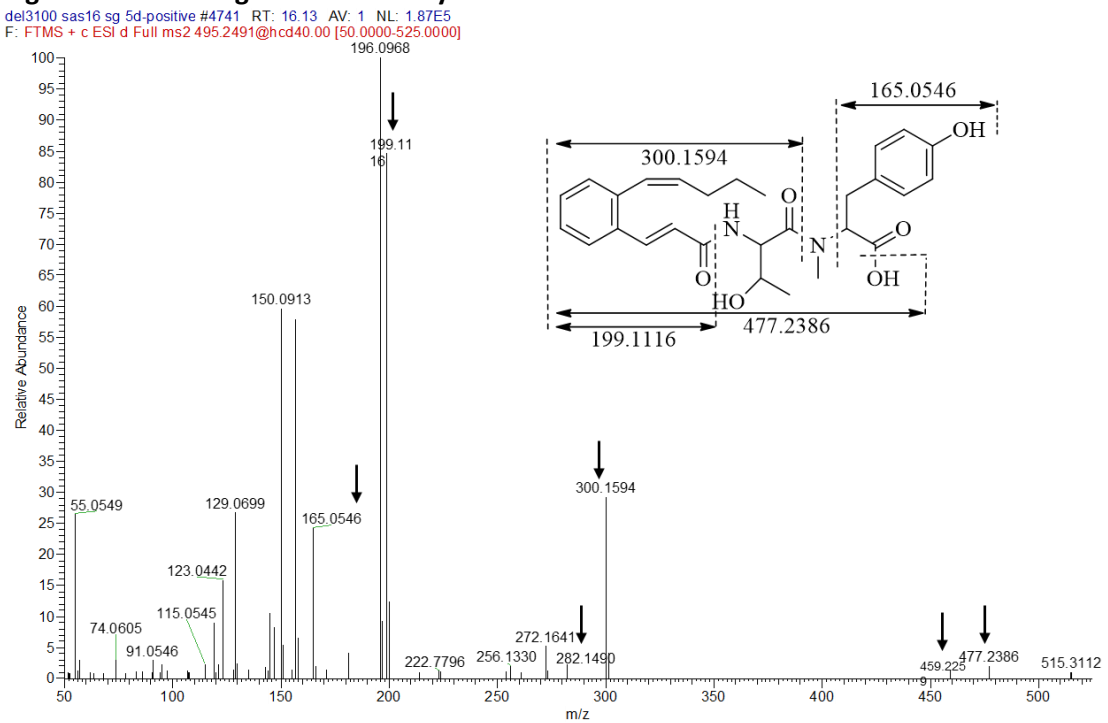

Figure S17. LCMS analysis of Tyr-CoA.

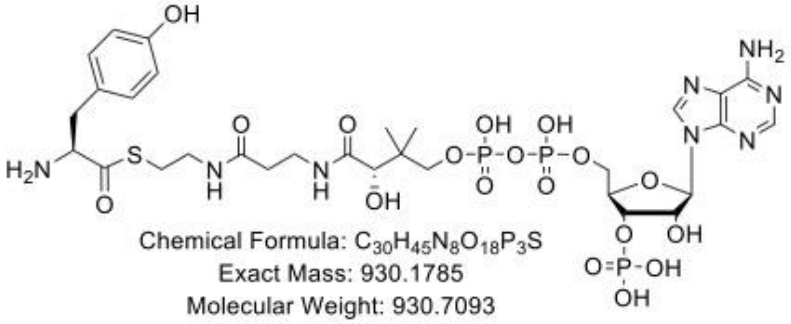

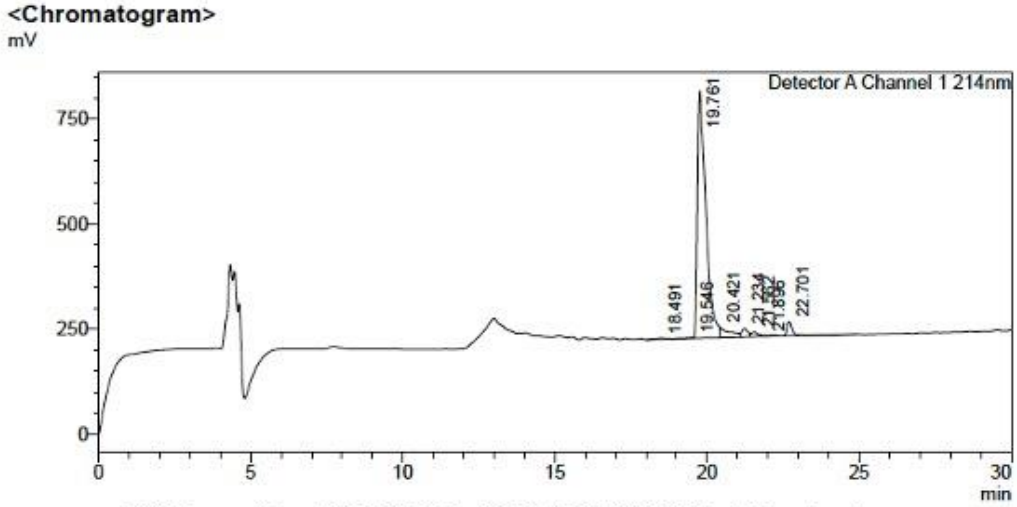

LCMS gradient 10-40% in ACN (0.1% TFA) in 30 minutes
RT = 19.76min

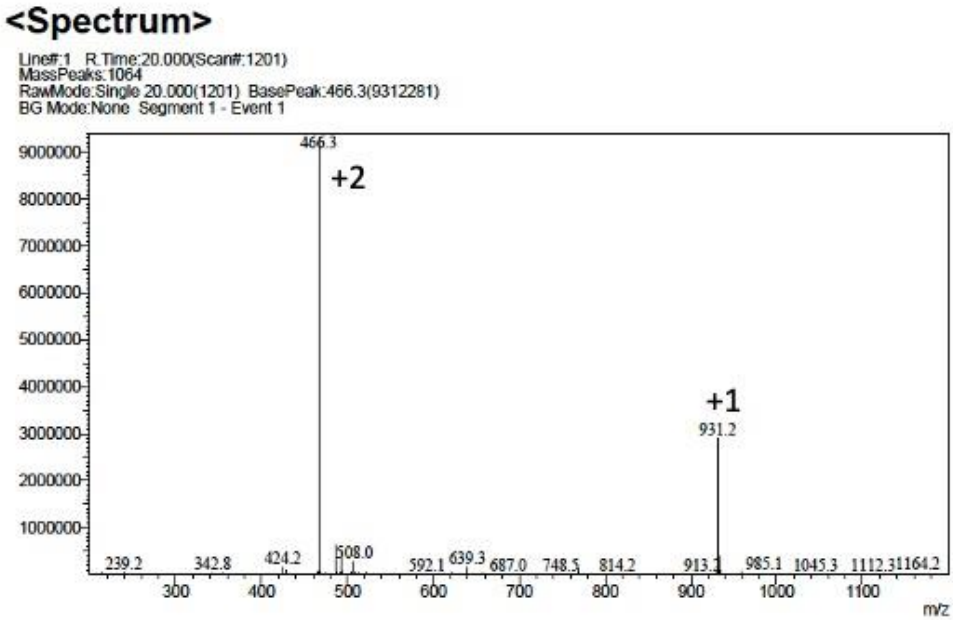

$[M + H^+]^+ = 931.2Da$; $MW_{exp} = 930.2Da$; $MW_{Expected} = 930.2Da$

Figure S18. LCMS analysis of NMe-Tyr-CoA.

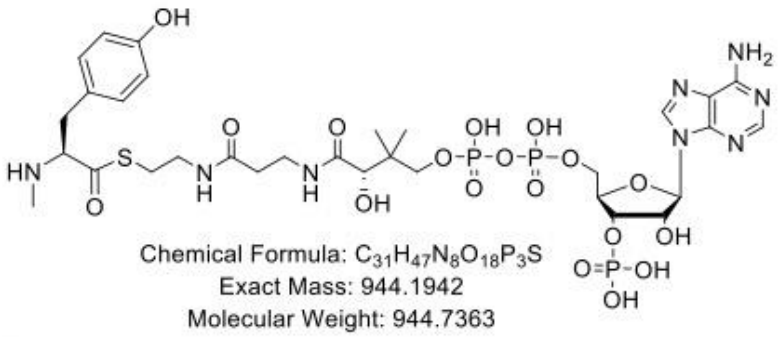

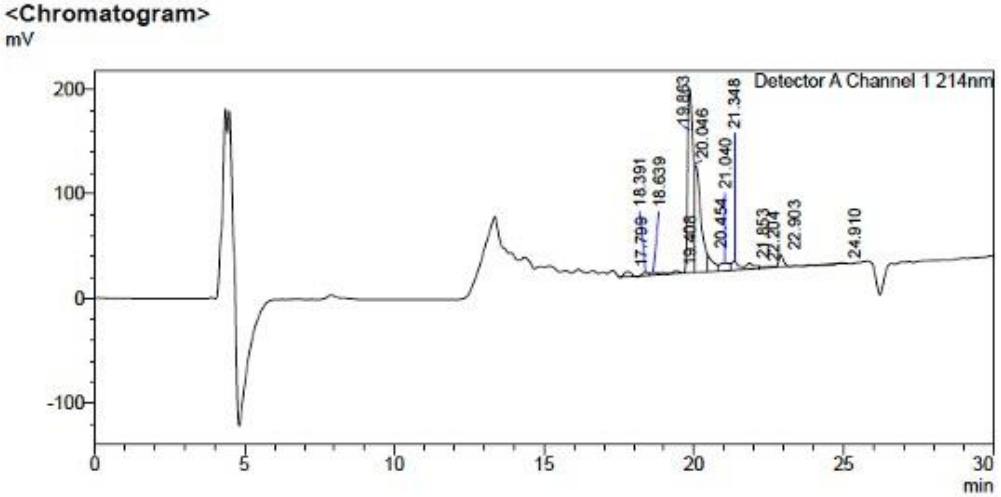

LCMS gradient 10-40% in ACN (0.1% TFA) in 30 minutes
RT = 19.86min

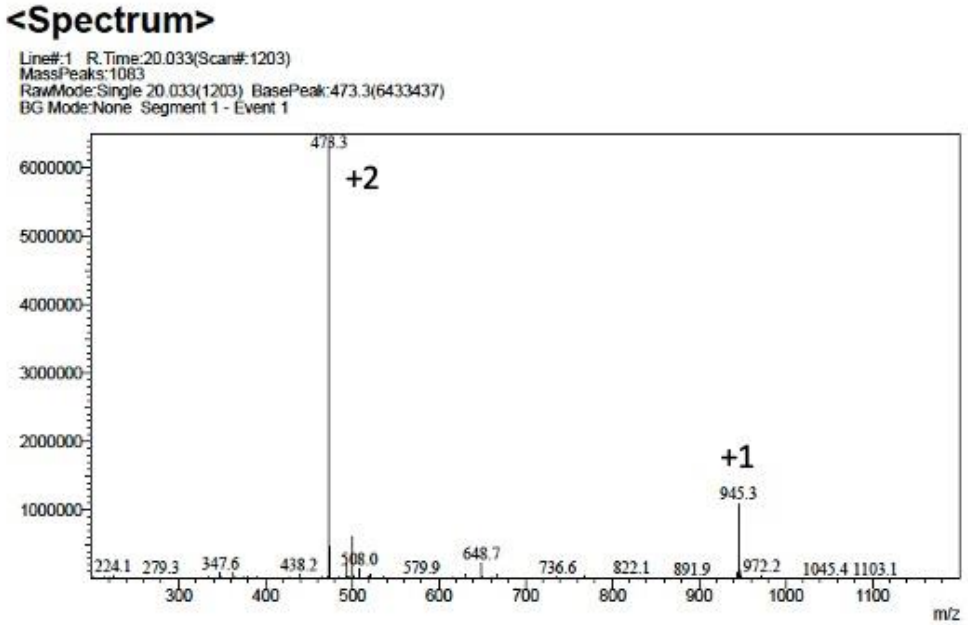

$[M + H^+]^{+} =$ 945.3Da; MW_{exp} = 944.3Da; $MW_{Expected}$ = 944.2Da

Figure S19. LCMS analysis of Cinnamoyl-Thr-Tyr-CoA.

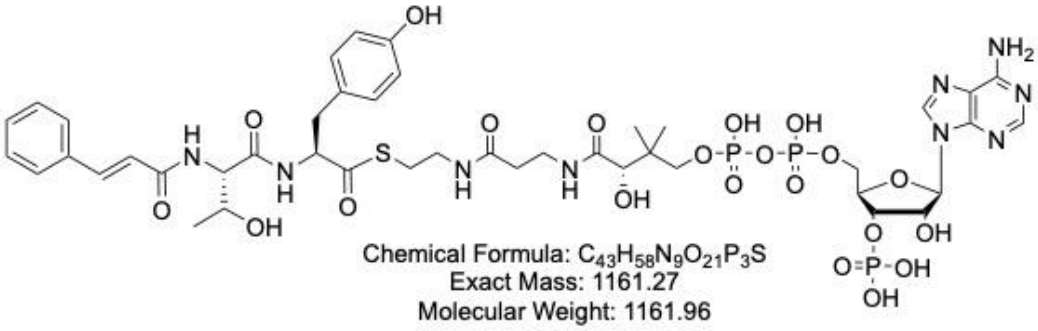

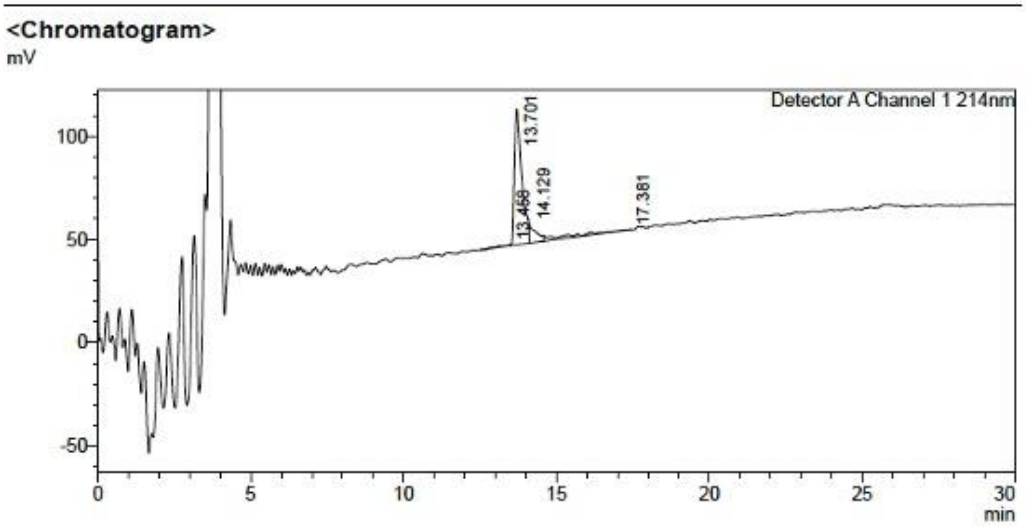

LCMS gradient 10-70% in ACN (0.1% TFA) in 30 minutes
RT = 13.46min

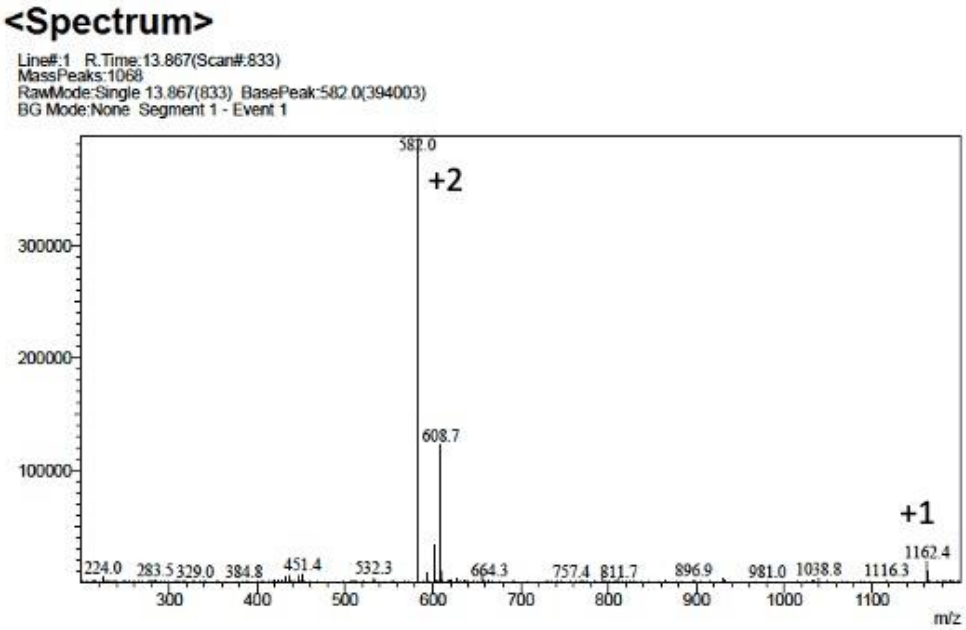

$[M + H^+]^{+} = 1162.4Da$; $MW_{exp} = 1161.4Da$; $MW_{Expected} = 1161.3Da$

Figure S20. LCMS analysis of Cinnamoyl-Thr-NMe-Tyr-CoA.

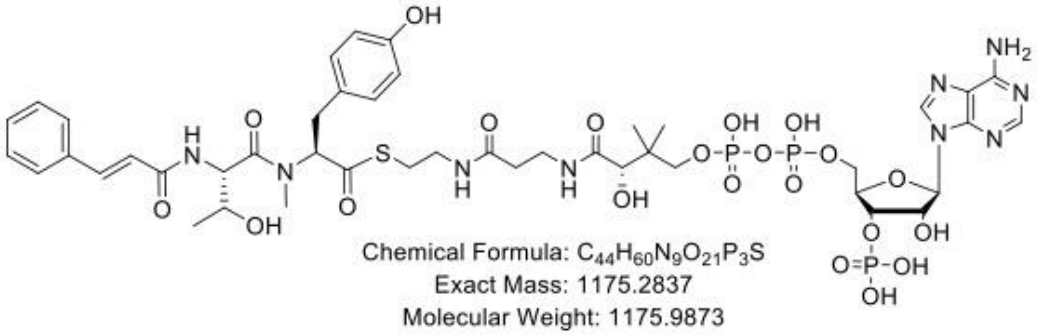

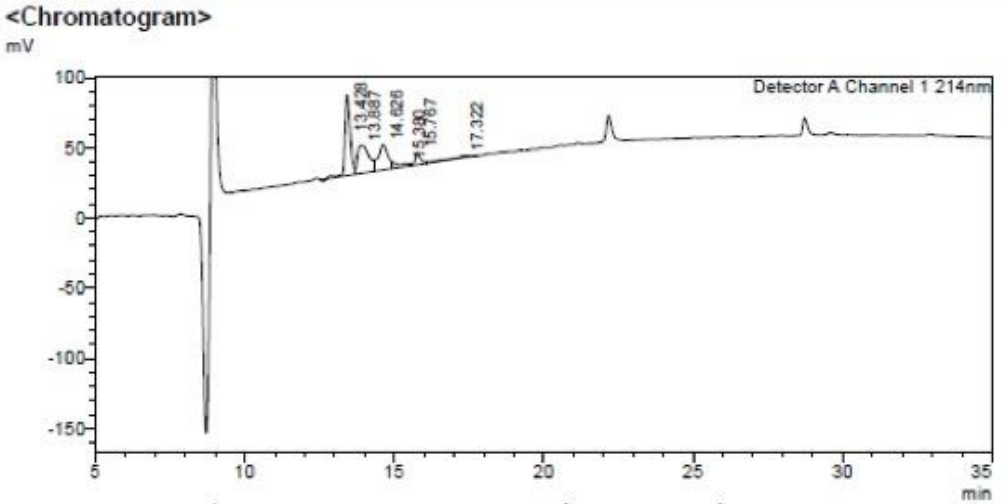

LCMS gradient 10-100% in ACN (0.1% TFA) in 30 minutes

RT =

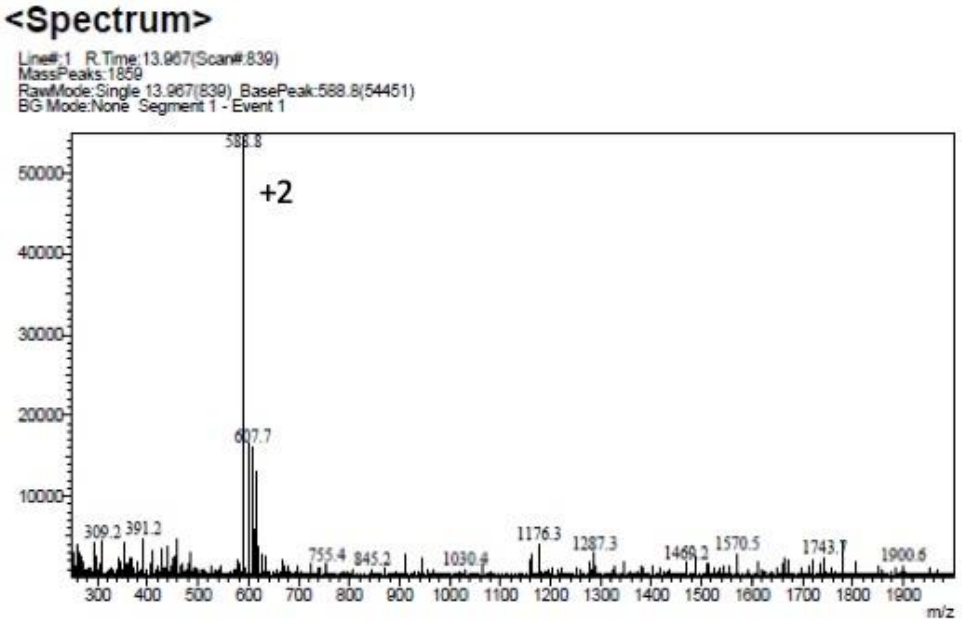

$[M + 2H^+]^{2+}$ = 588.8Da; MW_{exp} = 1175.6Da; $MW_{Expected}$ = 1175.3Da

Figure S21. LCMS analysis of Cinnamoyl-Val-NMe-Tyr-CoA.

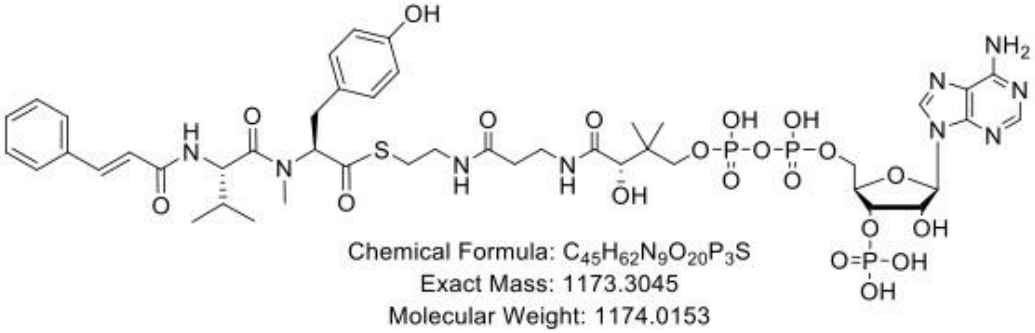

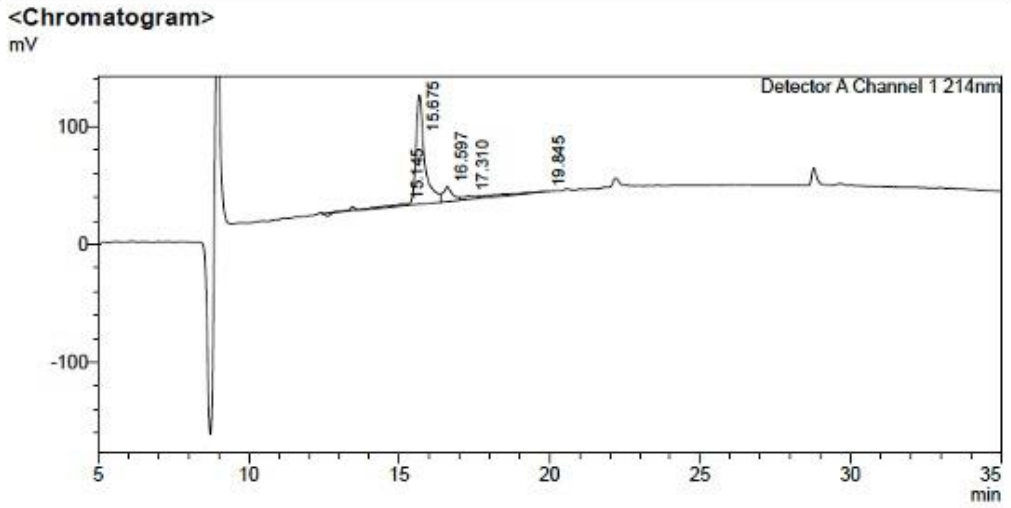

LCMS gradient 10-100% in ACN (0.1% TFA) in 30 minutes
RT = 13.4min

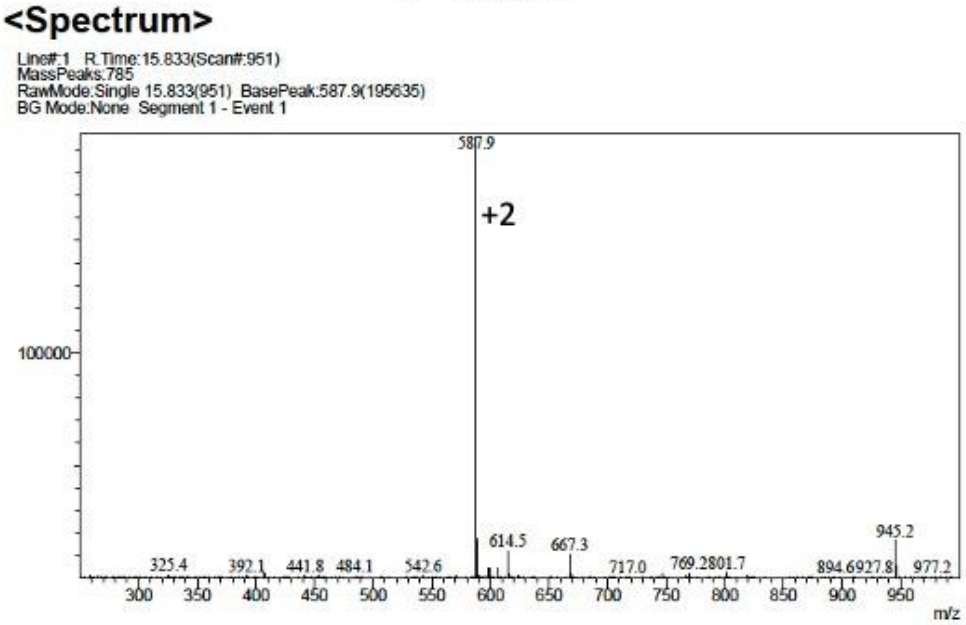

$[M + 2H^+]^{2+} =$ 587.9Da; MW_{exp} = 1173.8Da; $MW_{Expected}$ = 1173.3Da

Figure S22. LCMS analysis of Benzyl-Thr-NMe-Tyr-CoA.

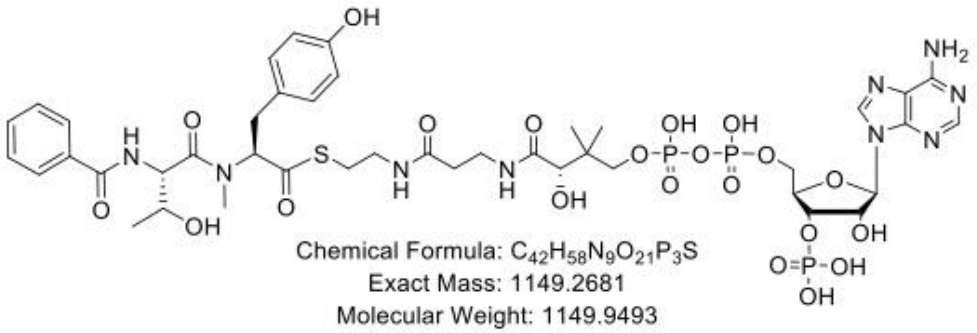

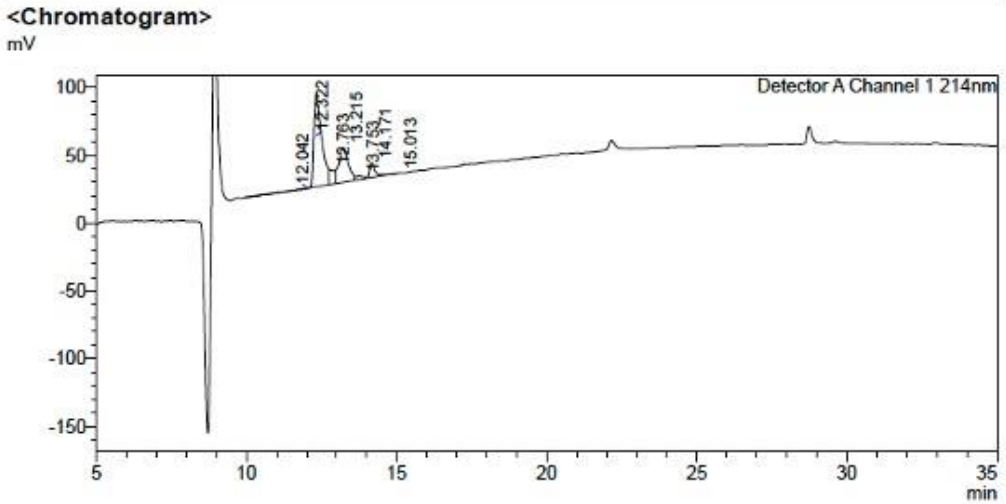

LCMS gradient 10-100% in ACN (0.1% TFA) in 30 minutes
RT = 12.32min

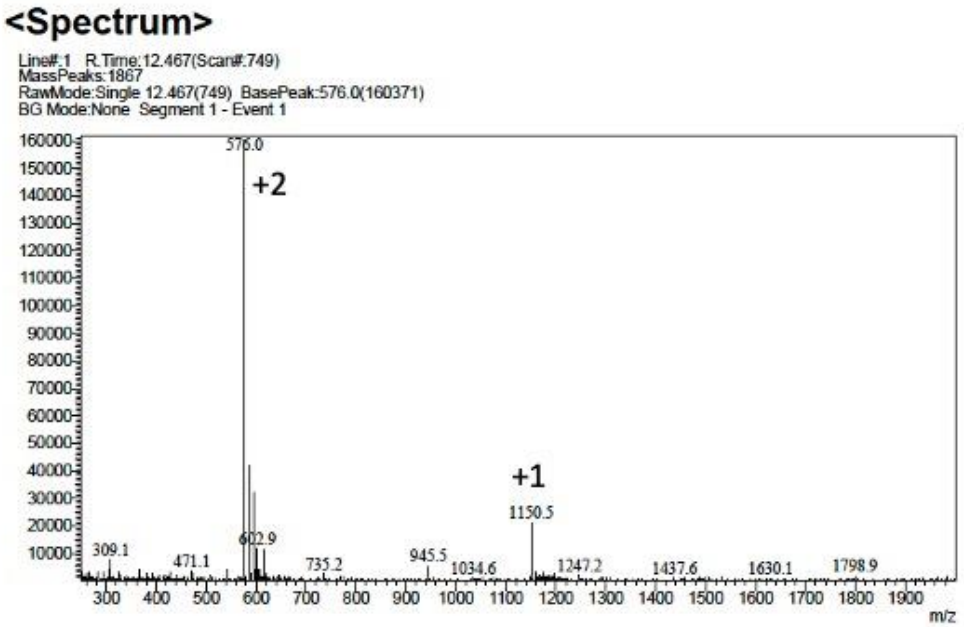

$[M + H^+]^{+=}$ 1150.5Da; MW_{exp} = 1149.5Da; $MW_{Expected}$ = 1149.3Da

Figure S23. HRMS and MS^2 analysis of Cinnamoyl-Thr-NMe-Tyr-NMe.

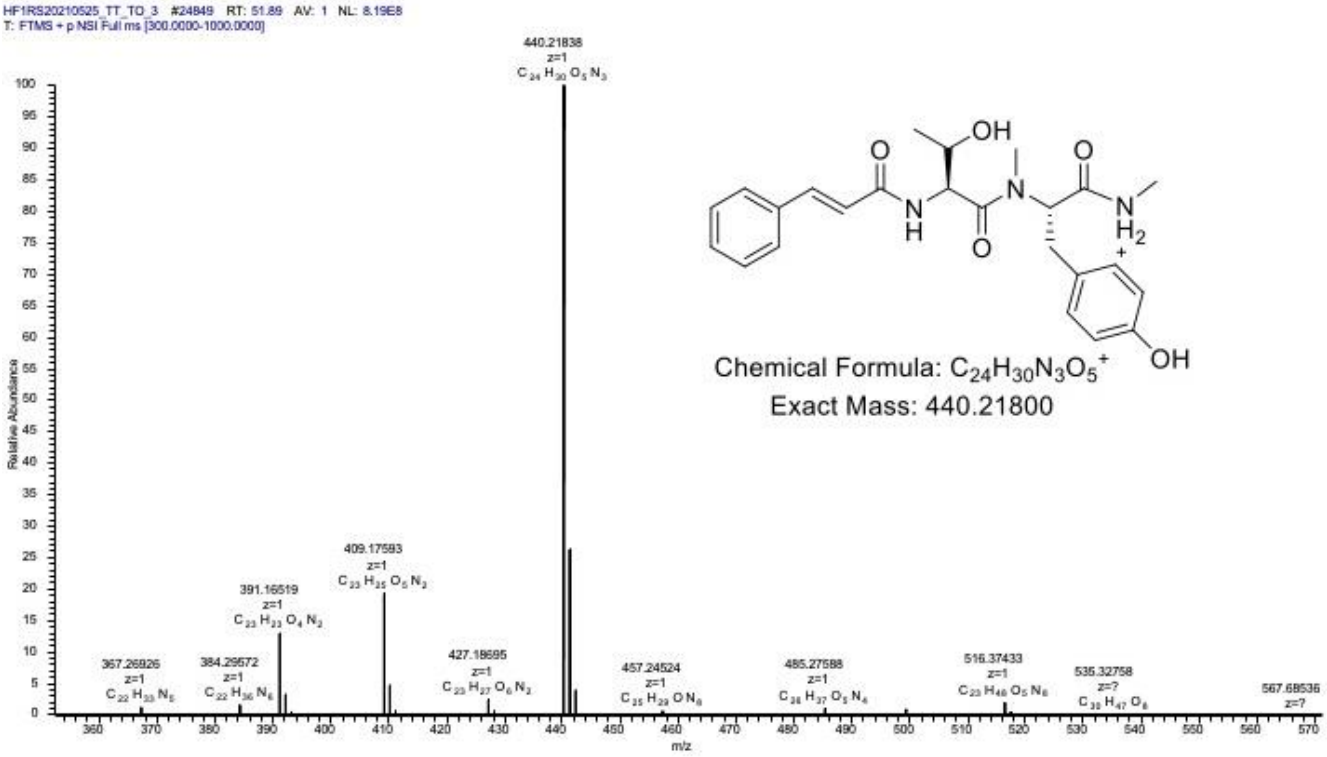

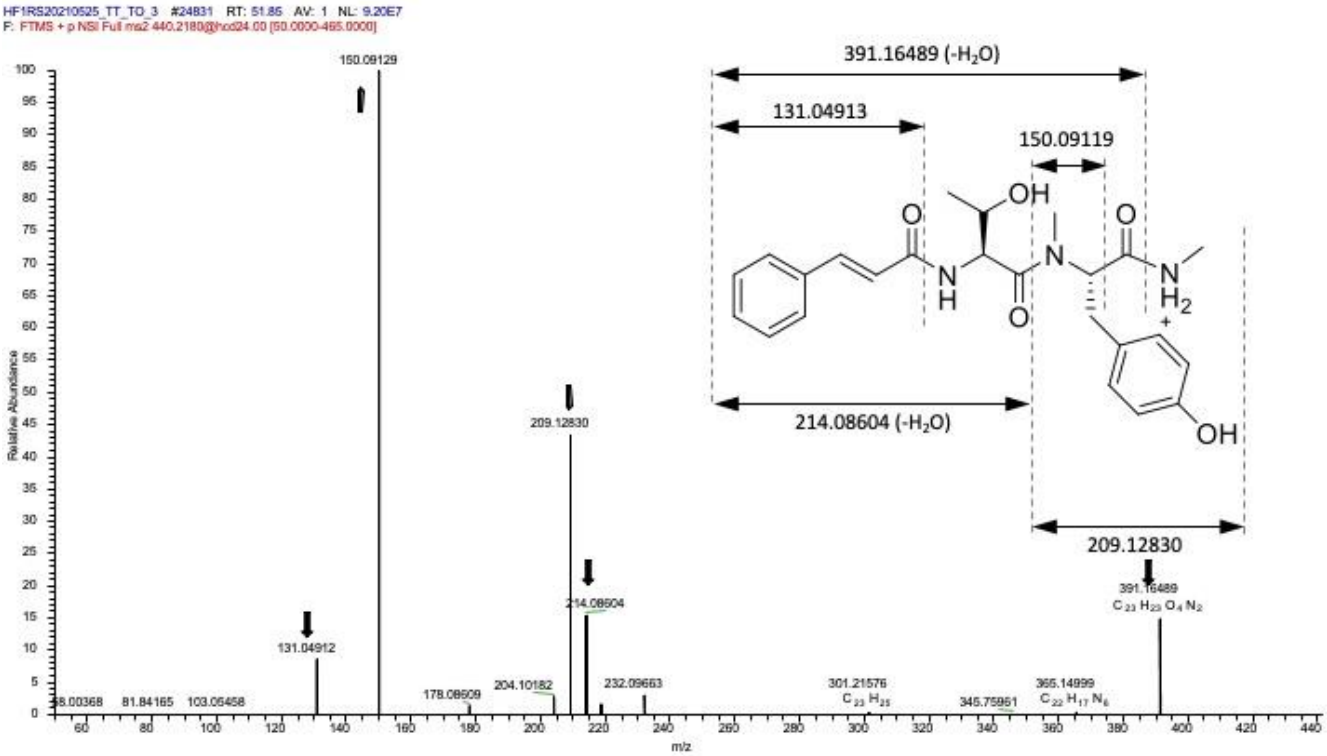

Figure S24. HRMS and MS^2 analysis of Cinnamoyl-Val-NMe-Tyr-NMe.

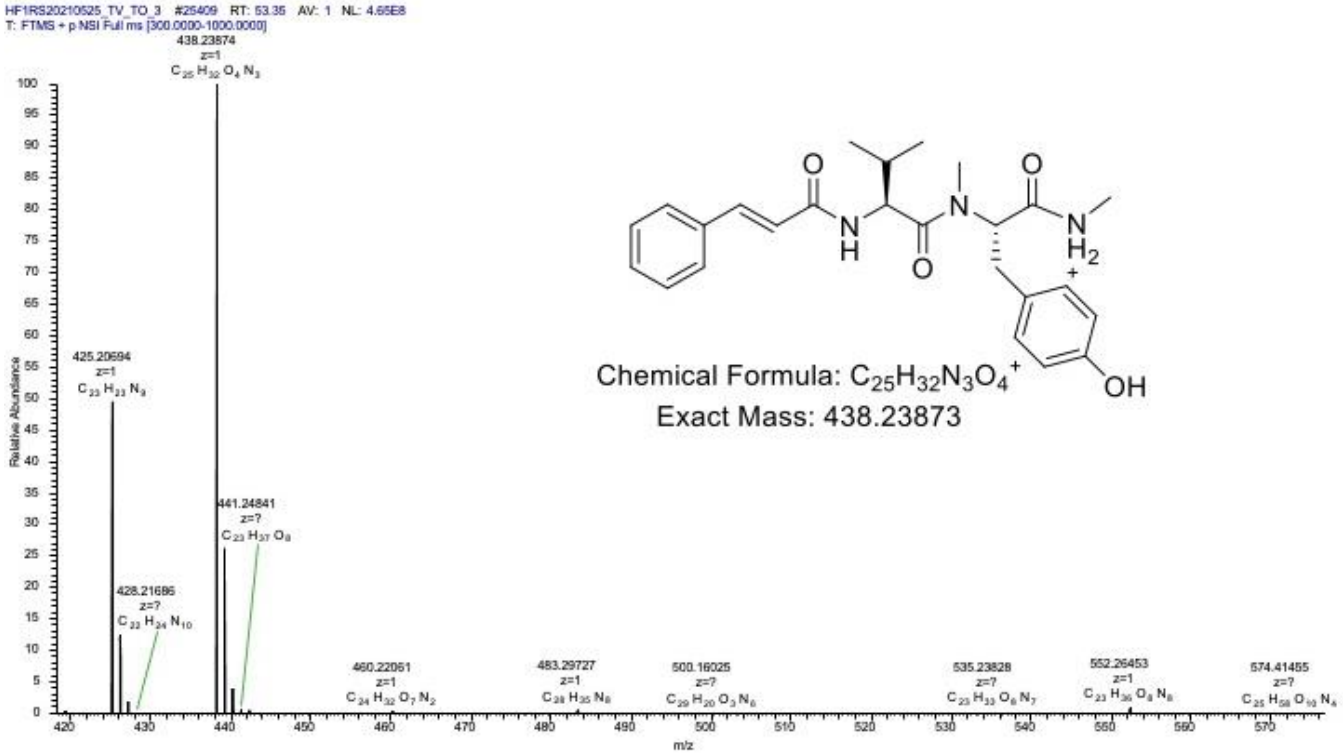

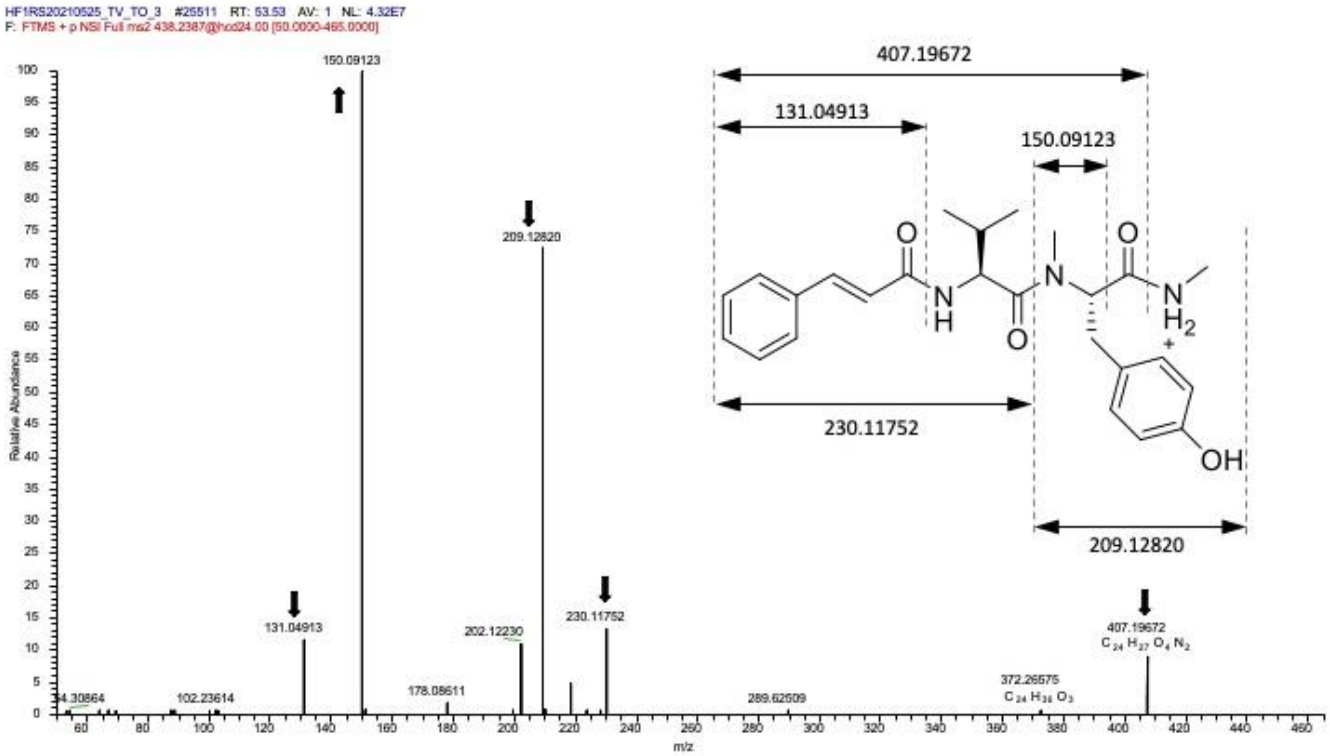

Figure S25. HRMS and MS^2 analysis of Cinnamoyl-Thr-Tyr-NMe.

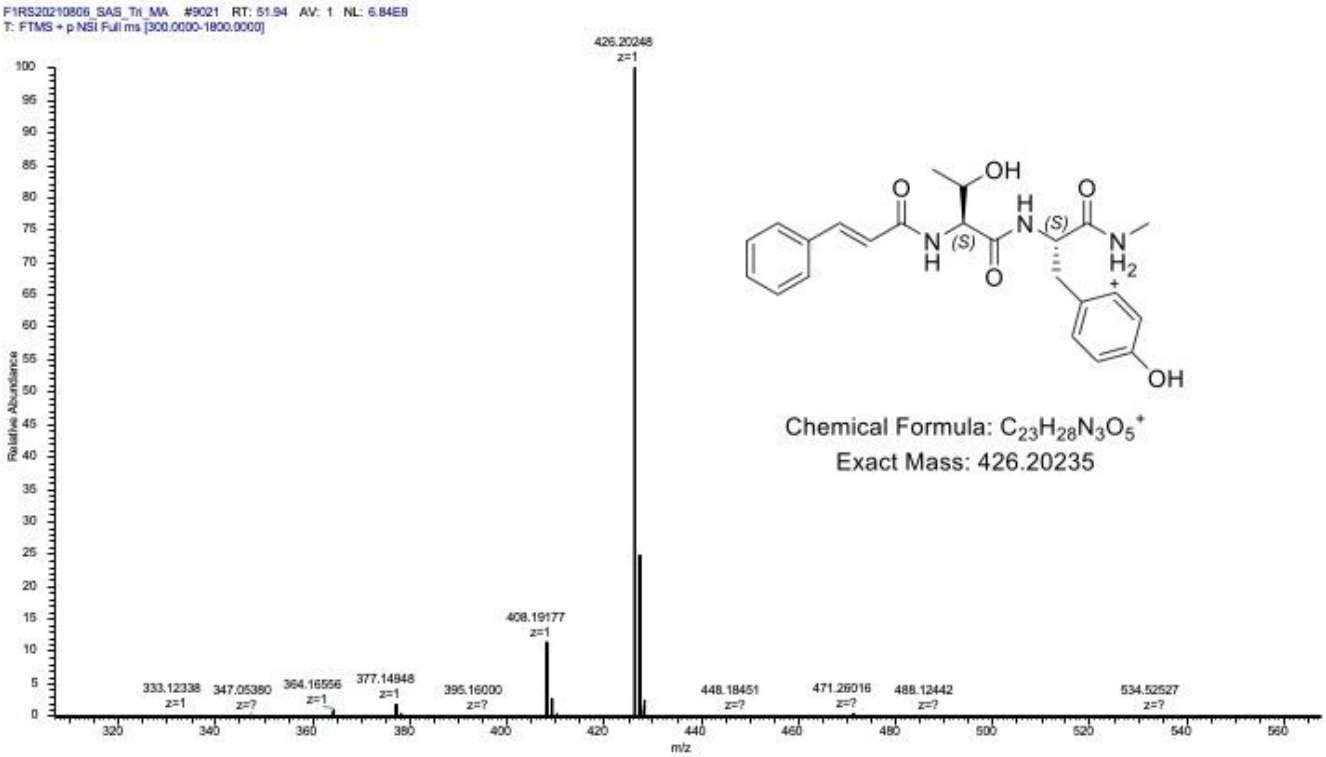

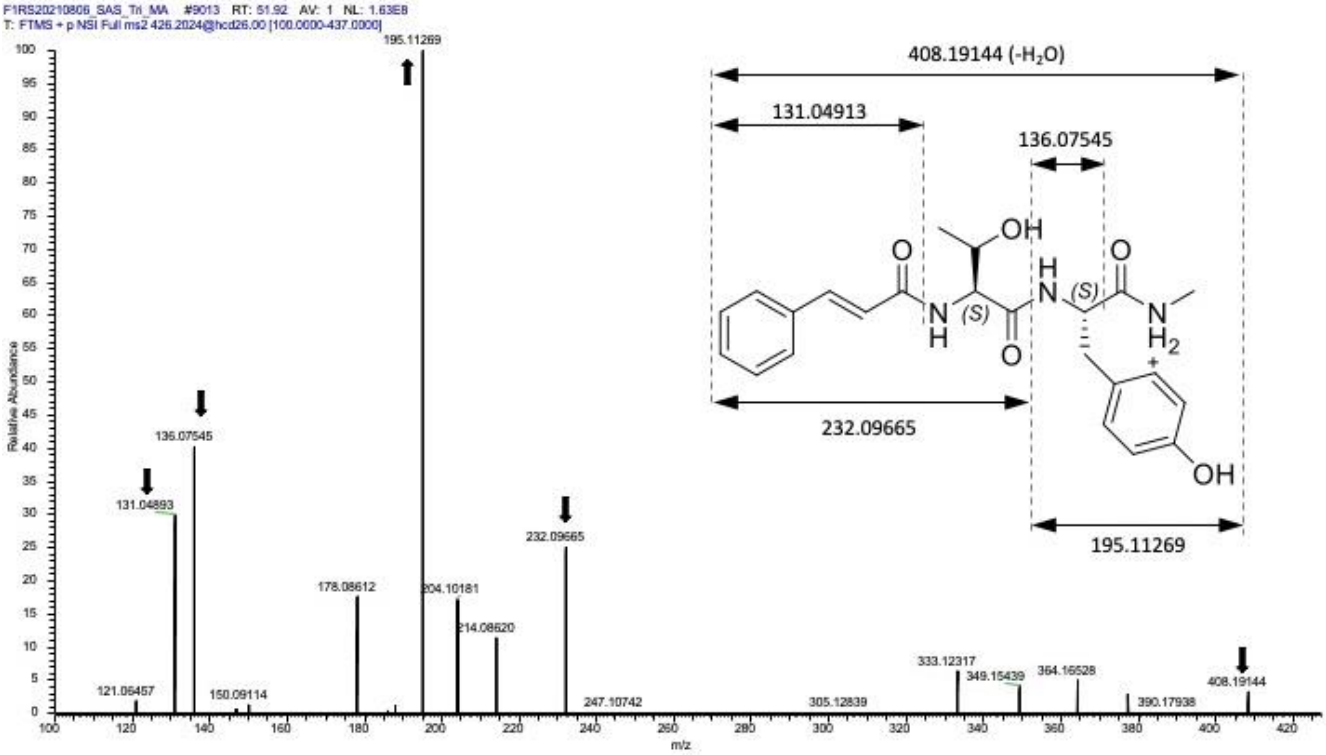

Figure S26. HRMS and MS^2 analysis of Benzyl-Thr-NMe-Tyr-NMe.

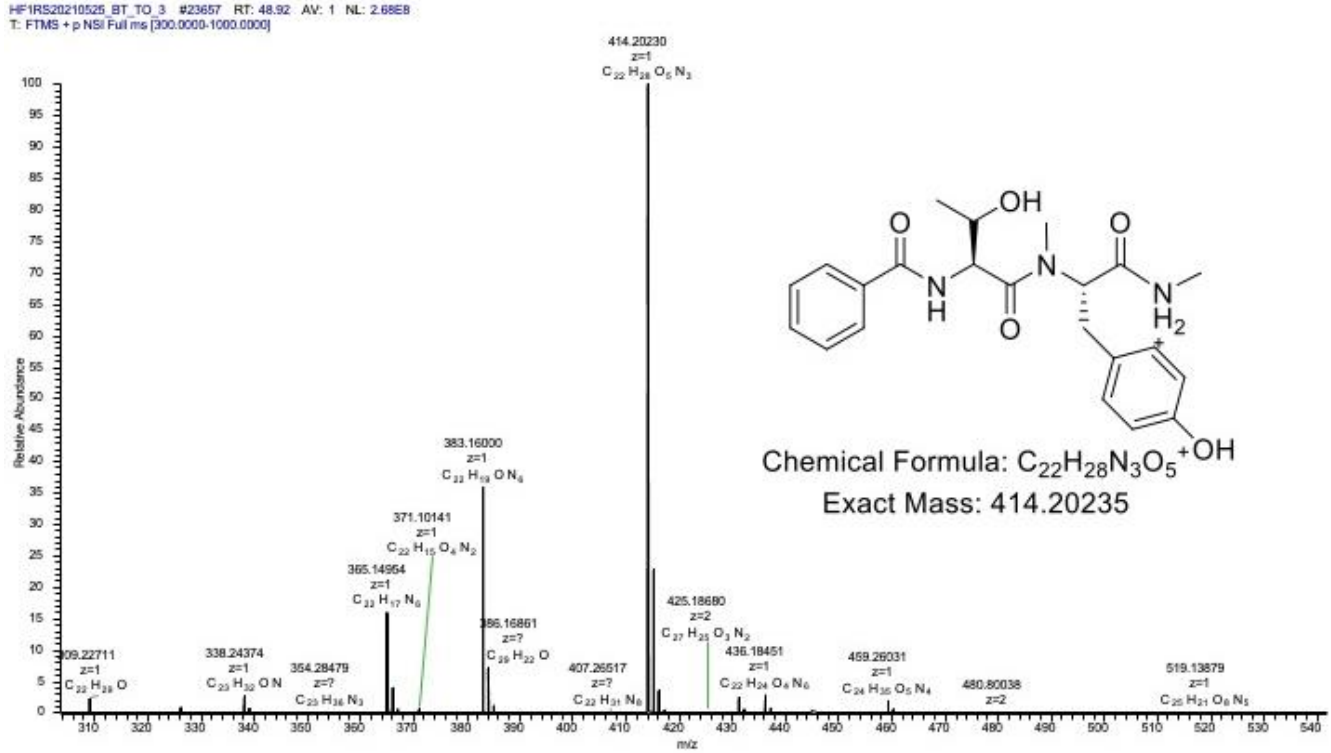

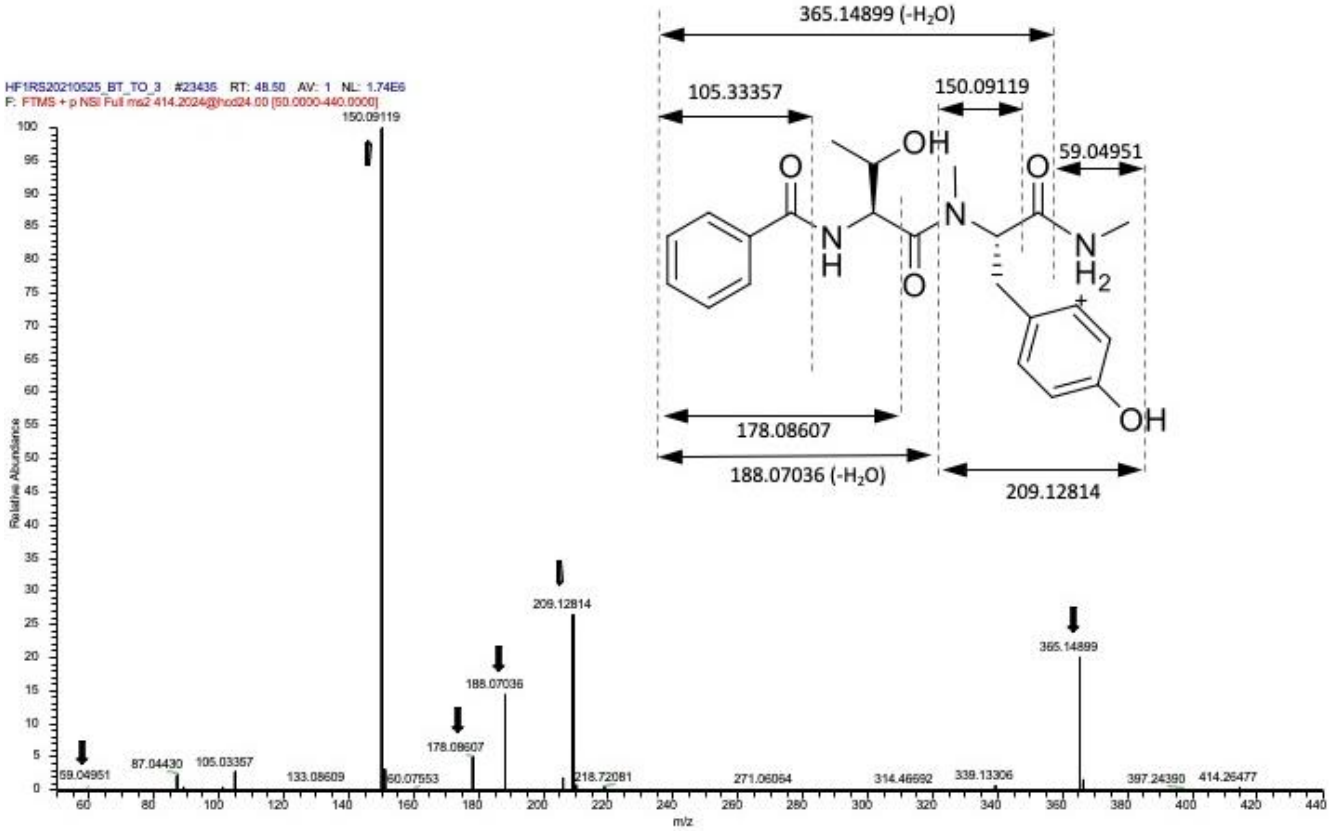

Figure S27. Putative peptide intermediate species captured in the biosynthesis of WS9326A by a tyrosine-based chain termination probe.

Dipeptide

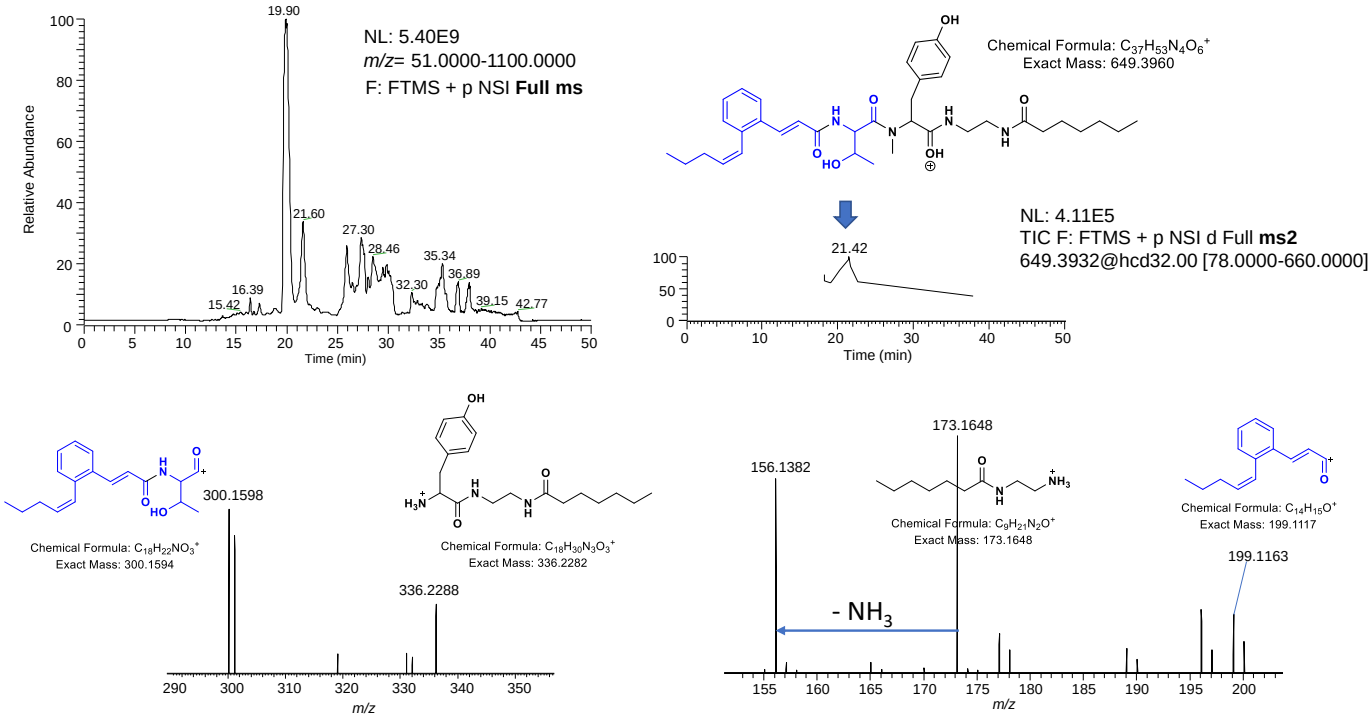

From top left, clockwise: TIC, HR- MS^2 and diagnostic fragments of *m/z* 649 dipeptide from extract analysis. In blue are the off-loaded biosynthetic species.

Unsaturated Dipeptide

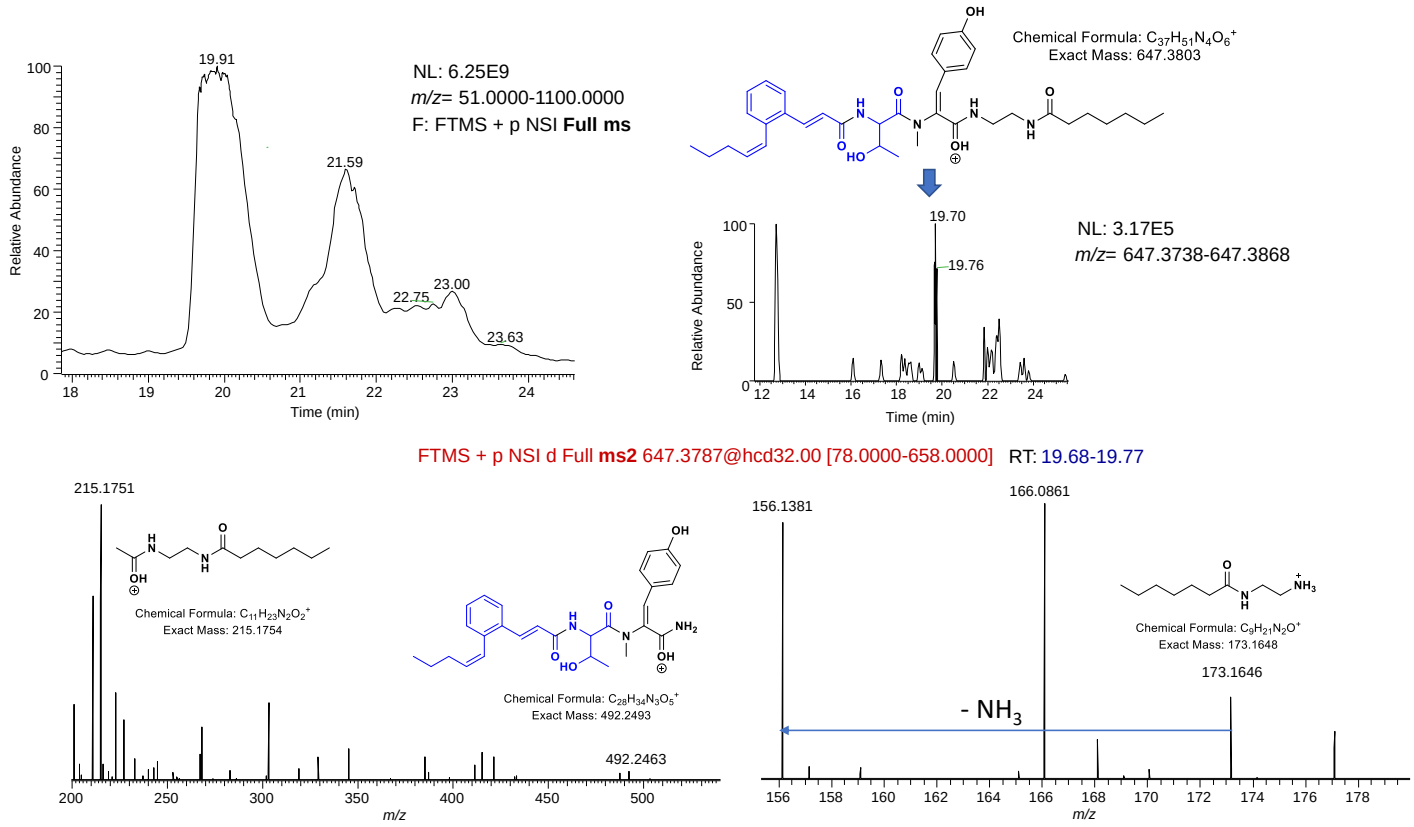

From top left, clockwise: TIC, EIC and diagnostic MS^2 fragments of *m/z* 647 dipeptide from extract analysis.

Tetrapeptide

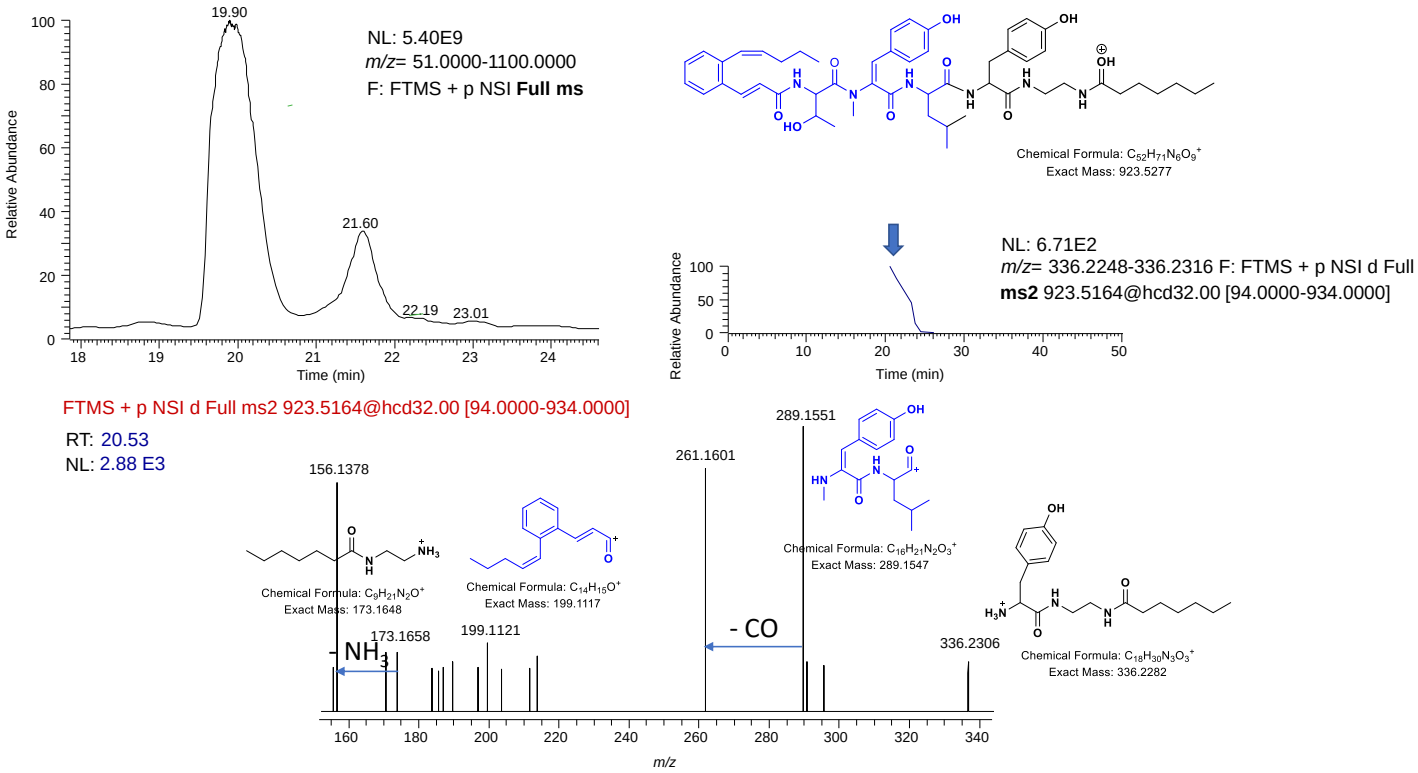

<u>From top left, clockwise</u>: TIC, HR-MS^2 detection and fragments of *m/z* 923 tetrapeptide from extract analysis.

Pentapeptide

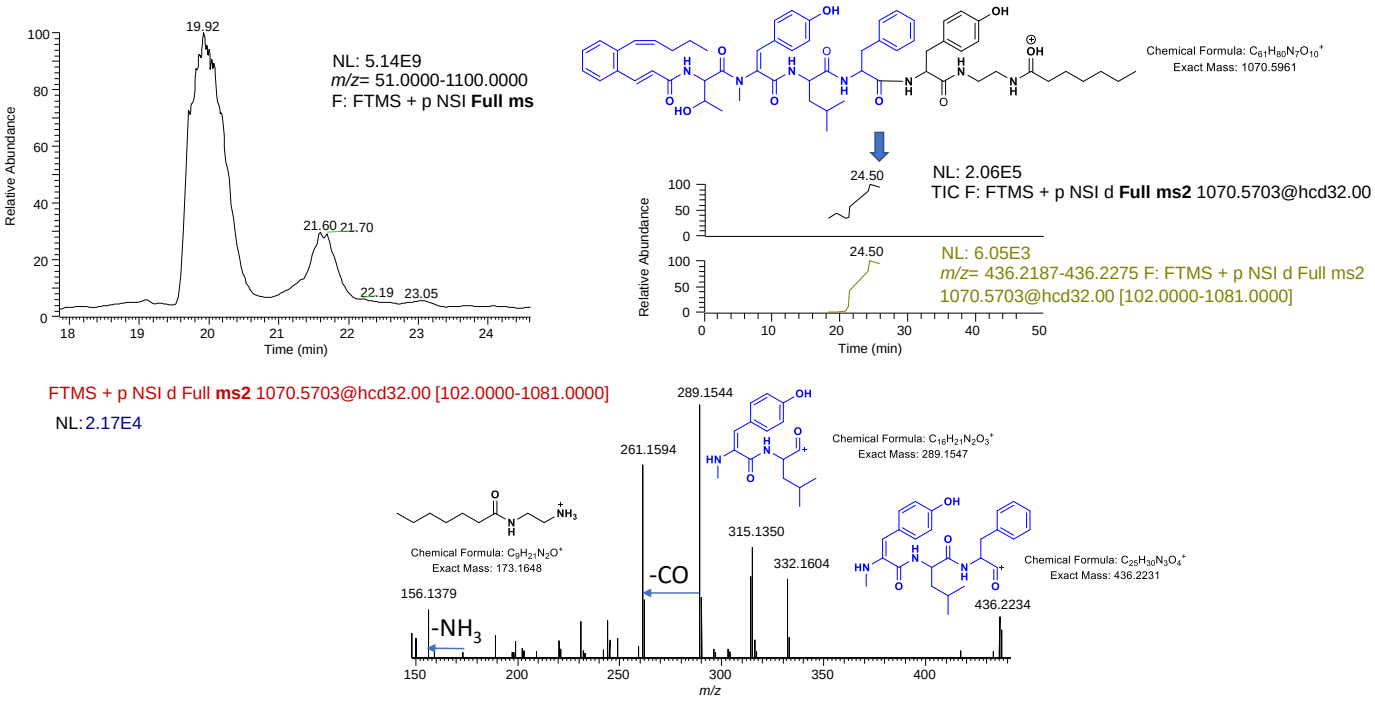

<u>From top left, clockwise</u>: TIC, HR-MS^2 detection and fragments of *m/z* 1070 pentapeptide from extract analysis.

Hexapeptide

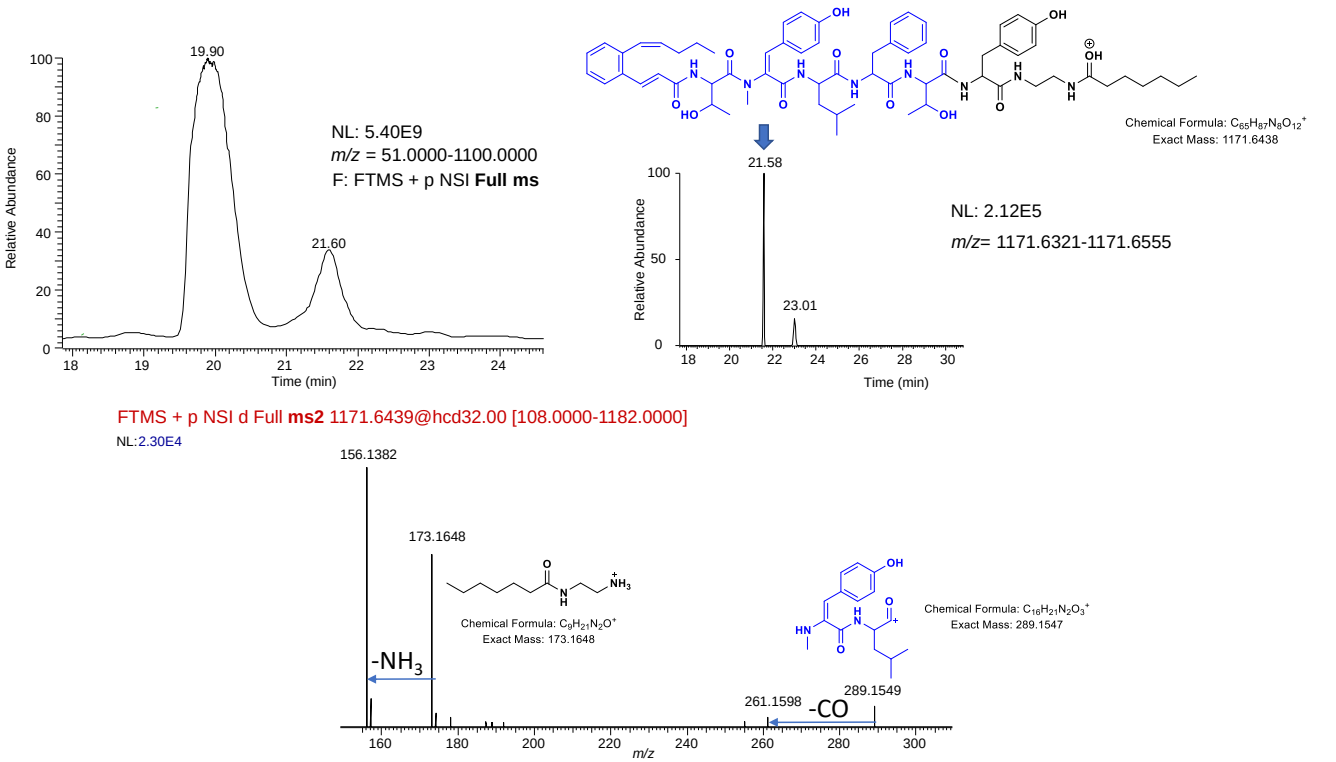

From top left, clockwise: TIC, EIC and HR-MS^2 fragments of *m/z* 1170 hexapeptide from extract analysis.

Methylation of tyrosine-based chain termination probe

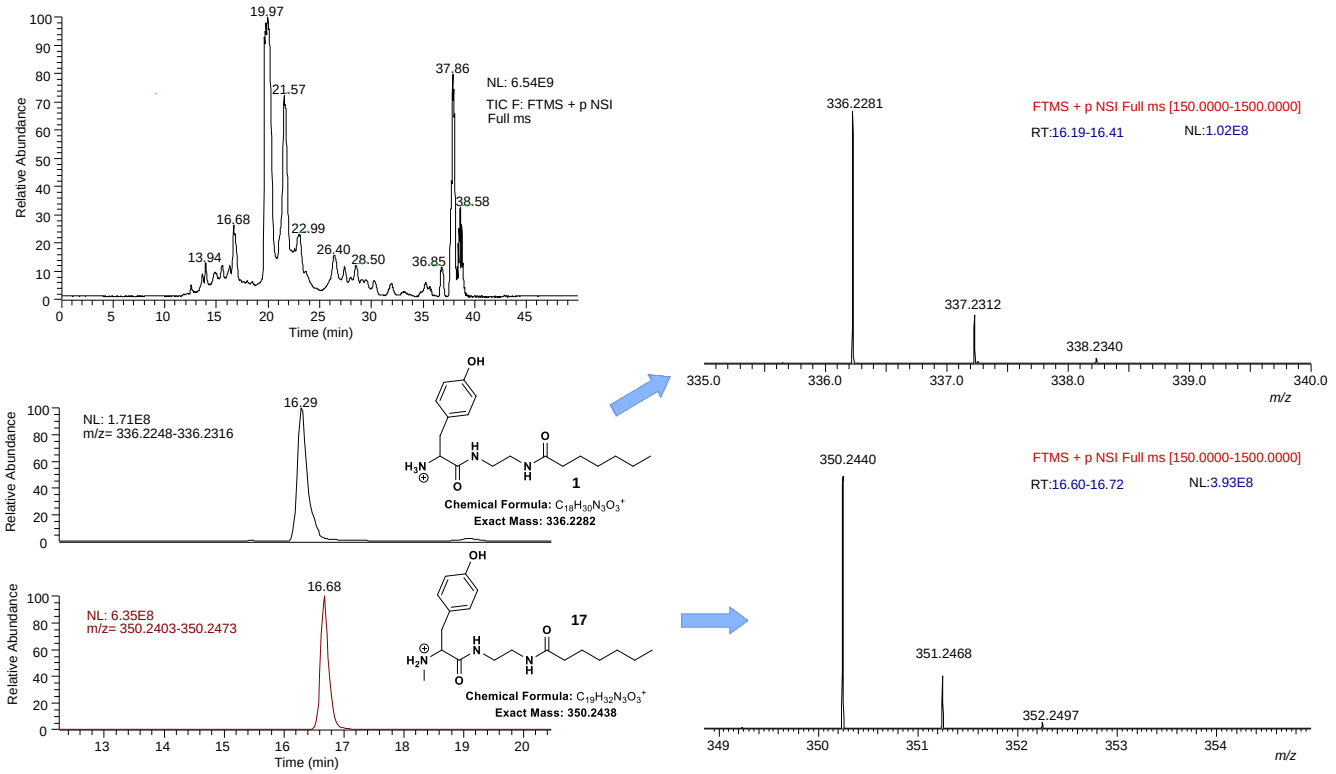

Left: TIC (top) and EICs (bottom) for probe **1** ([M+H]$^+$) and its methylated form (**17**, ([M+H]$^+$), found in the organic extracts of *S. asterosporus* strains supplemented with **1** over 5 days. Right: HR- MS analysis of **1** (top) and **17** (bottom).

Figure S28. Putative peptide intermediate species captured in the biosynthesis of WS9326A by a β-alanine based chain termination probe.

Dipeptide

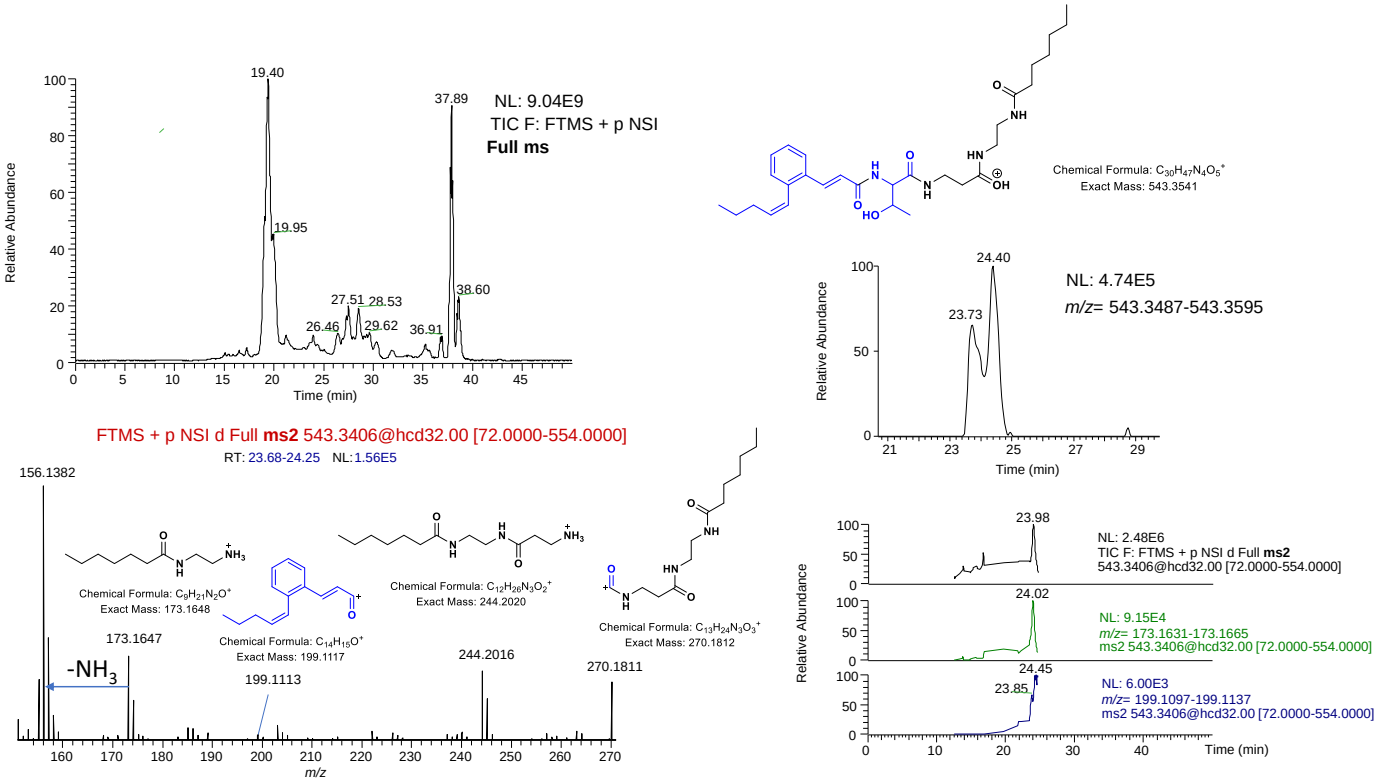

<u>From top left, clockwise</u>: TIC, EIC, HR-MS^2 detection and fragments of *m/z* 543 dipeptide from extract analysis.

Tripeptide

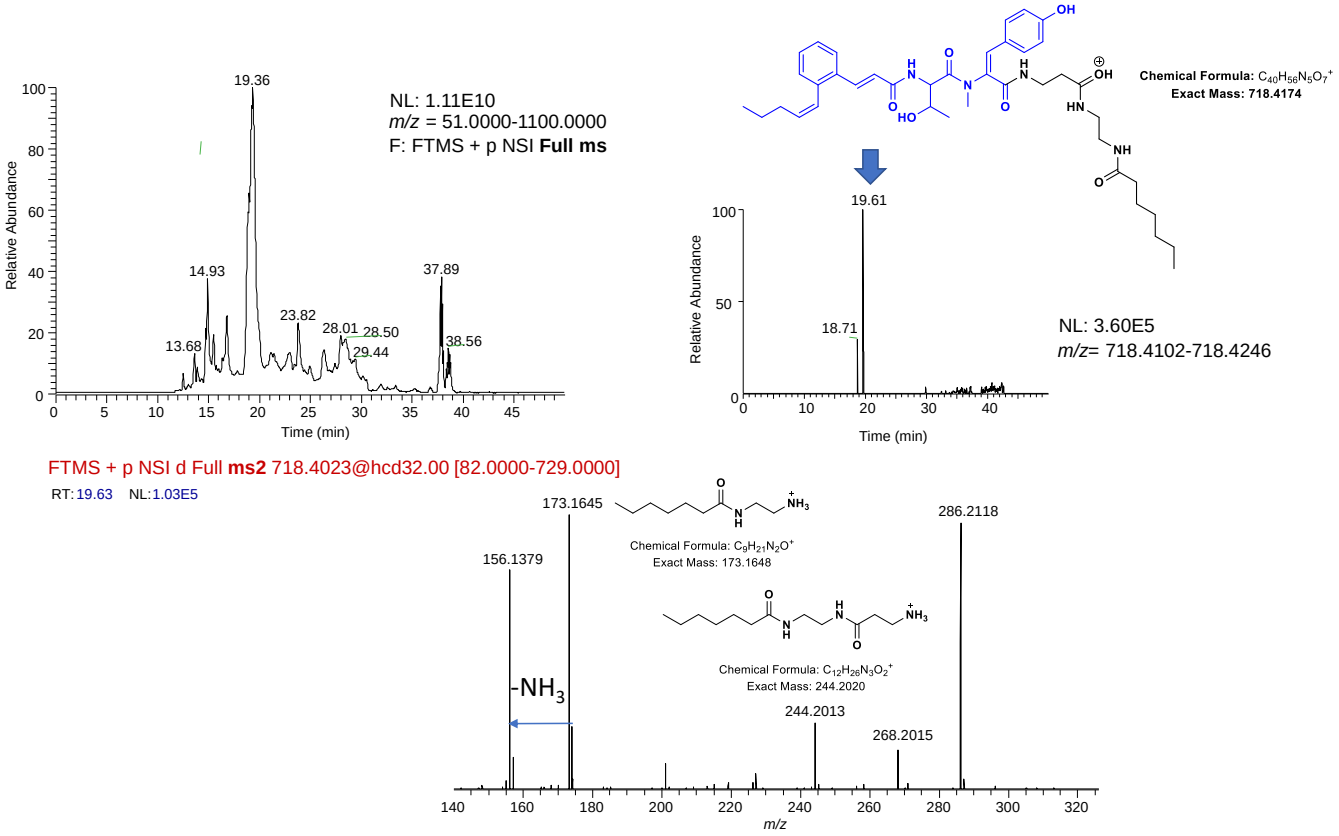

From top left, clockwise: TIC, EIC and HR-MS^2 fragments of *m/z* 718 tripeptide from extract analysis.

Tetrapeptide

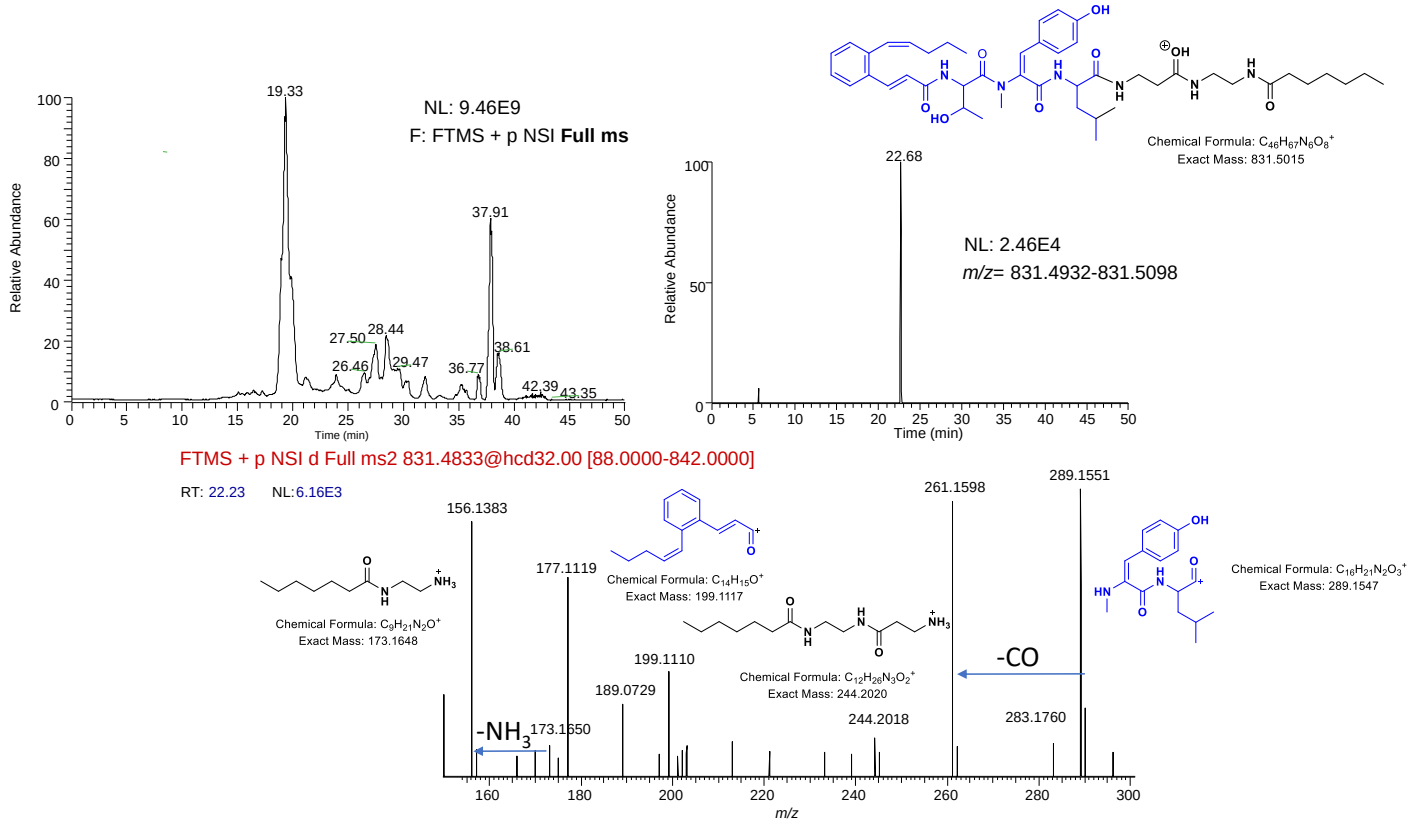

From top left, clockwise: TIC, EIC and HR-MS^2 fragments of *m/z* 831 tetrapeptide from extract analysis.

Hexapeptide

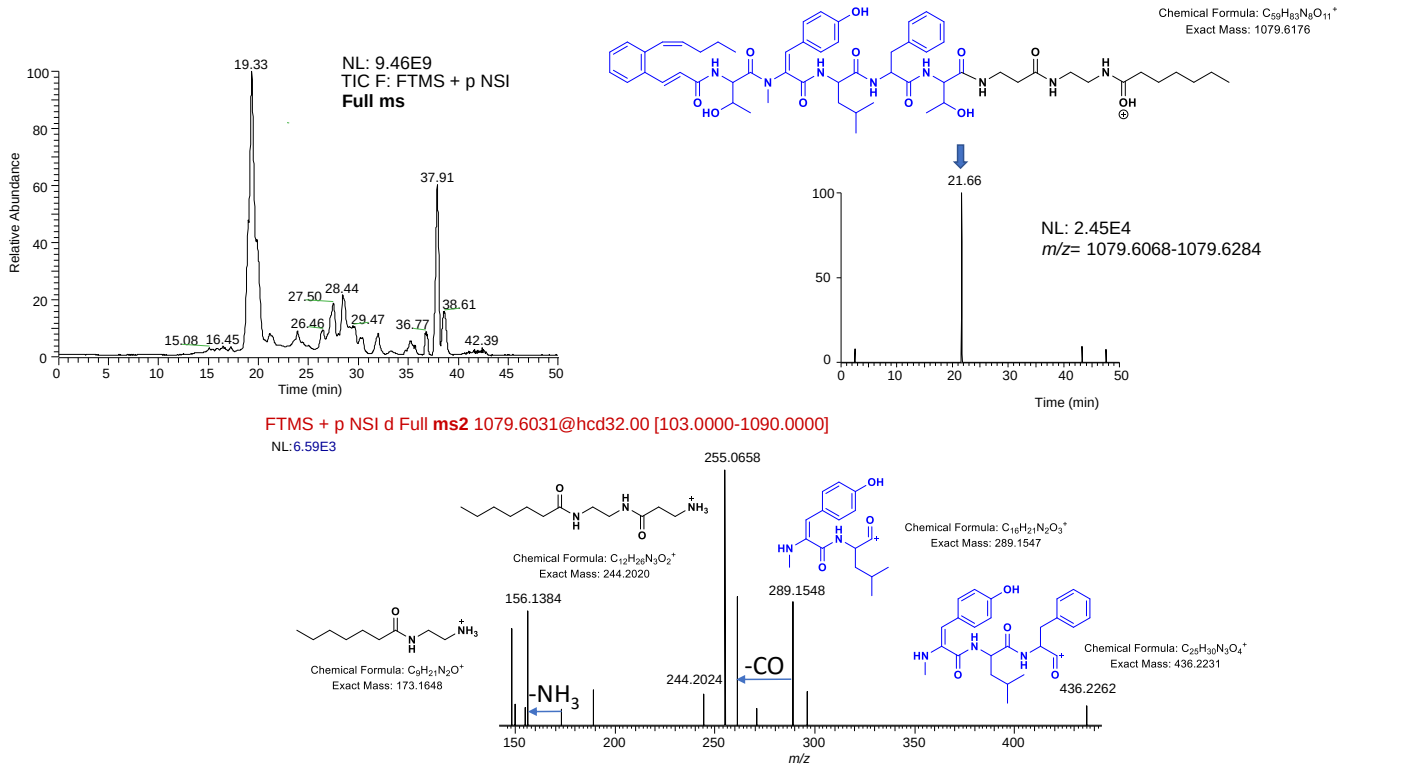

From top left, clockwise: TIC, EIC and HR-MS^2 fragments of *m/z* 1079 pentapeptide from extract analysis.

Figure S29. Putative peptide intermediate species captured in the biosynthesis of WS9326A by a glycine-based chain termination probe.

Dipeptide

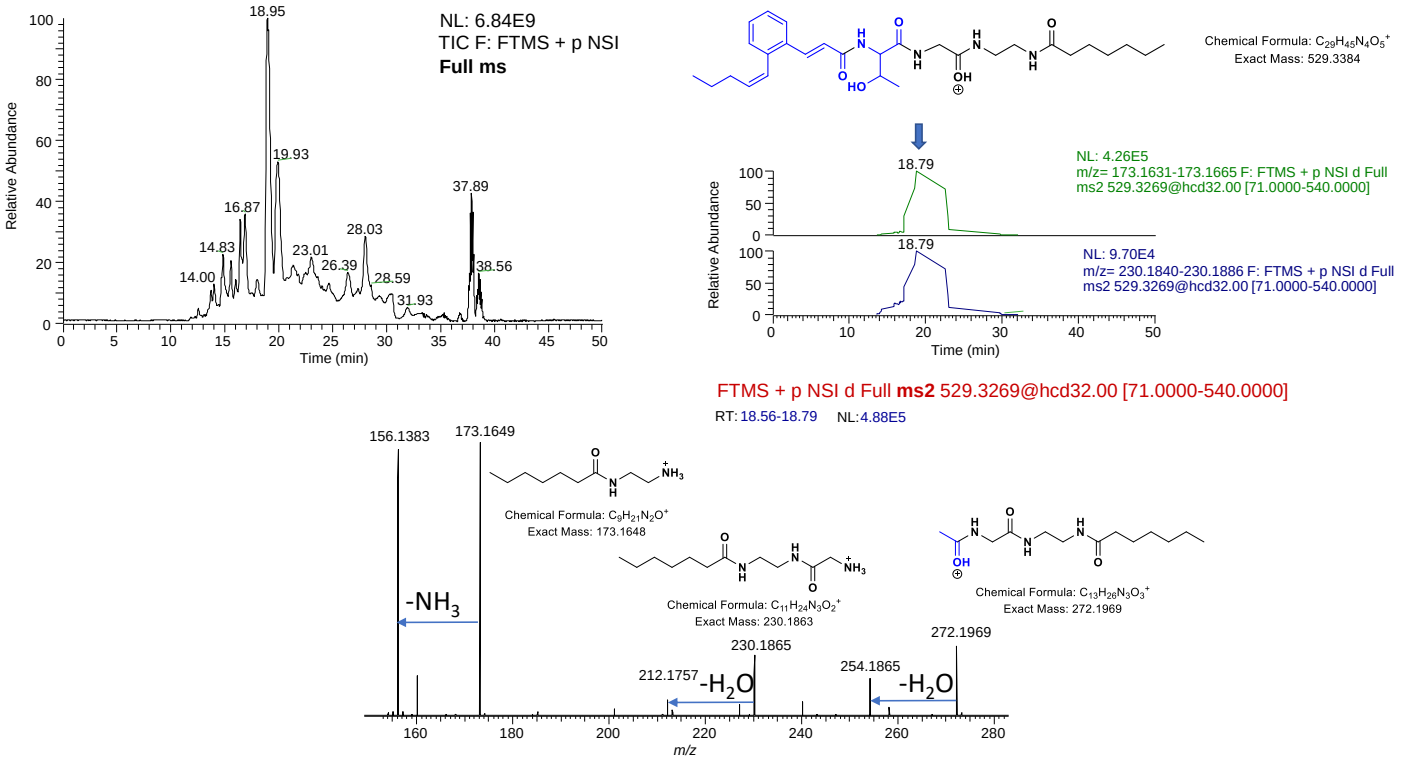

From top left, clockwise: TIC, HR-MS^2 detection and fragments of *m/z* 529 dipeptide from extract analysis.

Tripeptide

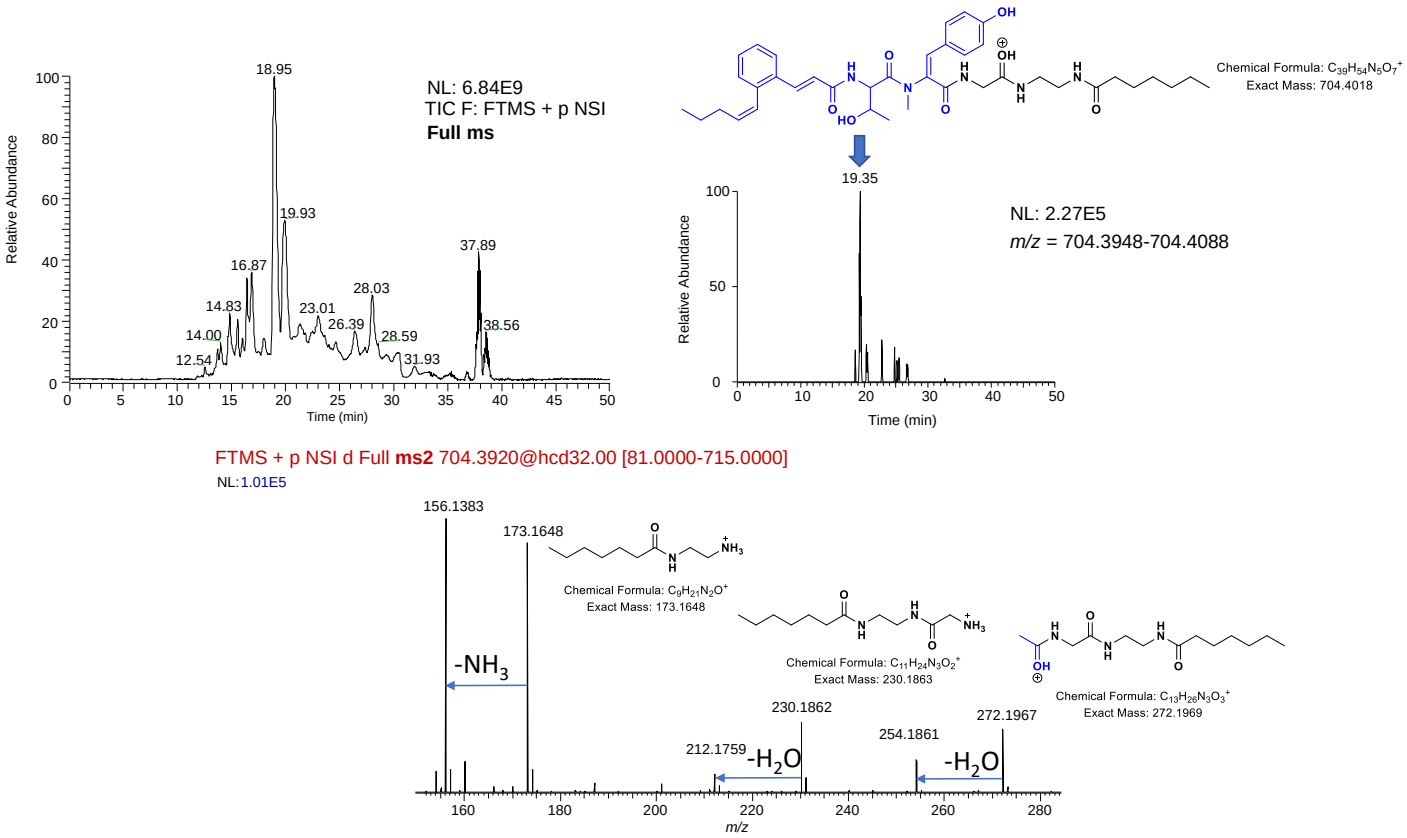

From top left, clockwise: TIC, EIC and HR-MS^2 fragments of *m/z* 704 tripeptide from extract analysis.

Tetrapeptide

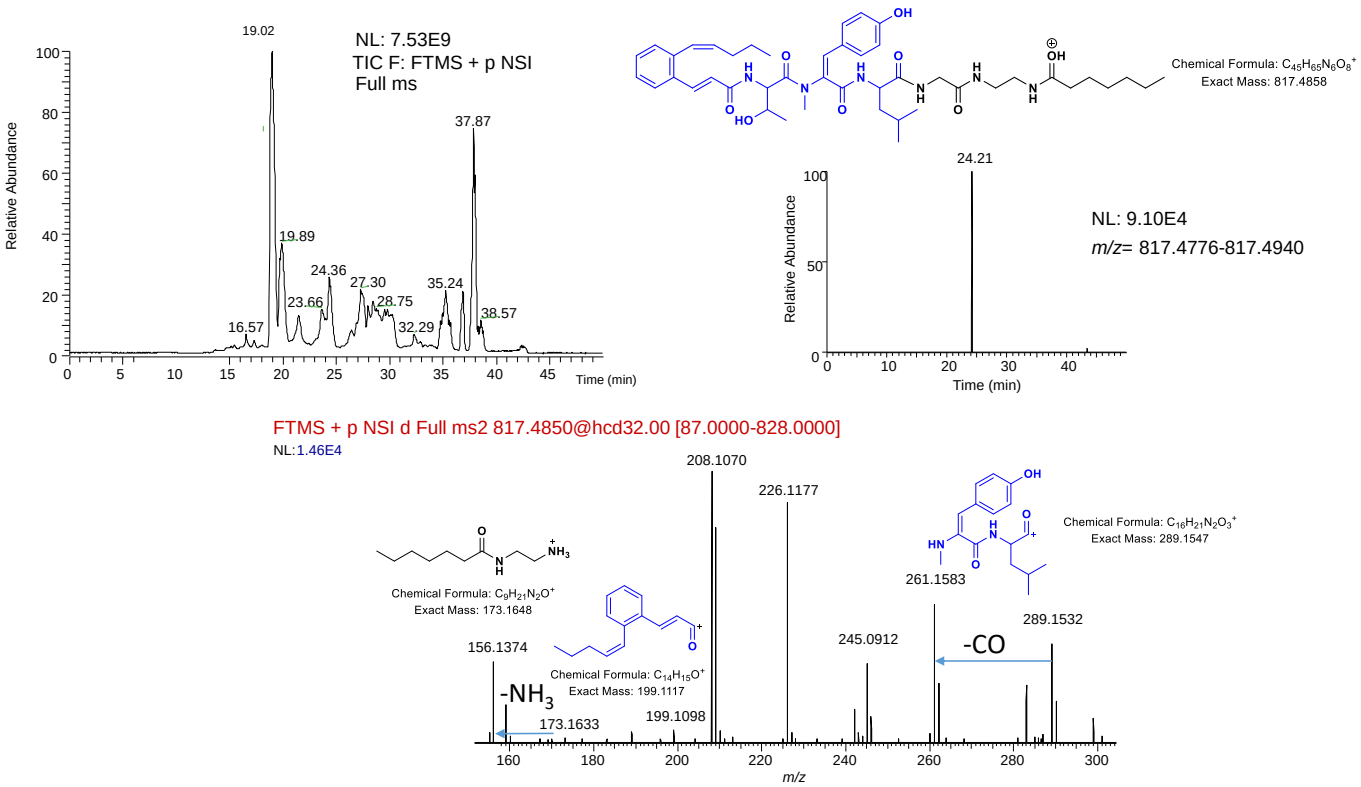

From top left, clockwise: TIC, EIC and HR-MS^2 fragments of *m/z* 817 tetrapeptide from extract analysis.

Hexapeptide

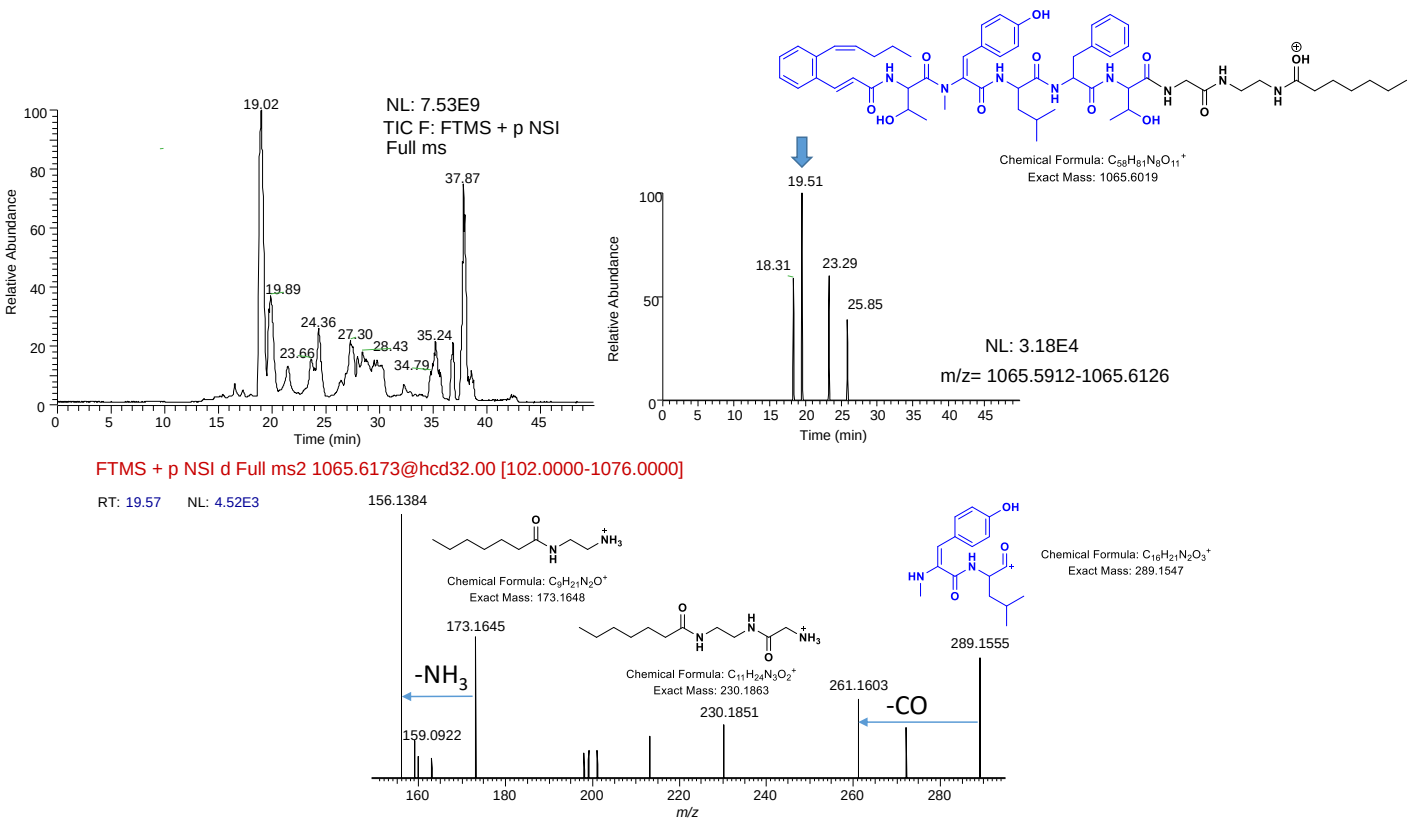

From top left, clockwise: TIC, EIC and HR-MS^2 fragments of *m/z* 1065 hexapeptide from extract analysis.

Figure S30. Putative peptide intermediate species captured in the biosynthesis of WS9326A by a chain termination probe in which the Tyr-residue has not been dehydrated. These include *m/z* 720, 1072 and 1081 (species for which tyrosine has not been dehydrated, intermediates in the formation of WS9326B) partial spectra and putative structures are shown.

***m/z* 720:**

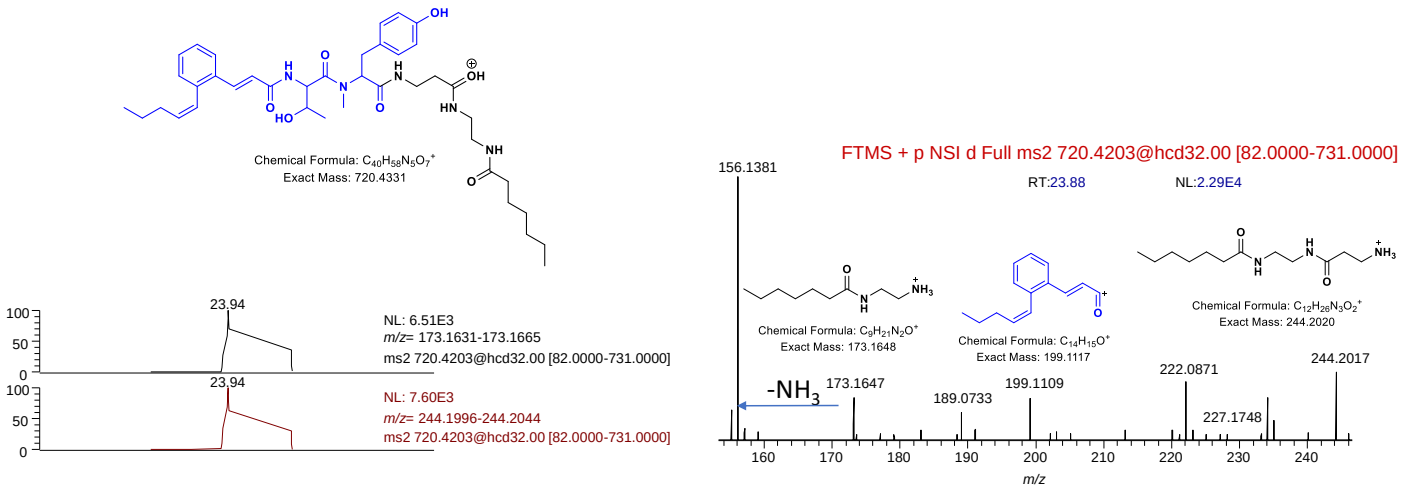

***m/z* 1072:**

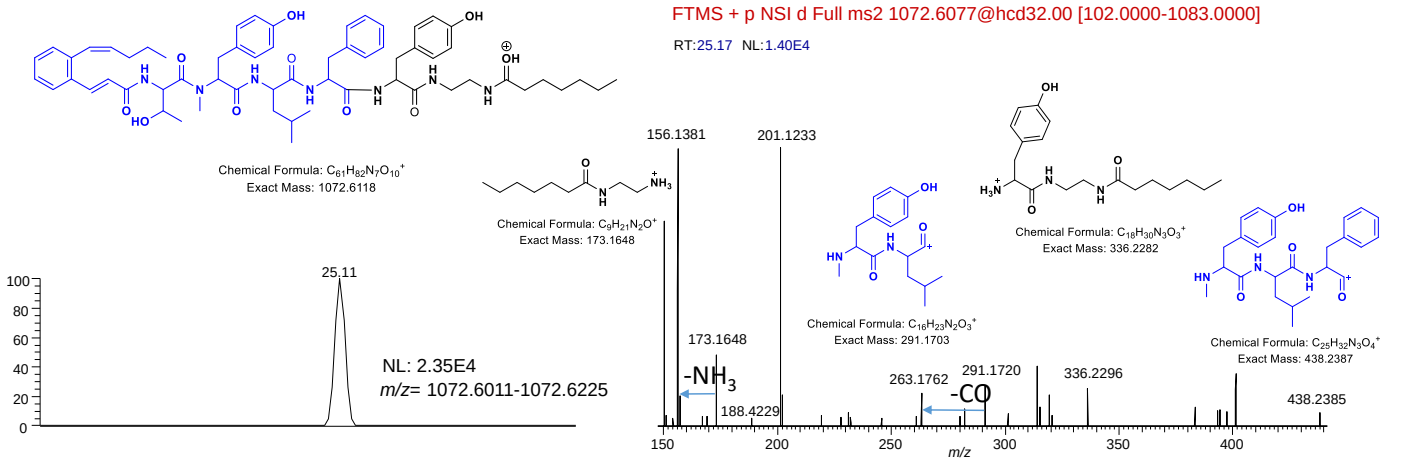

***m/z* 1081:**

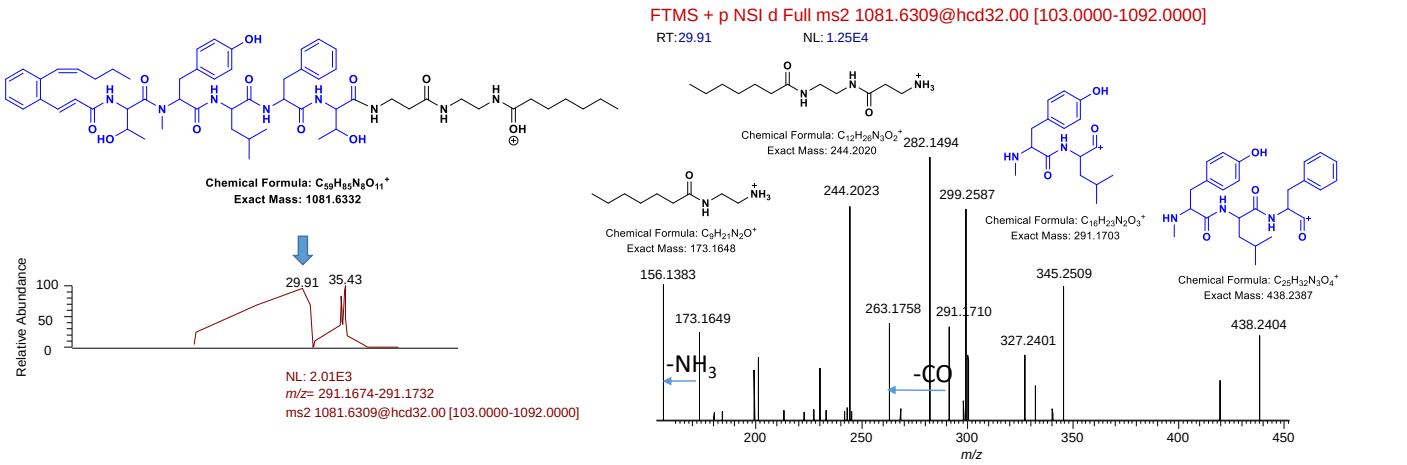

Figure S31. The genome region comparison of P450$_{Sas}$ to homologous P450 enzymes. Comparison of selected genes from the biosynthetic clusters that encode P450$_{Sas}$ homologues (UniProt ID left-hand side) including the P450 (yellow), NRPS (red, Sas17 homologue in dark red), transporter (blue) and enzymes responsible for the biosynthesis of the Z-pentenylcinnamoyl moiety (green), showing the similarity of the biosynthetic clusters containing P450$_{Sas}$ homologues. An analysis of the Sas17 NRPS homologues is shown on the right-hand side of the figure, showing two modules (Thr, N-Me-Tyr) with conserved C-A-PCP-C-A-NMt-PCP architecture. Such high levels of biosynthetic similarity support the hypothesis that all Sas16 homologues here will generate a Dht residue in the same acylated dipeptide biosynthetic intermediate.

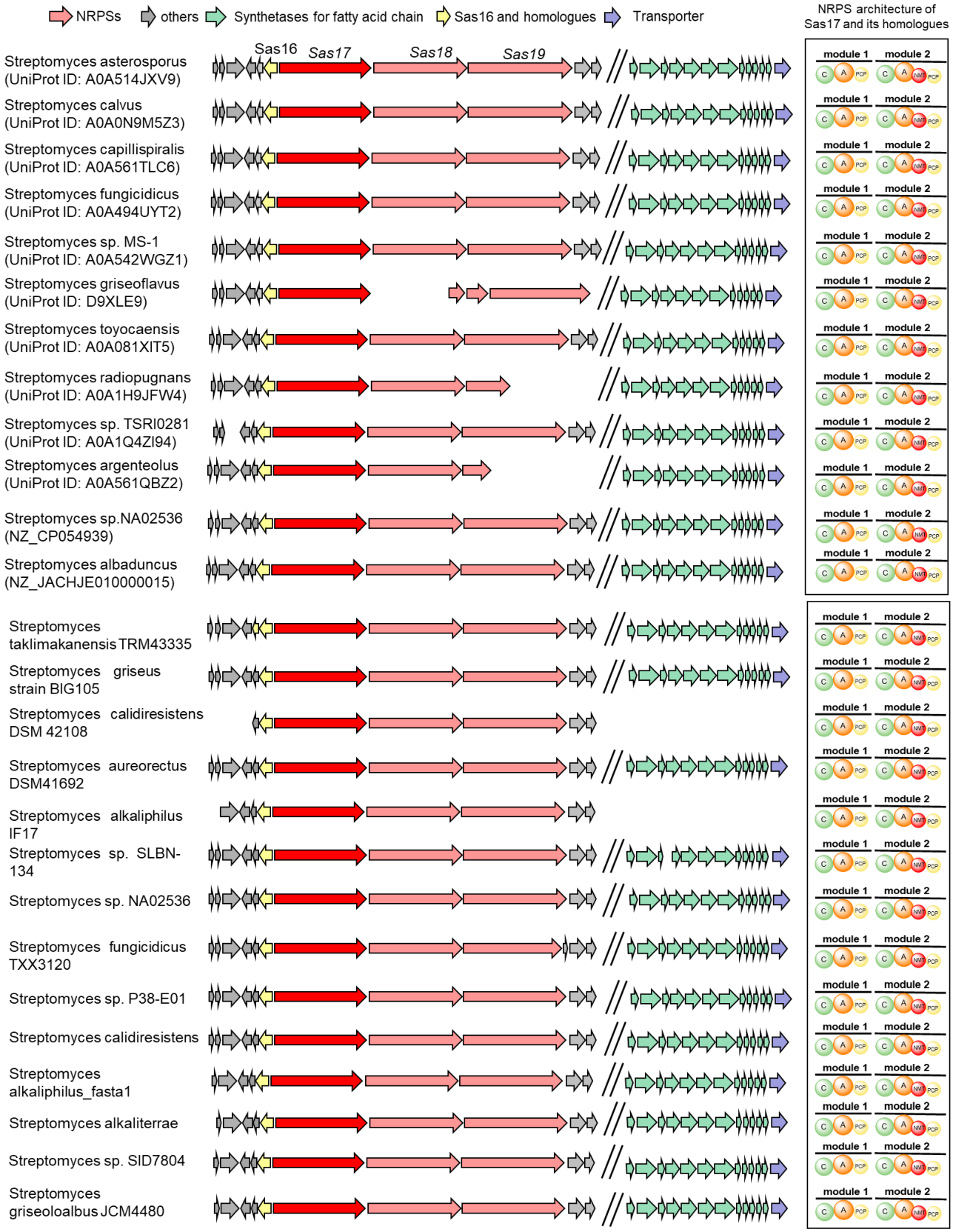

Figure S32. ^{1}H NMR spectrum of WS9326M in DMSO-d$_6$.

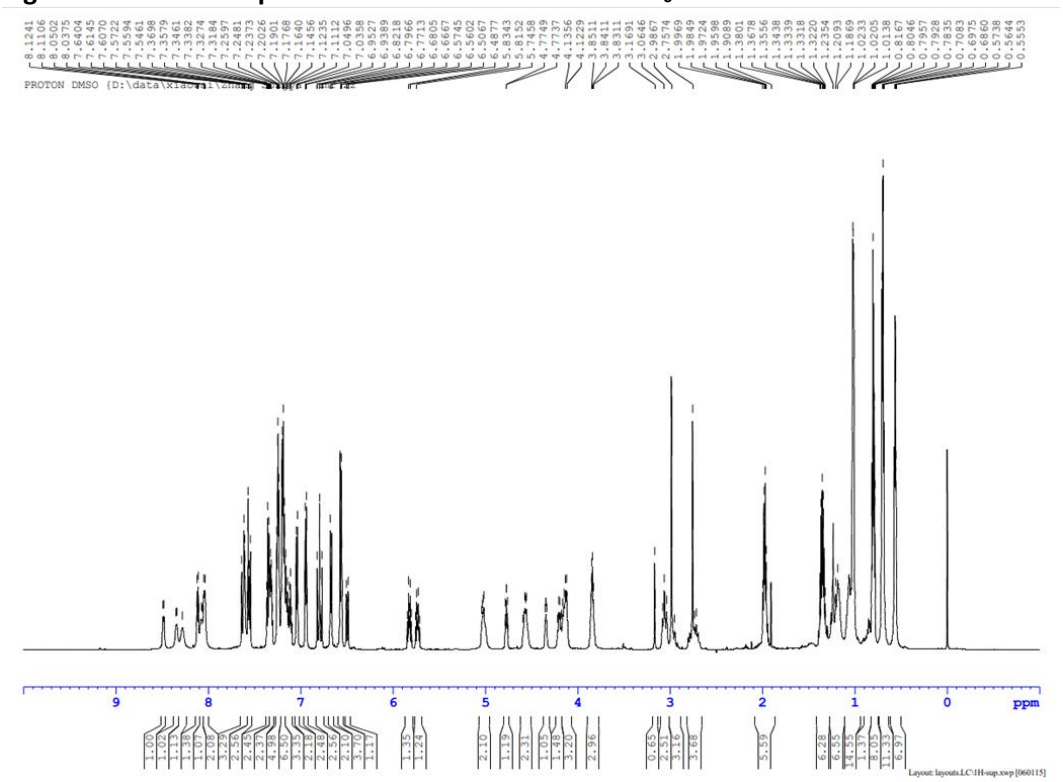

Figure S33. ^{13}C NMR spectrum of WS9326M in DMSO-d$_6$.

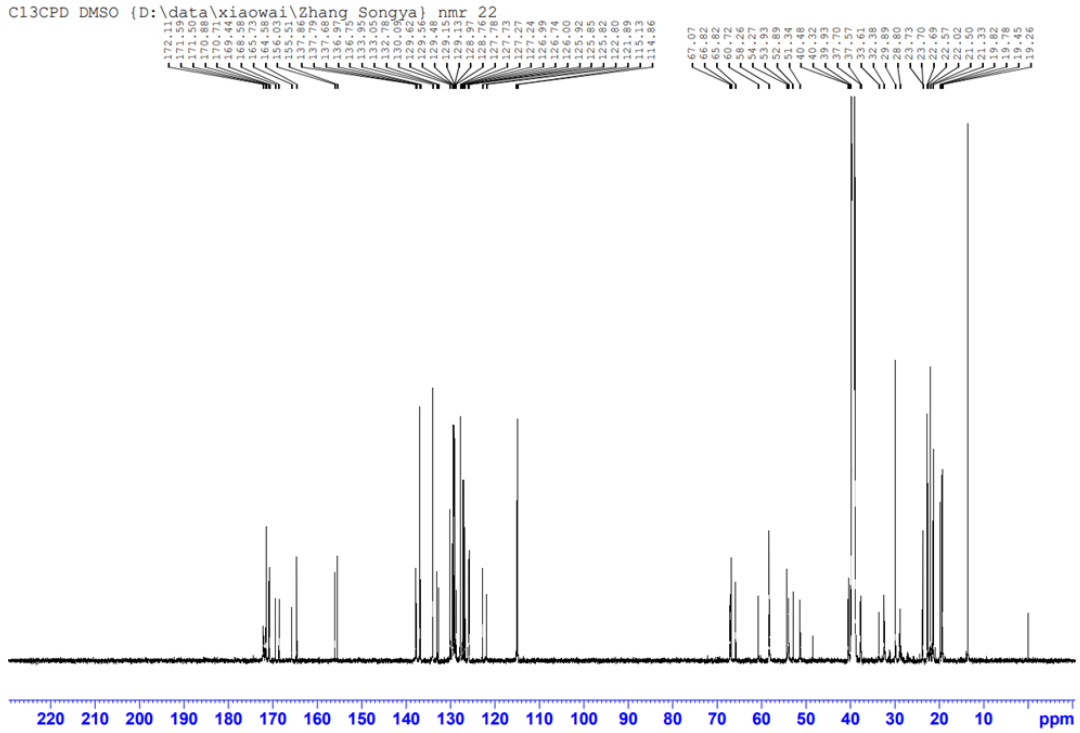

Figure S34. ^{1}H-^{1}H COSY spectrum of WS9326M in DMSO-d_6.

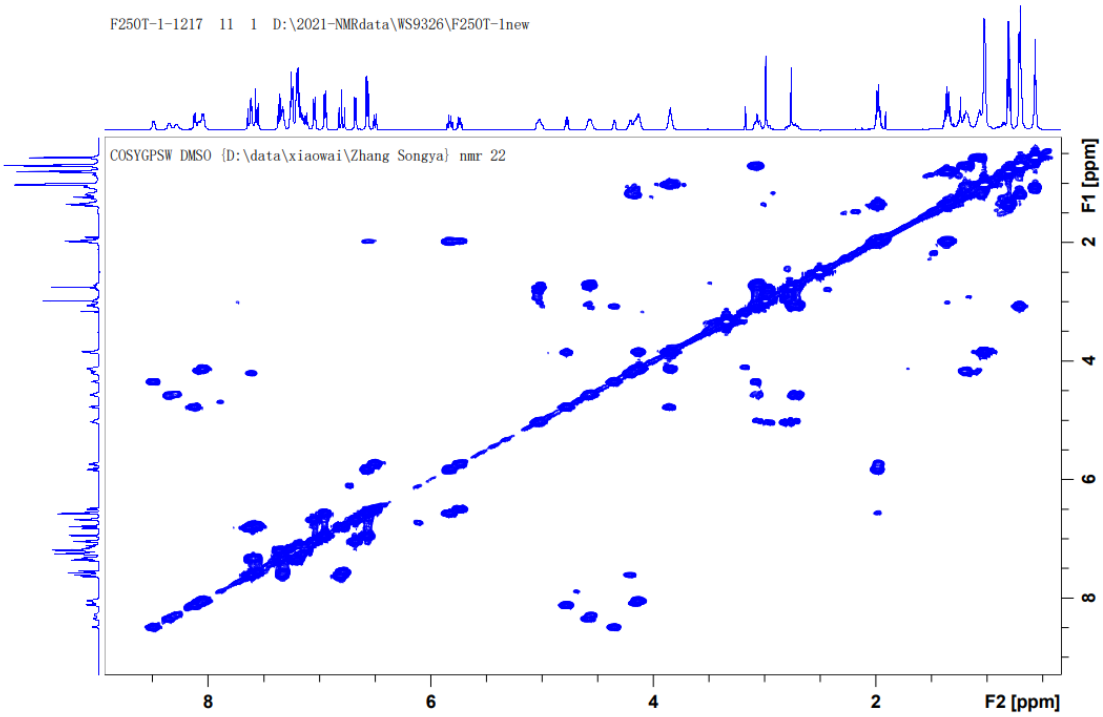

Figure S35. HSQC spectrum of WS9326M in DMSO-d_6.

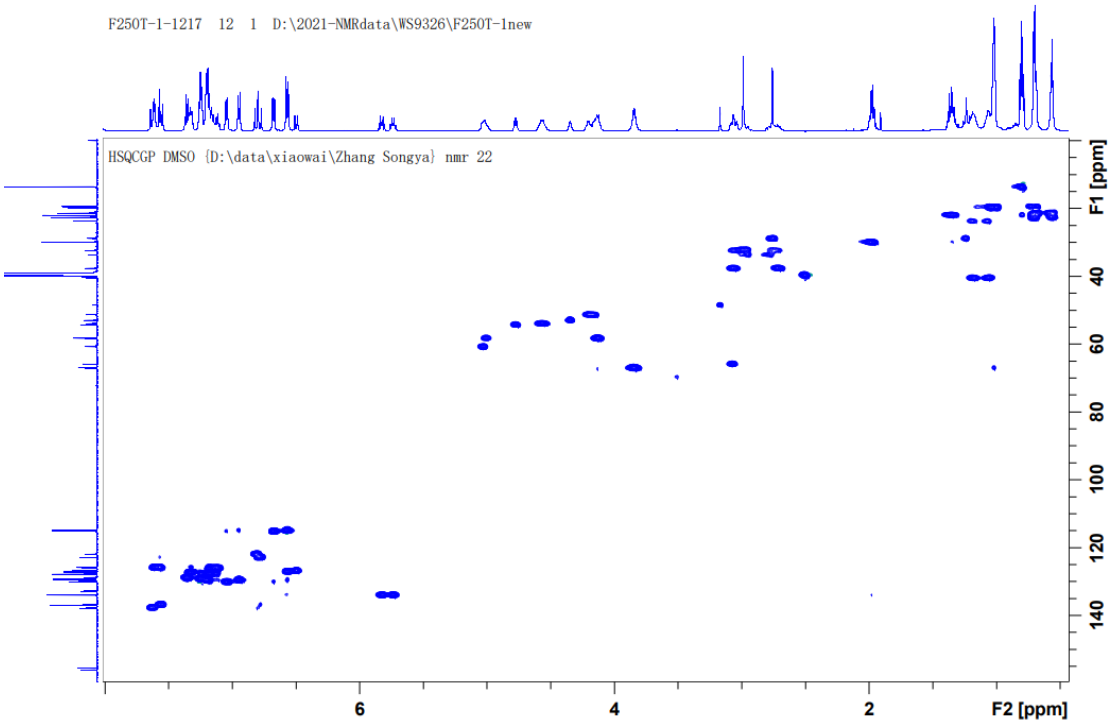

Figure S36. HMBC spectrum of WS9326M in DMSO-d_6.

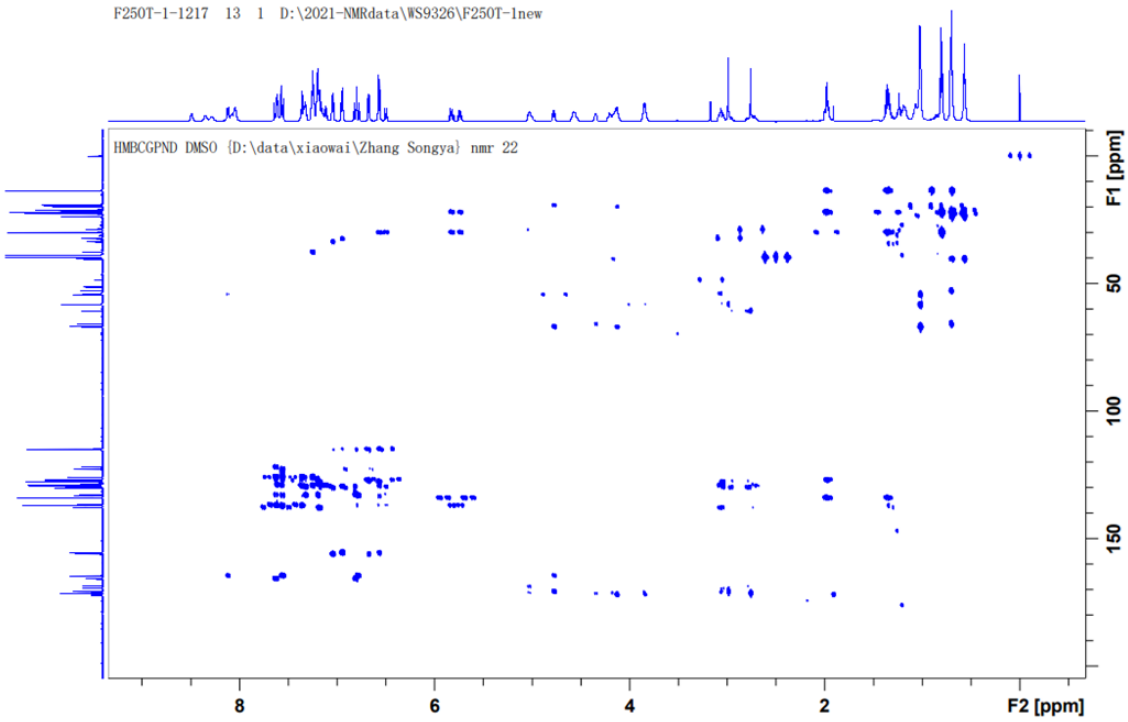

Figure S37. ^{1}H NMR spectrum of WS9326N in DMSO-d_6.

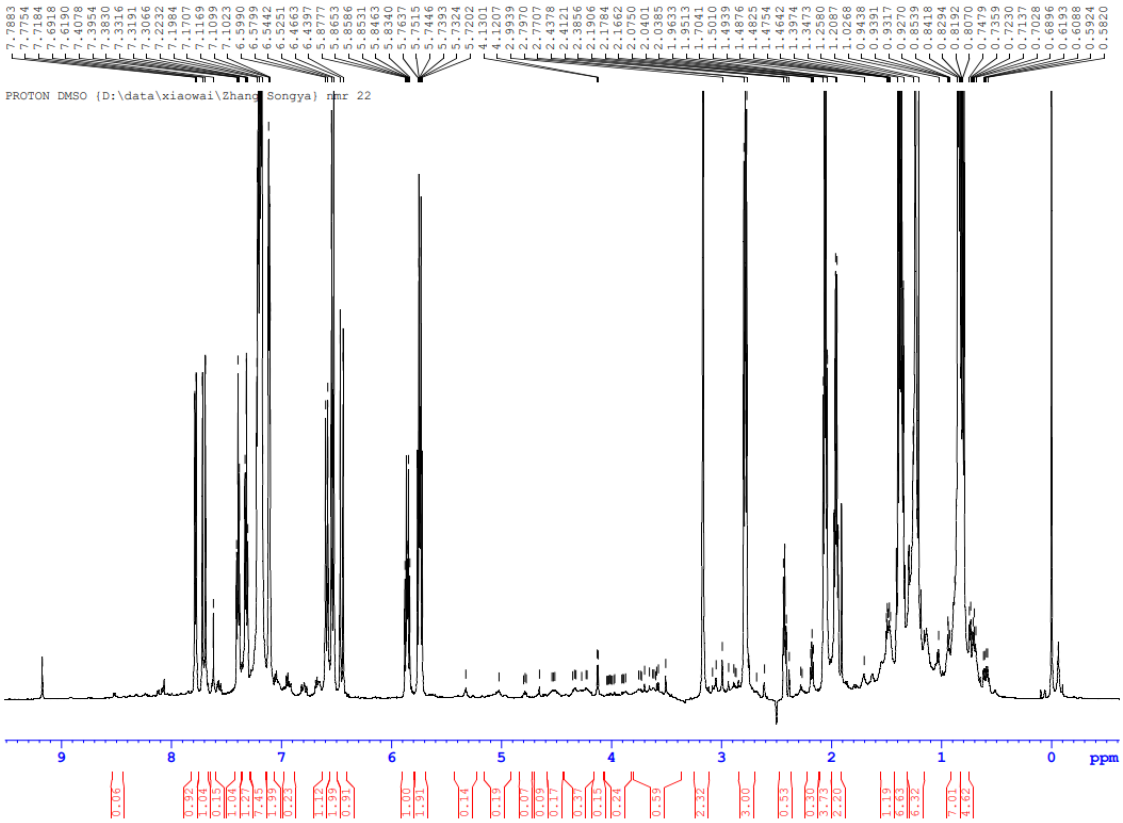

Figure S38. ^{13}C NMR spectrum of WS9326N in DMSO-d_6.

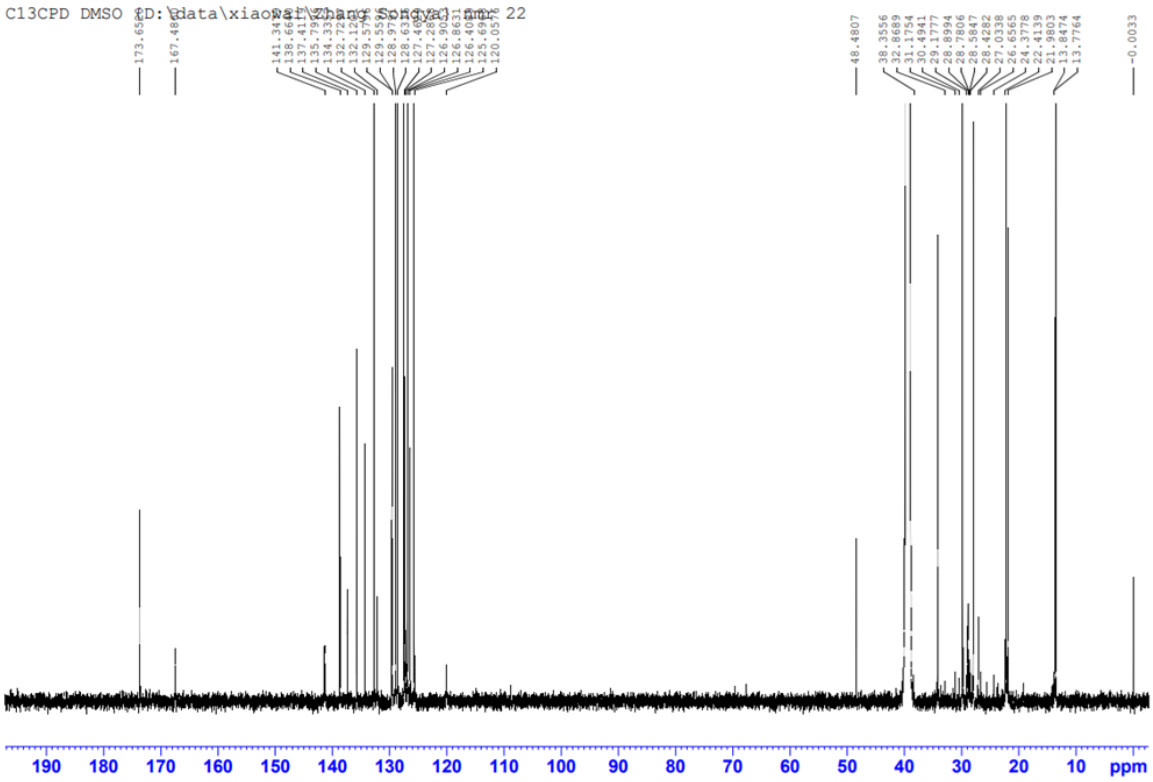

Figure S39. ^{1}H-^{1}H COSY spectrum of WS9326N in DMSO-d_6.

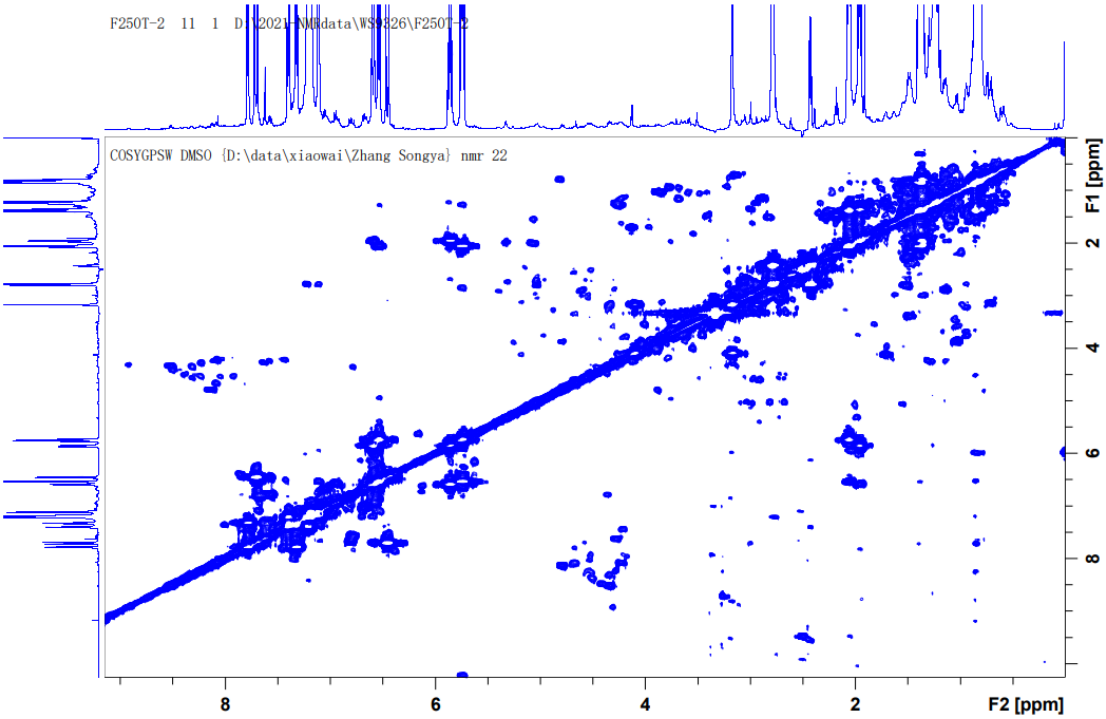

Figure S40. HSQC spectrum of WS9326N in DMSO-d_6.

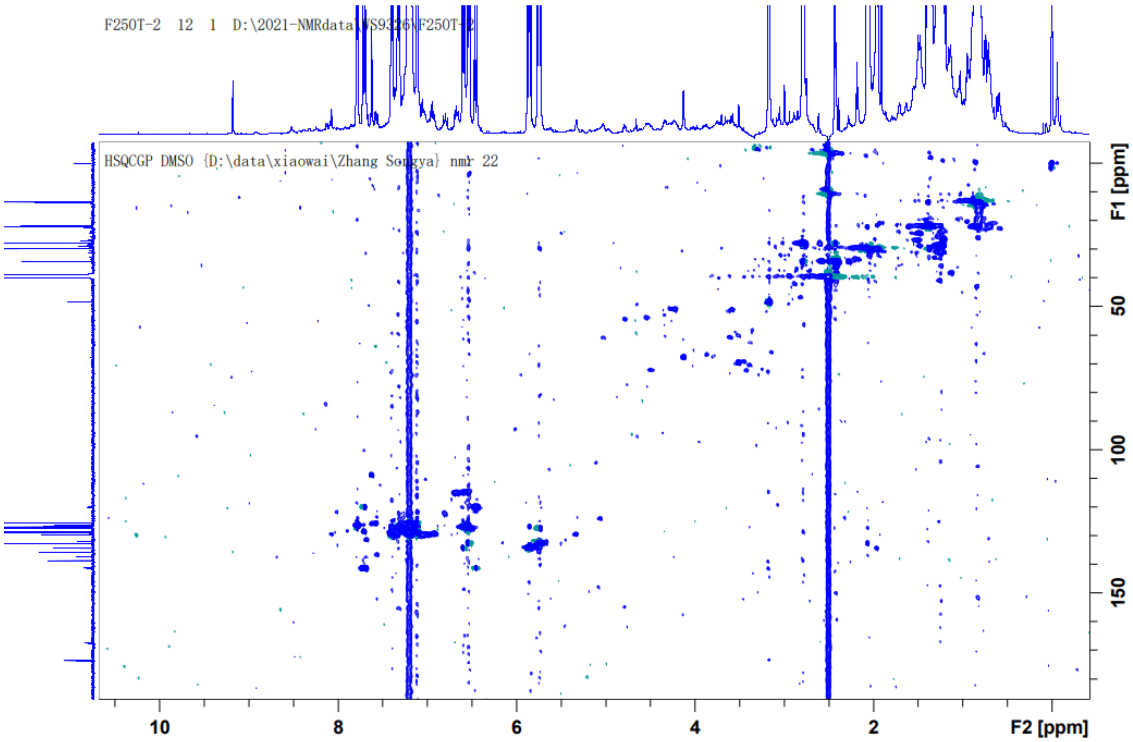

Figure S41. HMBC spectrum of WS9326N in DMSO-d_6.

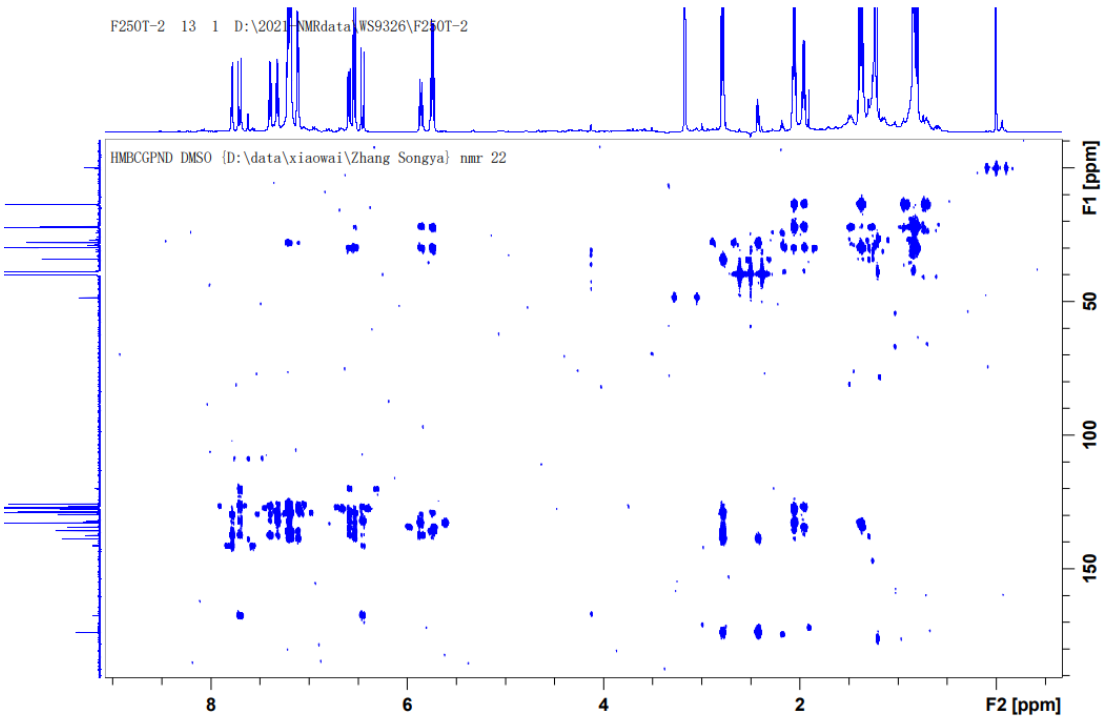

Figure S42. ^{1}H NMR spectrum of WS9326X in DMSO-d$_6$.

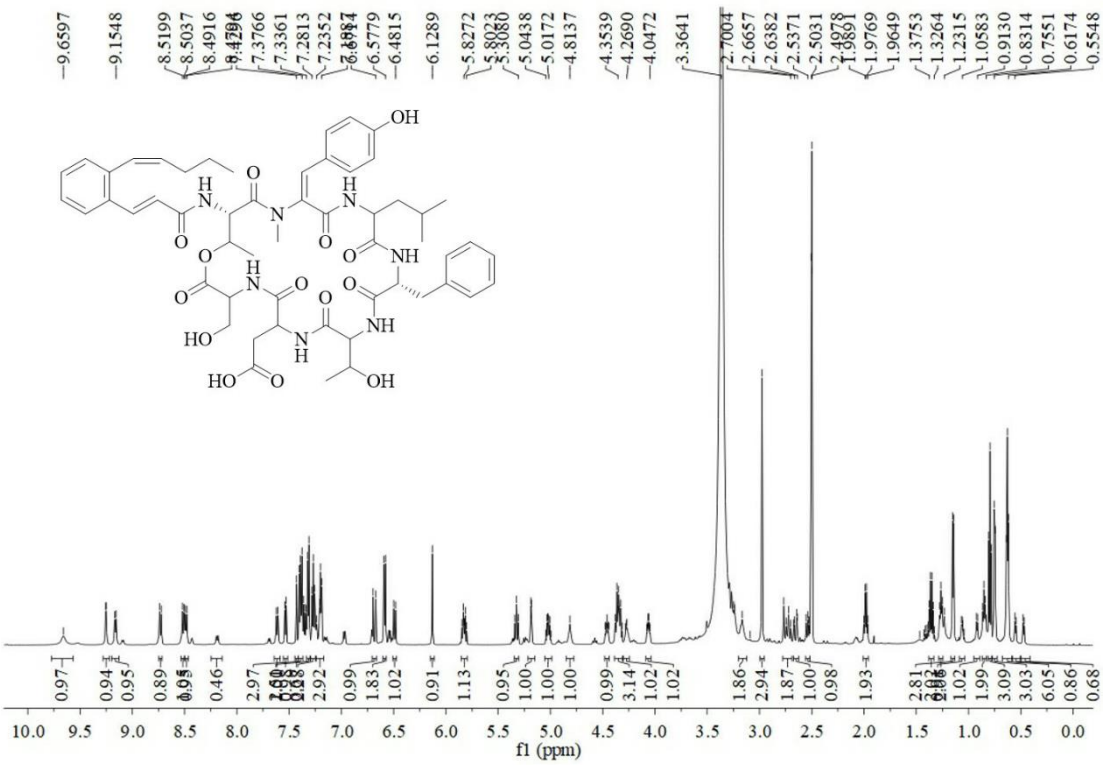

Figure S43. ^{13}C NMR spectrum of WS9326X in DMSO-d$_6$.

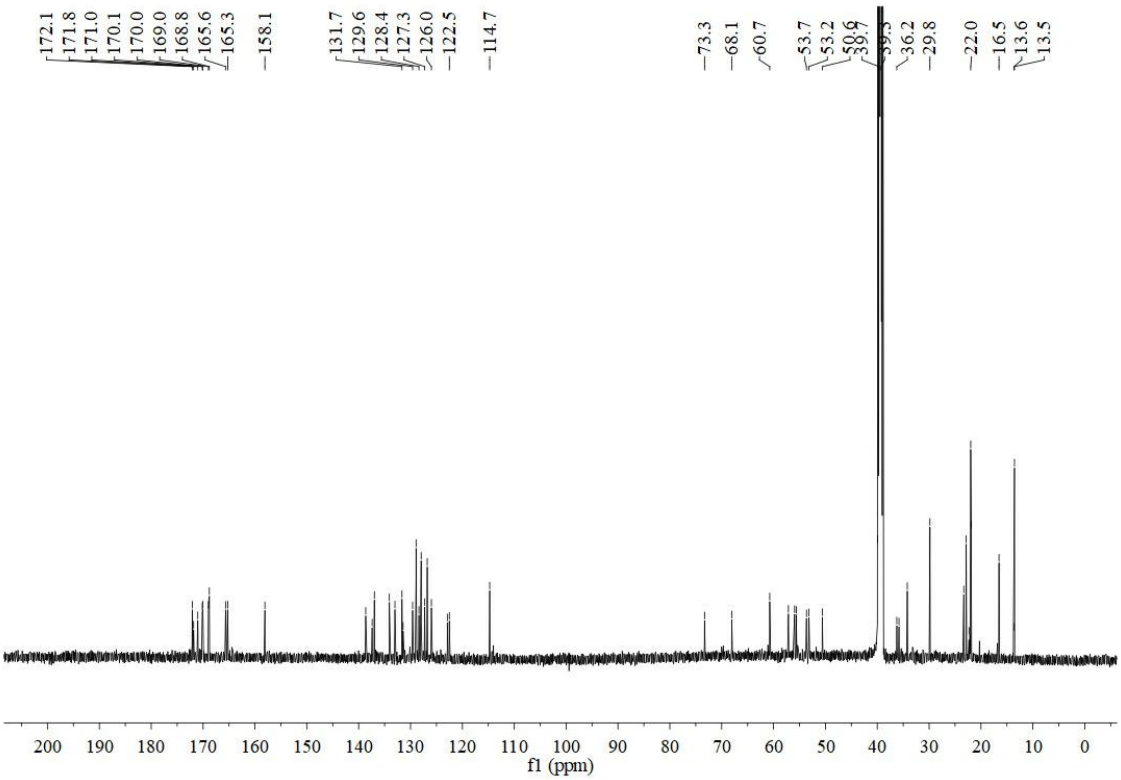

Figure S44. ^{1}H-^{1}H COSY spectrum of WS9326X in DMSO-d_6.

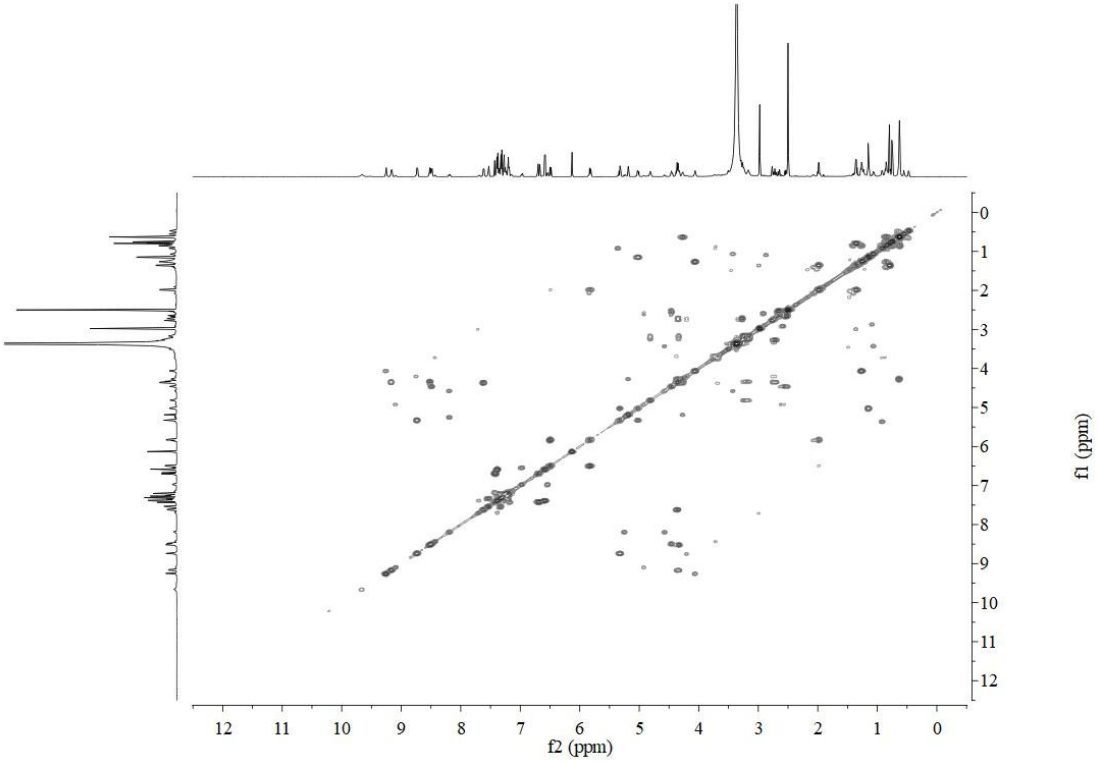

Figure S45. HSQC spectrum of WS9326X in DMSO-d_6.

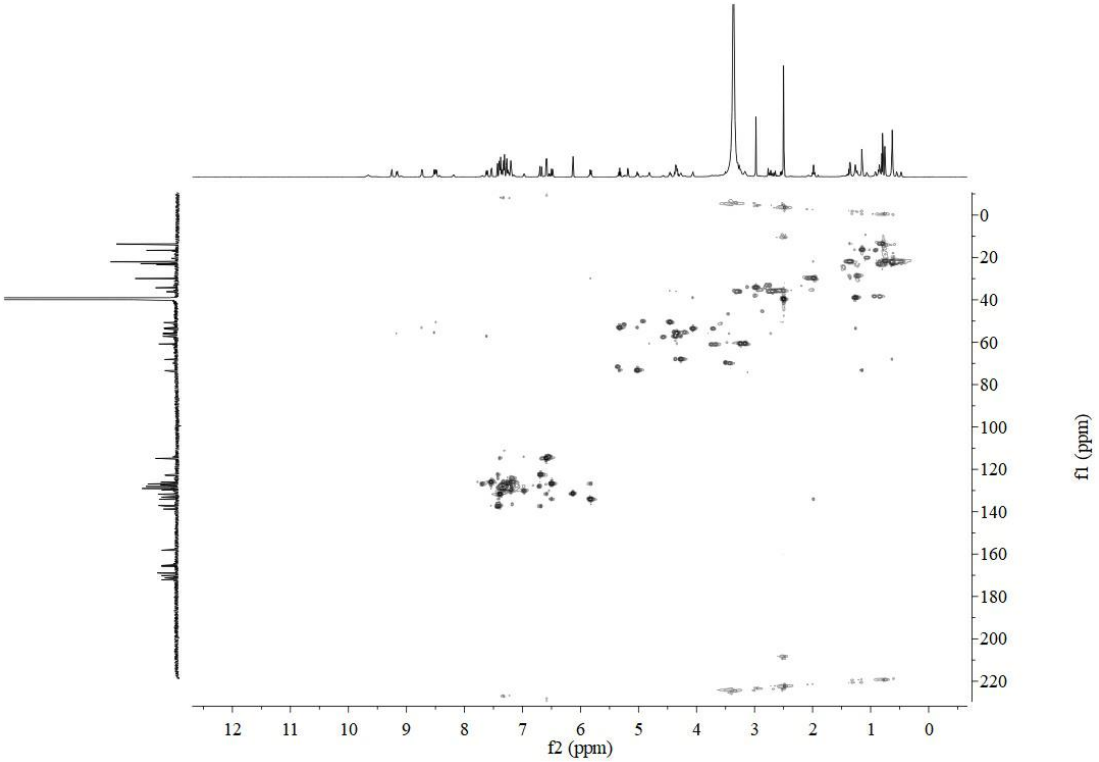

Figure S46. HMBC spectrum of WS9326X in DMSO-d_6.

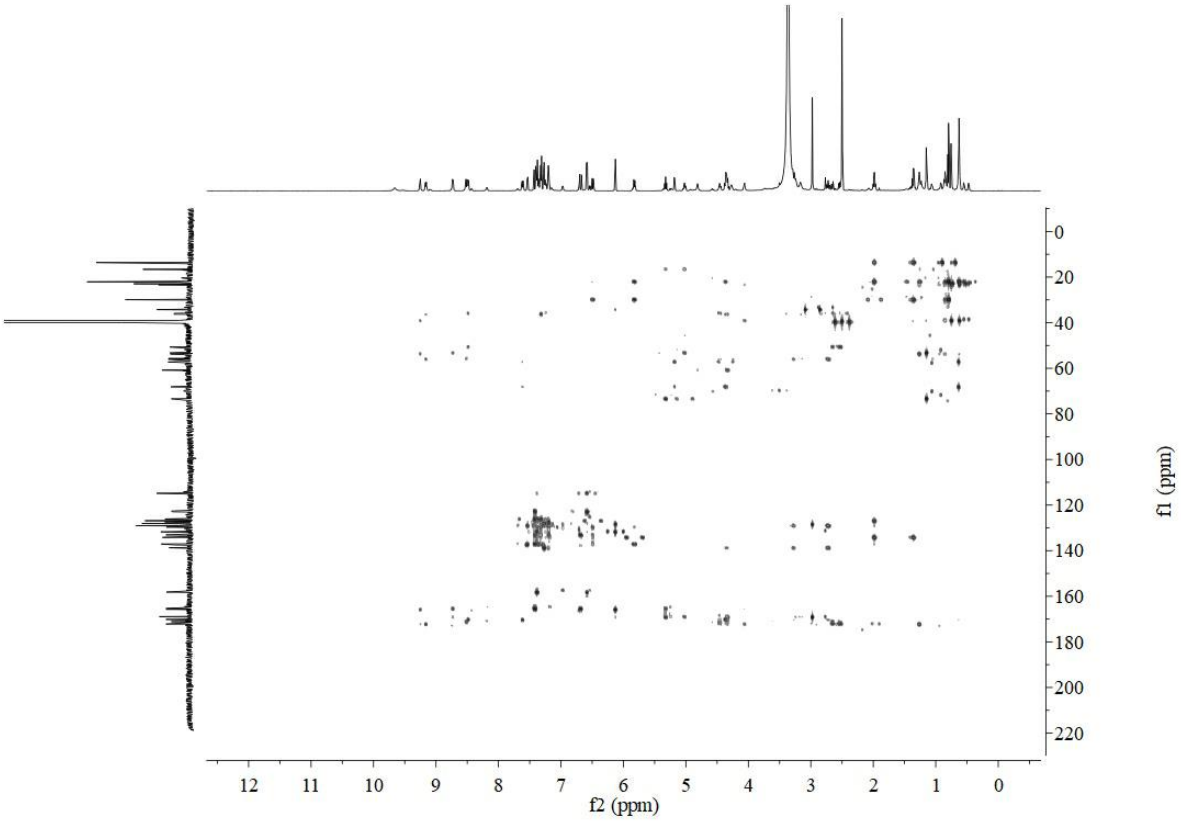

Figure S47. HPLC chromatogram of FDAA derivative of WS9326X and the corresponding standard amino acids.
The eluent for each chromatogram was monitored by extracted ion chromatogram mode.

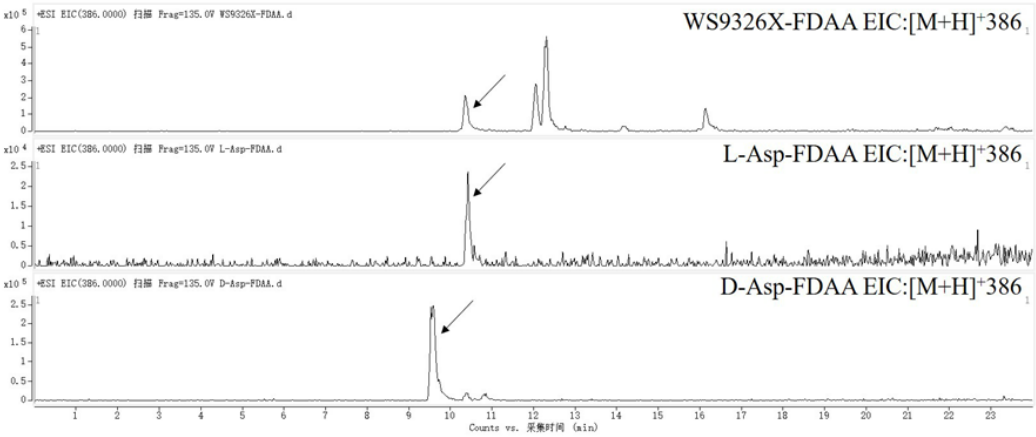

Figure S48. HPLC-MS/MS fragmentation analysis of WS9326X.

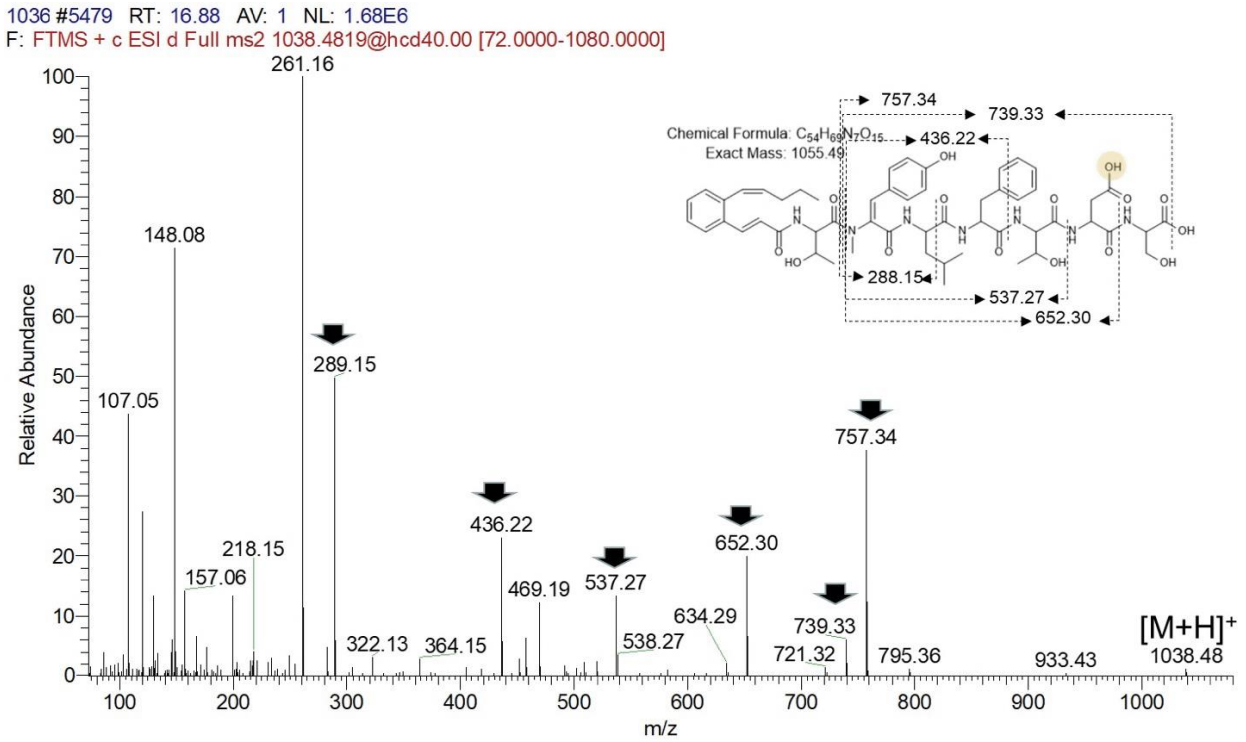

Figure S49. The HR LCMS chromatogram of WS9326X.

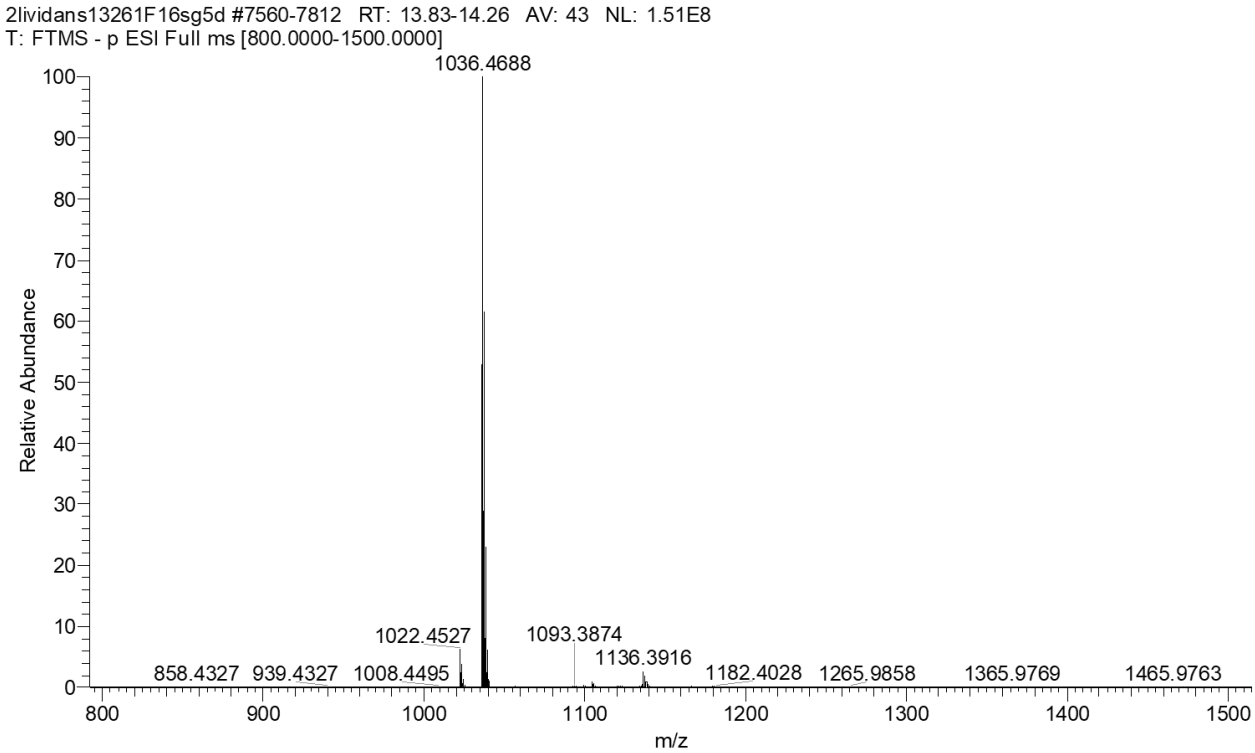

3. SI References

[1] B. Gust, G. L. Challis, K. Fowler, T. Kieser, K. F. Chater, *Proceedings of the National Academy of Sciences* **2003**, *100*, 1541-1546.

[2] M. Bierman, R. Logan, K. O'Brien, E. T. Seno, R. N. Rao, B. E. Schoner, *Gene* **1992**, *116*, 43-49.

[3] D. A. Hopwood, M. J. Bibb, K. F. Chater, T. Kieser, C. J. Bruton, H. M. Kieser, D. J. Lydiate, C. P. Smith, J. M. Ward, H. and Schrempf, *Genetic manipulation of streptomyces: A laboratory manual.*, The John Innes Foundation., Norwich, **1985**.

[4] S. Herrmann, T. Siegl, M. Luzhetska, L. Petzke, C. Jilg, E. Welle, A. Erb, P. F. Leadlay, A. Bechthold, A. Luzhetskyy, *Appl Environ Microb* **2012**, *78*, 1804-1812.

[5] R. Makitrynskyy, B. Ostash, O. Tsypik, Y. Rebets, E. Doud, T. Meredith, A. Luzhetskyy, A. Bechthold, S. Walker, V. Fedorenko, *Open biology* **2013**, *3*, 130121.

[6] L. Kalan, A. Gessner, M. N. Thaker, N. Waglechner, X. Zhu, A. Szawiola, A. Bechthold, G. D. Wright, D. L. Zechel, *Chemistry & Biology* **2013**, *20*, 1214-1224.

[7] S. G. Bell, F. Xu, E. O. D. Johnson, I. M. Forward, M. Bartlam, Z. Rao, L.-L. Wong, *J Biol Inorg Chem* **2010**, *15*, 315-328.

[8] M. Sunbul, N. J. Marshall, Y. Zou, K. Zhang, J. Yin, *J Mol Biol* **2009**, *387*, 883-898.

[9] J. Bogomolovas, B. Simon, M. Sattler, G. Stier, *Protein Expr Purif* **2009**, *64*, 16-23.

[10] H. Wang, X. Bian, L. Xia, X. Ding, R. Müller, Y. Zhang, J. Fu, A. F. Stewart, *Nucleic Acids Research* **2013**, *42*, e37-e37.

[11] S. Zhang, J. Zhu, D. Zechel, C. Jessen-Trefzer, R. Eastman, T. Paululat, A. Bechthold, *Chembiochem* **2018**, *19*, 272-279.

[12] L. Holm, P. Rosenström, *Nucleic Acids Res* **2010**, *38*, W545-W549.

[13] A. Miyanaga, R. Takayanagi, T. Furuya, A. Kawamata, T. Itagaki, Y. Iwabuchi, N. Kanoh, F. Kudo, T. Eguchi, *ChemBioChem* **2017**, *18*, 2179-2187.

[14] Y. Yasutake, N. Imoto, Y. Fujii, T. Fujii, A. Arisawa, T. Tamura, *Biochemical and Biophysical Research Communications* **2007**, *361*, 876-882.

[15] L.-H. Xu, S. Fushinobu, S. Takamatsu, T. Wakagi, H. Ikeda, H. Shoun, *Journal of Biological Chemistry* **2010**, *285*, 16844-16853.

[16] M. D. DeMars, F. Sheng, S. R. Park, A. N. Lowell, L. M. Podust, D. H. Sherman, *ACS Chemical Biology* **2016**, *11*, 2642-2654.

[17] K. Yasuda, Y. Yogo, H. Sugimoto, H. Mano, T. Takita, M. Ohta, M. Kamakura, S. Ikushiro, K. Yasukawa, Y. Shiro, T. Sakaki, *Biochemical and Biophysical Research Communications* **2017**, *486*, 336-341.

[18] S. Li, M. R. Chaulagain, A. R. Knauff, L. M. Podust, J. Montgomery, D. H. Sherman, *Proceedings of the National Academy of Sciences* **2009**, *106*, 18463-18468.

[19] O. Pylypenko, F. Vitali, K. Zerbe, J. A. Robinson, I. Schlichting, *J Biol Chem* **2003**, *278*, 46727-46733.

[20] J. R. Cupp-Vickery, T. L. Poulos, *Nature Structural Biology* **1995**, *2*, 144-153.

[21] M. J. Cryle, A. Meinhart, I. Schlichting, *J Biol Chem* **2010**, *285*, 24562-24574.

[22] K. Haslinger, C. Brieke, S. Uhlmann, L. Sieverling, R. D. Süssmuth, M. J. Cryle, *Angew Chem Int Ed* **2014**, *53*, 1-6.

[23] K. Zerbe, O. Pylypenko, F. Vitali, W. Zhang, S. Rouset, M. Heck, J. W. Vrijbloed, D. Bischoff, B. Bister, R. D. Sussmuth, S. Pelzer, W. Wohlleben, J. A. Robinson, I. Schlichting, *Journal of Biological Chemistry* **2002**, *277*, 47476-47485.

[24] J. Jumper, R. Evans, A. Pritzel, T. Green, M. Figurnov, O. Ronneberger, K. Tunyasuvunakool, R. Bates, A. Žídek, A. Potapenko, A. Bridgland, C. Meyer, S. A. A. Kohl, A. J. Ballard, A. Cowie, B. Romera-Paredes, S. Nikolov, R. Jain, J. Adler, T. Back, S. Petersen, D. Reiman, E. Clancy, M. Zielinski, M. Steinegger, M. Pacholska, T. Berghammer, S. Bodenstein, D. Silver, O. Vinyals, A. W. Senior, K. Kavukcuoglu, P. Kohli, D. Hassabis, *Nature* **2021**.